Electrokinetic Trapping of Biomolecules: Novel Nanofluidic Devices for Proteomic Applications

by

Ying-Chih Wang

S.M. Mechanical Engineering,
Massachusetts Institute of Technology, 2004

Submitted to the Department of Mechanical Engineering
in Partial Fulfillment of the Requirements for the Degree of
Doctor of Philosophy

at the

Massachusetts Institute of Technology

June 2007

Signature of Author.....
Department of Mechanical Engineering
May 10, 2007

Certified by.....
Jongyoon Han
Associate Professor of Electrical Engineering
Thesis Supervisor

Certified by.....
Scott Manalis
Associate Professor of Biological and Mechanical Engineering
Thesis Committee Chair

Accepted by.....
Lallit Anand
Chairman, Department Committee on Graduate Students

Electrokinetic Trapping of Biomolecules: Novel Nanofluidic Devices for Proteomic Applications

by

Ying-Chih Wang

Submitted to the Department of Mechanical Engineering
on June, 2007 in Partial Fulfillment of the
requirements for the degree of
Doctor of Philosophy

Abstract

Sample preparation has long been the most important and costly process in bioanalyses. Conventional identification methods involve multiple purification steps combined with mass spectrometry or immunosensing. While well-developed and widely utilized, these methods require extensive human labor and exhibit limited resolving power for low abundance analytes. Due to the shear complexity and abundance variation of biosamples, rapid and ultra-sensitive diagnostic measurements of disease markers are still out of reach. To address this issue, we developed a novel nanofluidic concentrator, utilizing the unique concentration polarization effect of sub 50 nm nanofluidic filters. With the distinct ionic and molecular interaction at the nanoscale, nanofluidic systems can potentially outperform current sample preparation and molecular detection techniques. Aiming to investigate and expand the applications of these techniques, this thesis work involves the design and development of a highly efficient nanofluidic preconcentrator, which can achieve a million fold detectability enhancements without complex buffer arrangements. This thesis also includes an integrated preconcentration-immunosensing device. By manipulating analyte concentrations, this integrated device not only increases the detection sensitivity, but also expands the dynamic range of given antibody-antigen couples. In addition, we also investigated the ion transfer at the micro-/nano-fluidic interface. Depending on the strength of the applied electric field across the nanochannel array, various phenomena such as concentration polarization, charge depletion, and nonlinear electrokinetic flows in the adjacent microfluidic channel can be

observed and studied *in situ* by fluorescent microscopy. In summary, the nanofluidic concentrator we developed in this thesis facilitates sample preparation and detection of biomolecules from complex biological matrices and facilitates a further understanding of nanoscale molecular/fluid/ion transport phenomena by providing a well-controlled experimental platform.

Thesis Supervisor: Jongyoon Han
Title: Associate Professor of Electrical Engineering and Biological Engineering

To my parents,

Chao-Yi and Tu Chiu-E Wang

and my wife,

Ya-Ling Chen

Acknowledgment

I have been very fortunate in being surrounded by many supportive friends and colleagues throughout my years of graduate study. Without their kind advice and help, this thesis would not have been made possible.

The long list of my indebtedness begins with my advisor, Professor Jongyoon Han, who introduced me to the field of micro/nano-fluidics and directed me with his insightful guidance. This thesis has benefited greatly from his generous support. I would also like to thank other thesis committee members of mine: Professor Scott Manalis, Professor Martin Bazant, and Professor Todd Thorsen. I very much appreciate their encouragement and enlightening input. I also thank Professor Dennis Freeman and Professor Joel Voldman for giving me the privilege of using their lab facilities.

Working with fellows in the MIT Micro/Nanofluidic BioMEMS Group has been a very delightful experience for me. I am grateful to all our group members (listed in no particular order): Jianping Fu, Pan Mao, Yong-Ak Song, Jeong Hoon Lee, Sung Jae Kim, Reto B. Schoch, Hansen Bow, Philip Dextras, Aniruddh Sarkar, Vincent Liu, Noel Reyes-Gonzalez, Arnaud Le Coguic, and Chang Soo Lee. In addition, there are many other people in this community, who have always been helpful to me: Man-Ho Choi, Anna L. Steven, Christopher Bergevin, Wendy Gu, Roozbeh Ghaffari, and Salil Desai. I appreciate their kind support and stimulating conversations.

I also thank all the staff members at MIT Microsystems Technology Laboratories, especially Kurt Broderick, for showing me the patience and skill it takes to survive and succeed when it comes to microfabrication.

In the meantime, I must thank many agents for their generous funds, including NIH funding sources, CDP center grant (GM68762), NIBIB EB005743, MIT Ferry Fund, NSF

CTS-0347348, and NCI CA119402. I cannot over emphasize how much I learned and gained from the encouraging environment supported by their generosity.

Above all, I would like to express my appreciation to my family for their selfless love and care. It is a great pleasure from me to dedicate this thesis to my beloved family.

Table of Contents

List of Figures

Chapter 1

Introduction

1.1 Opportunities in Micro/Nano-Fluidics Sample Preparation

Biosample preparation, also called sample purification or pre-fractionation, can be defined as a series of molecular separation or fractionation steps required for obtaining higher sensitivity and selectivity of downstream biosensing and molecular identification processes. Says Efraim Racker, a renowned biochemist, as one of the Ten Commandments of Enzymology:[1] "Don't waste clean thinking on dirty enzymes." It is not difficult to imagine that sample preparation has been the major challenge in proteomics studies, given the complexity of typical proteomic biosamples. A successful bioanalysis usually involves sample extraction, separation, amplification, and identification. For samples as complex as human serum proteome, more steps in the described sequence should be included in order to obtain a reliable readout.

Conventional bench top sample preparation is very time- and reagent-consuming, highly labor-intensive, vulnerable to cross-contamination and lacking fidelity in

identifying low abundance molecules. From the early 90s, scientists and engineers have been seeking an alternative technological platform called micro Total Analysis Systems (μTAS, also known as labs-on-a-chip), to overcome the inherent problems of existing techniques for biosample preparation. As recent developments in μTAS have shown promising solutions for the above mentioned problems and provided opportunities for mass-production and automatable analysis, many proteomic studies have adapted their conventional analysis into microfluidic platforms.[2-4]

Currently, the most common bioanalysis technologies in proteomics can be divided into two categories. The first is the most widely used: the combination of 2D gel electrophoresis or chromatography with Mass Spectrometry (MS). This method has been demonstrated to exhibit sensitivity in the μM to nM range. The second method uses immuno-enzyme assays such as Enzyme-Linked ImmunoSorbent Assay (ELISA) and Radio Immuno Assay (RIA) with sensitivity around nM to pM. The bottleneck of these immunoassay techniques is the identification of molecules with concentrations lower than pM, while there are novel techniques being developed to push the concentration sensitivity below fM level.[5-12] One critical problem of these bioanalysis tools (both MS and immunoassay) comes from their limited dynamic range of detection. None of these methods has a sufficient dynamic range to cover the concentration variation (from mM to zM) in human proteome. For example, human plasma, as shown in Figure 1-1 and 1-2, has majority protein species (albumin and immunoglobulin) at ~mg/ml concentration levels. In contrast, low abundance molecules such as cytokines and hormones only exist at ~pg/ml concentration levels, more than 9 orders of magnitude lower than highly abundant proteins. Such a dramatic range of concentration distribution has presented a formidable challenge to current identification methods. Currently, most biosensors show dynamic range of detection ~10^3. An analysis method that can detect molecules as low as a sub-pg/ml concentration and still have a dynamic range of more than 10^9 has not been realized yet.

To make the situation even worse, among the 10,000 proteins discovered, nearly 80% of them have molecular weights ranging from 20 to 80 kilo Dalton (kd). As a consequence, plasma protein identification with either MS or other tools is very challenging without one or more separation steps. (See Figure 1-1, the histogram of protein distribution according to their molecule sizes.) However, as demonstrated with our microchip IEF-MS coupling experiment (Figure 1-3), although separation can increase the resolution (the ability to pick up nearly overlapped samples) of the detector, the additional handling and purification steps also make some originally detectable samples fall below the detection limit.

With the recent development of micro and nanofabrication techniques, unique properties found in nanostructures have led to new inventions, and have been demonstrated to be a useful tool in areas of biomolecule detection, separation and other critical sample preparation elements.[13-15] As nanostructures and nanomaterials can be used to control and automate sample processing that is not possible on the macroscopic scale, nanofluidic devices have been built for sorting and separating well defined target biomolecules.[16, 17] These engineered biomolecule sieving structures can be fabricated with anisotropic structures and lead to more precise and rapid sample processing.

Because nanofabricated structures have similar size dimensions to most biomolecules, they are often used as molecular sieving structures to build customized separation devices. In addition, the size similarity between biomolecules and nanostructures also promises advances in the field of biosensing.[18-20] Due to the existence of surface diffusion layers, a major limiting factor in low concentration analyte detection is the prolonged incubation time to reach equilibrium. Nanoscale biosensors offer significant advantages in terms of its faster reaction kinetics, as smaller sensors have less surface area for conjugations.[21] As a result, nanotechnology has been used widely to address the need for ultra-sensitive biomolecule sensing, which have proven benefits in both increasing signal to noise ratio and reducing the scale of characteristic diffusion lengths.

Examples like cylindrical nanowires, planar ion-sensitive field-effect transistors and nanosphere sensors, for example, have been widely recognized for their ability to detect low concentration analytes. [20, 21]

In addition, the unique ion transport phenomena associated with nanofluidic channels have found applications in fields such as fuel cells, sample preconcentrations,[22, 23] and chromatograph separations.[24] Current studies suggest that the (nearly) overlapping of Debye screening layers in nanofluidic channels can give them better proton conductivity than conventional media. These new proton-exchange membranes could be used to develop next generation micro fuel cells. Besides, because the surface screening layers have profound effects on biomolecules and ions, nanofluidic devices are also the ideal platform for us to study novel ion selective transfer phenomena.

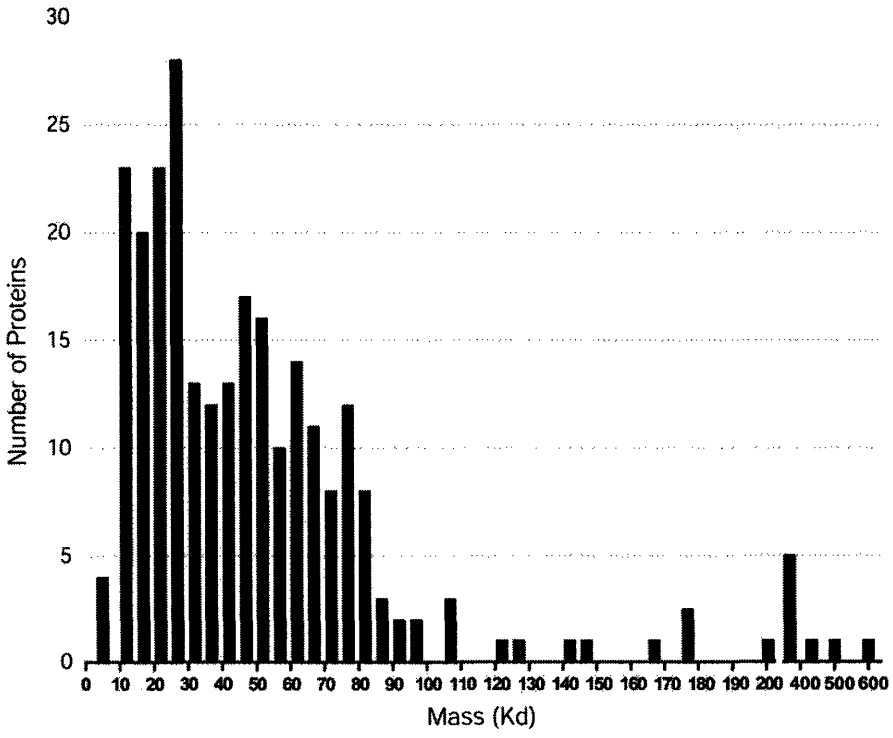

Figure 1-1 The histogram of proteins observed in the plasma
The figure is composed from 289 proteins currently being identified. (Adapted from works of Anderson *et al.*[25])

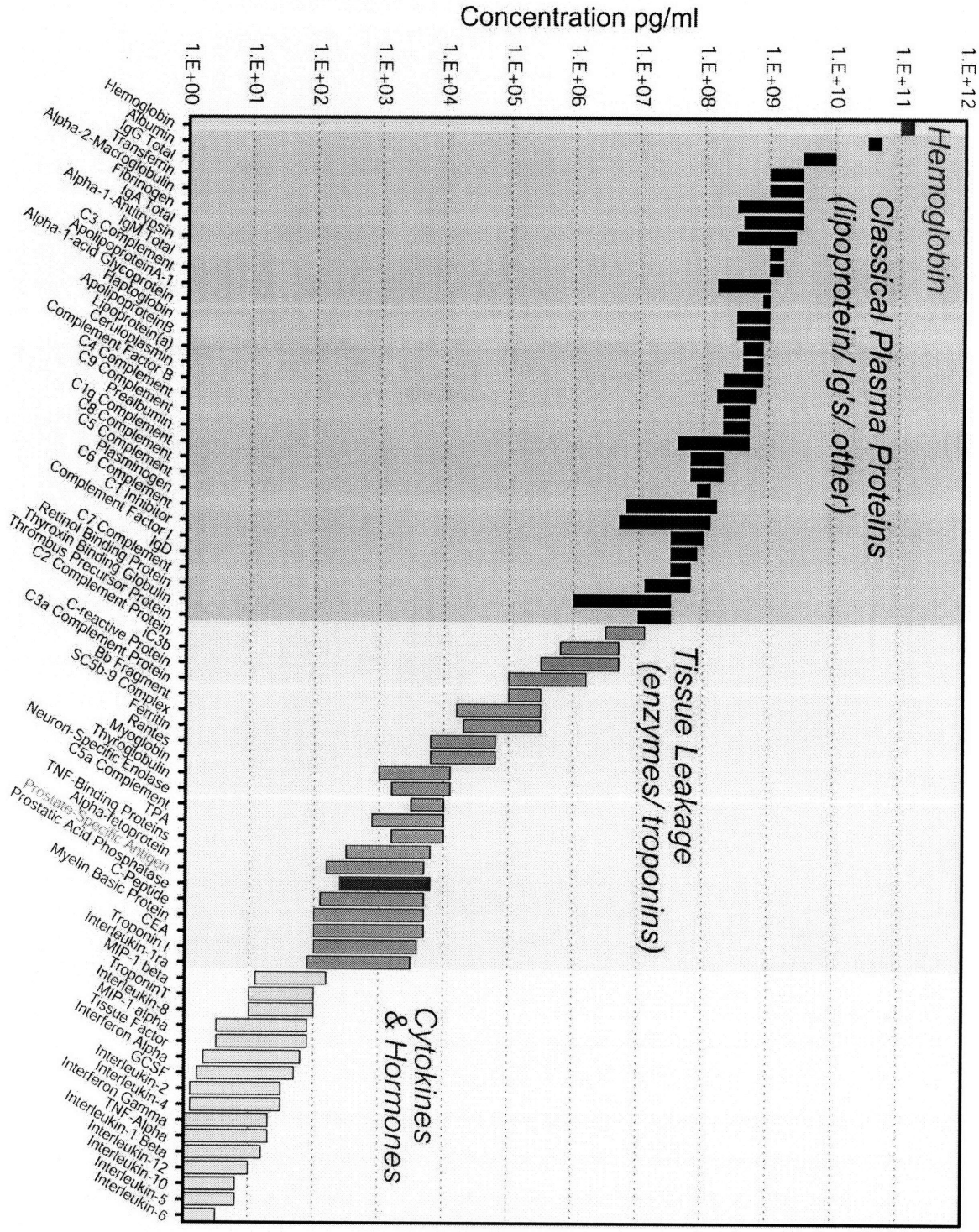

Figure 1-2 Human plasma proteome, normal range of abundances.
(Adapted from works of Anderson *et al.*[25])

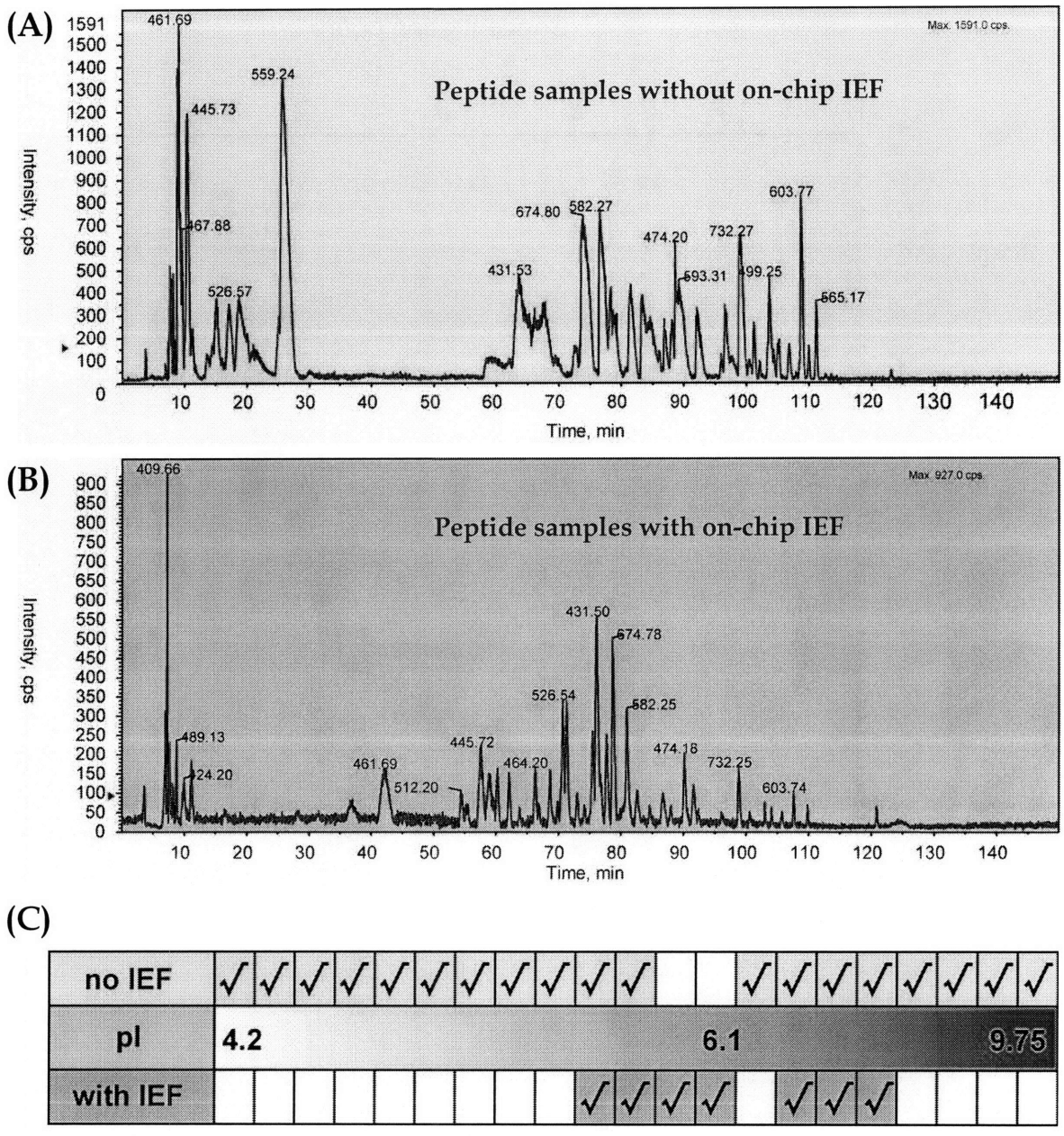

Figure 1-3 TOF-MS base peak chromatography of human serum albumin digest

The light background data (A) shows the readouts from original peptide digest and the dark background one (B) is the digest after on-chip isoelectric focusing (Peptides between pI 5-7 were isolated with microfluidic device. (C) More peptides were identified with a separation step.[26]

Table 1-1: Mass spectrometry readout of peptides in human serum

Before IEF	pI	After IEF
DDNPNLPR	4.21	
QNCELFEQLGEYK	4.25	
AAFTECCQAADK	4.37	
YICENQDSISSK	4.37	
DVFLGMFLYEYAR	4.37	
LVNEVTEFAK	4.53	
AEFAEVSK	4.53	
FKDLGEENFK	4.68	
RPCFSALEVDETYVPK	4.68	
CCTESLVNR	5.99	CCTESLVNR
YLYEIAR	6	YLYEIAR
QTALVELVK	6	QTALVELVK
LKECCEK	6.13	LKECCEK
PLLEK	6.43	
SLHTLFGDK	6.46	SLHTLFGDK
NECFLQHK	6.74	NECFLQHK
HPYFYAPELLFFAK	6.75	HPYFYAPELLFFAK
LCTVATLR	8.25	
RHPDYSVVLLLR	8.75	
KVPQVSTPTLVEVSR	8.75	
FQNALLVR	9.75	

*http://us.expasy.org/tools/protparam.html

1.2 The Importance of Signal Amplification in the Sample Preparation

For the study of protein expressions in cell complements, tissues or biofluids, capabilities of isolating and amplifying target protein molecules are critically needed. As demonstrated in Figure 1-2, most signaling and pharmacodynamical biomarkers present at very low concentrations in a complex mixture. One major problem hampering the developing of present-day proteomics techniques is the lack of amplification techniques. Although some well-established methods such as sedimentations, chromatographic separations and electrophoretic separations have been successfully coupled to resolve thousands of samples either in sequence or in parallel, these purification techniques still cannot resolve the issue associated with low target concentration satisfactorily.

Since the identification and detection of scarce samples is extremely difficult without a proper (signal) amplification step, the first motivation for biomolecule sample

preconcentration is rather straightforward: the scarcity of these biomarkers imposes notable challenges on the detection systems. Typically, these information-rich signaling molecules have extremely low concentrations (nM-fM), concentration levels that most detection systems can barely handle. Therefore, an integratable preconcentration scheme will be able to largely eliminate the difficulty imposed on the detector and provide better sensitivity and signal-to-noise ratio.

Secondly, while tracking multiple biomarkers (also called sample multiplexing) has been identified as a critical measure of diagnostic reliability in pharmaceutical, clinical and proteomic applications, simultaneous measurements are extremely difficult because markers are distributed across concentrations with over 10 orders of magnitude differences. Monitoring multiple species is important because biochemical reactions/ metabolism usually involve multiple pathways. As an extreme example, if one is to diagnose the malnutrition and inflammatory responses of the liver due to an infection, both serum albumin (normally ranging from 35-50 mg/ml) and interleukin 6 (normally ranging from 0-5 pg/ml) have to be measured. Monitoring these two molecules spontaneously with one biotransducer (sensor) would be very challenging due to their shear abundance variation (10 orders of magnitude). Since a preconcentration device can enhance the concentration of a given biosample, it can increase the sensitivity and therefore the dynamic range of detection without modifying the biosensor. As a result, the preconcentration could become the enabling technique for biomolecular multiplexing.

The third reason for performing sample amplifications comes from the need for multiple purification steps when processing complex human samples. As shown in Figure 2, there are estimated more than 10,000 protein species present in the blood serum. Aside from immunoassays, most biomolecule detectors have no specificity over targets, and have only limited resolving power in terms of sample species. As one of the most powerful and widely used detectors, mass spectrometry (MS), which has peak capacity around 3000 and a dynamic range of detection around 10^4, requires some separation or

purification steps before samples can be transferred to the detector. However, after extensive separation steps, biomolecule detection become far more challenging due to non-specific sample loss. The implementation of a preconcentration device can readily be an approach to the sample complexity issue.

Some separation techniques, such as isoelectric focusing (IEF) and immunological chromatography, provide certain level of preconcentration. IEF is known to focus and concentrate proteins and enhance the nominal concentration by ~500 fold or so. Also, techniques such as surface enhanced laser desorption/ionization mass spectrometry (SELDI-MS) can pull out certain subsets of proteome and enrich their concentration by several orders of magnitudes, to achieve better detection. However, there have been no generic, widely-accepted and applicable solutions for protein signal enhancement available. Recent efforts have been focusing on applying novel methods for sample preconcentration in lab-on-a-chip devices, mostly using nano and microfluidic technologies. While most on-chip preconcentration approaches evolve from conventional capillary electrophoresis and chromatographic column techniques, these preconcentration techniques play an increasingly important role in chip-based sample preparation and identification systems.

1.2.1 Need for Sample Preconcentration as a World-to-chip Interface

Means of preconcentration plays a more important role in chip-based systems due to the critical scaling problem. Samples are handled in μL scales in conventional biotechnologies, using pipettes. Even though microfluidic miniaturization and integration have demonstrated great advantages for the field of biotechnology, microchannels typically have length scales around 10-100 μL and can process small sample volumes very effectively (~nL level). Considering the 1 μL or more of samples being loaded, more than 99.9% of them will not be processed. This means only limited volume and number of target molecules is available for microchip-based detection. The

problem is exacerbated when it comes to detection of low-abundance species. Because microchips usually have confined geometries that reduce the detectable volume by one to a few orders of magnitude, the total amount of sample for detection and overall detection sensitivity are significantly limited.

Since the detection sensitivity in microsystems is often challenged by the limited sample volume available, it is of special interest to have an efficient sample concentrator that can take typical ~μL or more sample volumes and preconcentrate molecules into a sampler volume so that sample can be separated and detected with much higher sensitivity and efficiency.

Therefore, coupling sample amplification scheme to biosample preparation steps cannot only increase the limits of detection for biosensing but also address one of the most challenging problems in proteome and disease marker discovery. This is a more critical issue in microchip-based fluidic systems because volume-limited microfluidic systems are largely challenged at their sensitivity. Not surprisingly, numerous efforts have been devoted to addressing these issues by building an efficient and robust preconcentration device.

1.3 Current Signal Amplification and Preconcentration Techniques

Several research groups have reported ways to preconcentrate samples in lab-on-a-chip devices. Earlier on-chip preconcentration approaches have largely evolved from conventional capillary electrophoresis and chromatographic column techniques. Recently, novel preconcentration schemes, evolved from unique micro/nano-fluidic properties, have been developed in response to the critical need for protein signal amplification in biosensing.

By having an efficient sample concentrator that can take typical microliter or more sample volumes and concentrate molecules into a smaller volumes, samples can be separated and detected much more sensitively. The basic preconcentration strategies applied to microfluidic devices can be classified into three broad categories: electrokinetic manipulation, chromatographic preconcentration[27-29] and membrane preconcentration.[30-32] More precisely, the electrokinetic manipulation can be divided into three subcategories including field-amplified sample stacking (FAS),[33] isotachophoresis,[34, 35] micellar electrokinetic sweeping,[36, 37] and electrokinetic trapping.[38-42]

1.3.1 Field Amplified Stacking (FAS)

Field-amplified stacking is a technique first introduced by Mikkers *et al.* in late 70s.[43] The mechanism relies on manipulating buffer concentration to achieve local field amplification. As shown in Figure 1-4, FAS concentrates samples by injection a low conductivity sample plug into high conductivity background buffers.

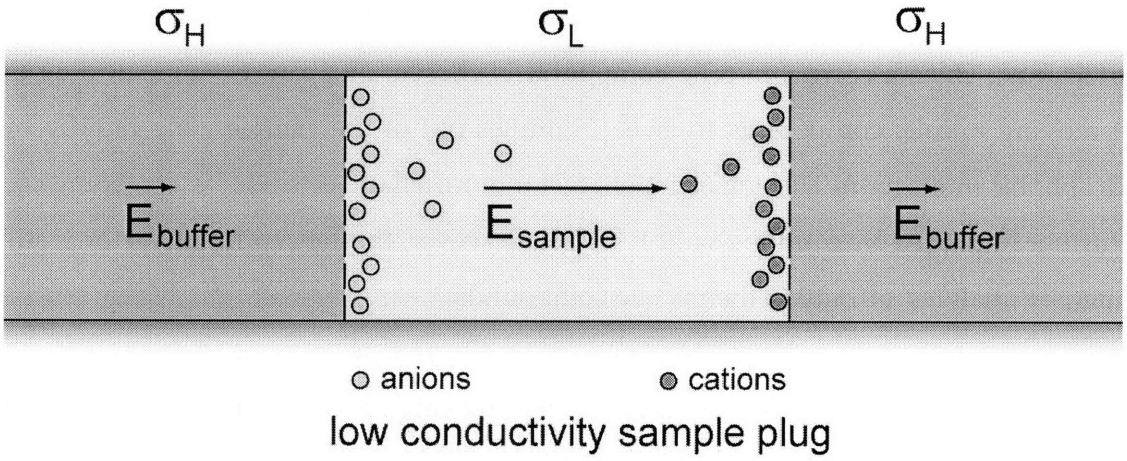

Figure 1-4 Schematic illustration of field amplified stacking in a microchannel

The relation between the electric field (E) and buffer concentration (C) can be defined by the relative conductive (γ) as:

$$\gamma = \frac{c_L}{c_H} = \frac{\sigma_L}{\sigma_H} = \frac{E_{buffer}}{E_{sample}} \qquad (2.1)$$

When a low conductivity (σ_L) sample plug is introduced into capillaries or microfluidic channels with high conductivity running buffer, most of the potential drop will occur in the injected sample zone. This locally amplified field will therefore drive/stack samples to the ends of the plug, and the stacked plug will be narrower but higher in concentrations. With a given plug size, one can increase the enhancement factor by increasing the relative conductivity ratio of the two buffers.[44] Even though FAS is one of the oldest, simplest preconcentration schemes to implement on microchips, the band broadening at the stacking boundary caused by hydrodynamic mixing, either from flow injection or mismatched electro-osmotic flow (EOF), limits the performance. FAS has been used on microchips, the volume-defined sample plug was enhanced by about 100 fold.[44] A continuous FAS was reported by Jacobson *et al.* that can stack samples at the sample-buffer interface during the injection.[45]

Micellar electrokinetic sweeping,[36] on the other hand, is achieved by changing the electrophoretic mobilities of samples by associating them with micelle compounds (surfactants). Once a correct micelle compound is chosen, one can use a small plug of fast moving micelle compounds to sweep samples out of the sample zone rapidly by hydrophobic interaction. The enhancement factor of micellar electrokinetic sweeping can be further improved by coupling with FAS.[36] However, the concentration factor is still limited by analytes' affinity to the micelle compounds.

Isotachophoresis[34] is another extensions of the stacking concept of FAS. In the case of isotachophoresis, with the knowledge of sample molecule's electrophoretic mobilities, the sample plug is sandwiched by leading electrolyte (LE) and terminating electrolyte (TE), instead of the same high conductivity buffer as in FAS. In the order of descending mobilities, the sample constituents will separate into distinct zones between high

mobility LE and low mobility TE (relative to sample constituents) upon the application of the separation voltage. Moreover, once the steady state gradient is achieved, the boundaries between samples can be maintained by a self-focusing mechanism which alleviates the dispersion problem of FAS. Recently, Jung *et al.* reported an on-chip transient isotachophoresis by introducing TE and LE into a T-junction simultaneously to achieve fast sample loading and separation.[35] Both FAS and isotachophoresis use buffer manipulation to achieve local field enhancement that helps sample stacking.

1.3.2 Electrokinetic Manipulations

While FAS and its related techniques are well-established, their merit as a sample preparation device is limited since these techniques usually require special buffer arrangements or reagents in the system. An alternative approach is using electrokinetic manipulation to trap biomolecules. By modifying the electrophoretic mobility of analytes, after balancing with the bulk flow as shown in Figure 1-5, the focused analytes molecules can remain stationary. The electrophoretic mobility of analytes can be controlled via various approaches, temperature gradient focusing, for example, uses temperature gradient to change overall mobility of given molecules.[38, 39, 46] This focusing mechanism can occur whenever the net molecular velocity profile is converging by either controlling the flow and/or electric field of the two zones.[47] Such collection can be achieved in a continuous fashion and does not require any special buffers or ionic strength arrangements. However, the overall efficiency of the collection would be critically dependent on the specific electrophoretic mobility of the target.

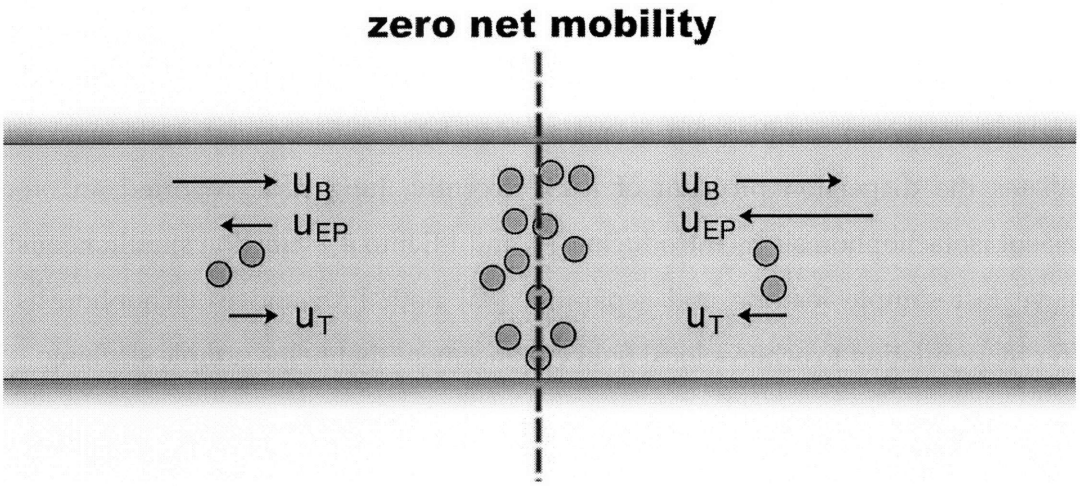

Figure 1-5 Schematic illustration of electrokinetic manipulation in a microchannel
Methods such as temperature gradient focusing or electrokinetic trapping can create one of multiple zones where analyte mobility equals to zero (bulk + electrophoresis mobility). As a result, continuous accumulation can be achieved as long as the zero mobility zone is well maintained.

Electrokinetic trapping is yet another class of techniques that can preconcentrate samples via electric field application. It is achieved by applying electric field across either porous membrane or nanofluidics channel with sub 50nm pore size. By controlling the pore size and buffer concentration, the thickness of the electrical double layer (EDL) can be on the order of the pore radius. Therefore, upon the application of the electric field, a phenomenon called concentration polarization will be induced. This polarization force has been used to stack charged samples with very high efficiency.[40, 41, 48] Advantage of electrokinetic trapping is that the preconcentration can be less sensitive to specific molecular electrokinetic properties (such as electrophoretic mobility) therefore provides a generic way for various types of molecules. However, concentration polarization and related phenomena are generally poorly understood, and the linearity and stability of the trapping is sometimes an issue. Unlike FAS, electrokinetic trapping can concentrate both cations and anions at the same boundary. This is because both ionic species are 'repelled' by concentration polarization process from the membrane/nanochannel. The work described by this dissertation falls in this category.

Meanwhile, the thesis also aims to study the concentration polarization phenomena in greater details.

1.3.3 Chromatographic preconcentration

Chromatographic preconcentration is also called solid-phase extraction (SPE). Fundamentally, this method relies on the different partition coefficients of each solute between adsorbed vs. free state of solute. Known as Nernst Partition Law, the ratio of concentrations of solutes species at a phase boundary is a constant for most given solutes and bulk phases:

Partition coefficient

$$K_{N(C,1,2)} = \frac{[C]_{phase1}}{[C]_{phase2}} \qquad \textbf{(2.2)}$$

In other words, with a given surface (fixed phase2, for example), when changing the fluid bulk phase, the equilibrium solute concentration in the fluid (phase1) will be changed, depending on the partition coefficient. As a result, it is possible to find buffers with distinct partition coefficient that can provide a dramatic absorption/releasing behavior when buffers have been switched.

As shown in Figure 1-6, chromatographic preconcentration usually involves two steps. First, analytes are retained by affinity binding onto an appropriated stationary subject. Then, with the application of the elution buffer, the analytes can be eluted into a more concentrated form. Depending on the chosen stationary subject, SPE can be divided into non-selective and selective ones. For example, Dodge *et al.* have demonstrated a chip-based assay by immobilizing Protein A on the surface and then mobilizing bound molecules with a glycine-HCL buffer.[49] To increase the surface-to-volume ration, Sato *et al.* packed a bed of polystyrene beads in a microchip to adsorb more samples.[50]

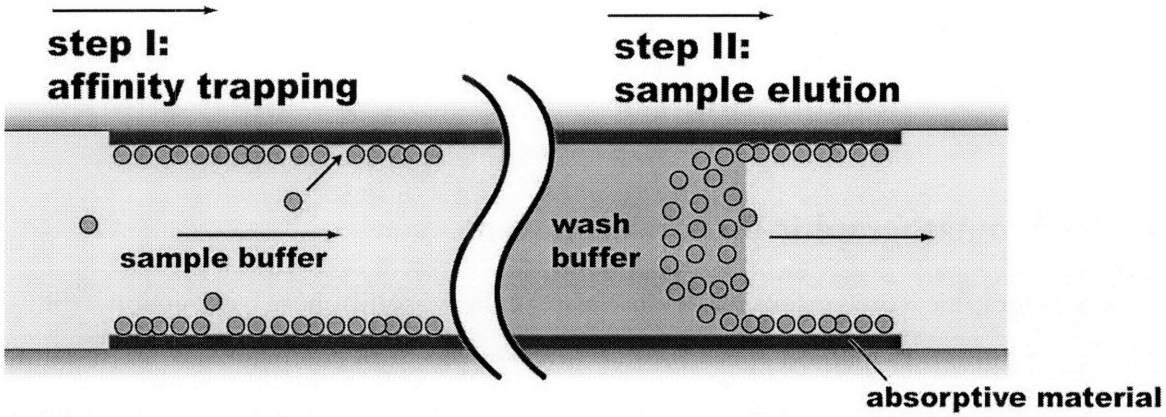

Figure 1-6 Schematic illustration of surface affinity-based preconcentration
Affinity-based preconcentration relays on different field amplified stacking in a microchannel.

1.3.4 Membrane preconcentration

Porous membranes have long been used in applications such as desalting and molecular weight cut-off separation. By adjusting the pore size, the system would allow the passage of buffer ions and small molecules but exclude larger molecules of interest. Several groups have developed an integrated preconcentration/separation system using porous membrane between adjacent microchannels, showing about 1000x fold signal enhancement.[31, 32, 48]

The concept is introduced in Figure 1-7. By arranging a porous membrane in the fluid pathway, larger molecules will be retained, allowing the transfer of small molecules only. These techniques are widely used in spin columns as a preparation step for bioanalytical separations.

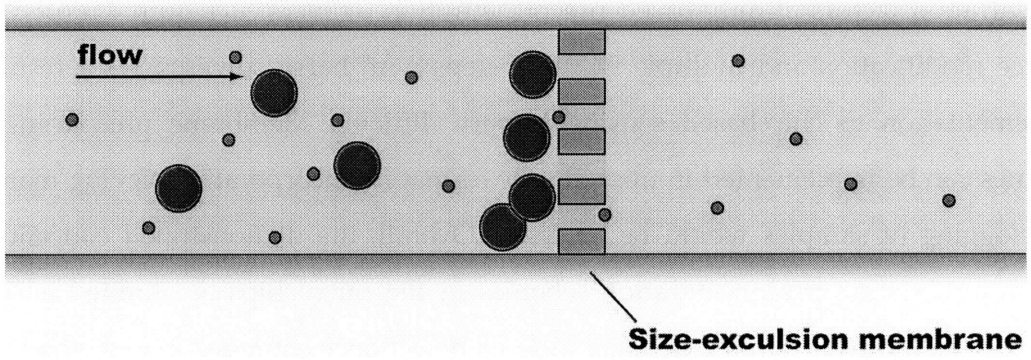

Figure 1-7 Schematic illustration of membrane preconcentration

1.4 Limitation of current techniques

While numerous preconcentration methods have been developed, an efficient and flexible preconcentration method is still missing. When it comes to building lab-on-a-chip bioanalysis systems that are capable of completing automated sequences (extraction, elution, injection, separation and detection), a scheme that is simpler to integrate with other detectors and separation systems would be desirable. In order to accommodate various detectors in microfluidic systems, a new preconcentration technique without the need for embedded electrodes, membranes, or complex buffer arrangement would be ideal.

Many of the above mentioned techniques were originally developed for capillary electrophoresis and are not ideally suited for proteomic sample preparations. While FAS methods are among the simplest and most widely used concentration techniques for small analytes, they still require special reagents and buffer arrangements.

Furthermore, the existence of the extensive low concentration buffer sample plug inevitably makes the use of high voltage power supply. For most electrokinetic trapping and membrane preconcentration systems, an in-line porous membrane is usually required and is cumbersome at times for downstream coupling. Despite the high

concentration factors affinity-based preconcentration delivers, it requires reproducible surface modification and multiple washing steps with harsh solvents. As a result, the implementation to chip-based sensing is very difficult. Membrane preconcentration schemes can be implemented in microfluidic format by incorporating sieving materials, but clogging of samples would be an issue. Overall, the demonstrated concentration factors for existing preconcentration schemes in the microchips are limited and their coupling with down/up-stream separation or detection techniques is very challenging due to operational constraints.

1.5 Scope and Outline of this Thesis

In this thesis, the author has developed a novel electrokinetic preconcentration, using nanofluidic channels. This invention features a charge selective nanochannel array and two micro/nano-fluidic junctions. By taking advantage of the concentration polarization phenomena, one can build a highly efficient yet flexible preconcentration device that can possibly be used to address the most challenging issue we face in developing a chip-based biomolecule analysis system. Also, we have explored the fundamentals and applicability of the above mentioned nanofluidic preconcentrator, with the long term objective of developing a fully integrated separation-preconcentration-detection system.

While the unique properties of nanoscale systems provide great opportunities for proteomic research, challenges such as robust large-scale manufacturing and ill-understood novel physics can hamper the development of this field. A solid physicochemical model of these nanofluidic systems is still absent, therefore, current efforts are focusing on studying the physics behind these nanochannels and nano-microfluidic junctions. In this thesis, the author used nanofluidic device as a model experimental system, and experimentally studied various scientific issues arising from the system, including the existence of nonlinear electrokinetic regime, concentration polarization, and over-limiting current behavior in the device.

With these considerations in mind, the achieved objectives of this thesis are to: (1) Design and fabricate nanofluidic preconcentrators with various microchannel/ nanochannel dimensions to optimize and explore the detailed biomolecule accumulation mechanism, and also to determine the upper size limit at which we can still maintain stable charge depletions; (2) Combine preconcentrator with detection system (ELISA, for example) to demonstrate the applicability of the system. In this work, we will use the optimized preconcentrator coupling with bead-based ELISA to improve the detection limit posed on ELISA systems.

The rest of this thesis describes the study of the ion transfer, charge depletion, concentration polarization phenomena, and the development as well as the implementation of a novel nanofluidic preconcentrator. Basic theoretical background for electrokinetic flow and ion transport in nanochannels is discussed in Chapter 2 and Chapter 3. Following these, the unique and efficient biomolecule electrokinetic trapping or preconcentration initiated by nanofluidic channels is described in Chapter 4. In the end, Chapter 5 illustrates the importance of preconcentration in immuno-biosensing and the integration between the novel preconcentration and bead-based immuno-sensors.

Chapter 2

Ion Transport in Nanofluidic Channels

The main rationales for the earlier μTAS (also called lab-on-a-chip) development include faster sample processing, massive parallelization and automation, and significantly less reagent and sample consumption.[51] In these microfluidic platforms, the handling of fluids and samples can be done easily, allowing the integration between various purification and detection components. Microfluidic systems exhibit unique properties, mainly because scaling down size dimensions significantly changes the relative importance between different driving forces (diffusion, conventions, field-driven forces). On the other hand, when we move from micro to nanometer size scales, the surface charge screening effect starts to dominate and has a big impact over any other driving forces.[15] Recently, many emerging physical phenomena have been reported at the nanoscale. These novel nanoscale properties have opened up the opportunity to learn new science using the platform.[52, 53] Moreover, nanofluidics have also been demonstrated as valuable tools in the field of proteomics, molecular separations and renewable energies.[16, 22, 40]

The surface charge screening layer, also called the surface double layer (DL), can generate fluid motions (electroosmotic flow) by inducing electrokinetic slips on the

surface and drag polar water molecules along membranes, porous structures or microfluidic channels. The application of electroosmosis can be traced back to decades ago, in porous clay diaphragm experiments.[54] However, the effect of the electrical double layer in microchannel (from one to several hundred μm) has negligible impacts on bulk properties because of its limited nanoscale characteristic length. Nanofluidic channels, on the contrary, have a characteristic dimensional in the scale of 10-50 nm. As nanofluidic devices have comparable critical dimensions with electrical double layers at low ionic strength, they have created a franchise of exciting new phenomena. In this chapter, we will cover some general concepts and basics such as surface charge, surface conductance and electrical double layer.

2.1 The Adsorption at the Solid-liquid Interface

In solid-liquid interfaces, the presence of a higher density electrolytes (ions) layer is usually described by terms of electrical double layer or the Debye layer. While electrical double layer (EDL) or double layer is usually referred to the layer defined by Helmholtz model or Gouy-Chapman-Stern model containing both counter- and co-ions, the Debye layer (named after the Dutch physical chemist Peter Debye) is referred to a relatively rough conceptual layer where counter-ions dominate and has yet no definite structure. As a result, these two terms are often cross-referenced to illustrate the idea of the surface charge shielding layer.

When substances brought into contact with aqueous medium, the wetting process of the solid surface starts spontaneously and can be considered irreversible. Given enthalpies of wetting listed below:[55]

$$\Delta_W H = \left(\gamma^{SL} - T\frac{\partial \gamma^{SL}}{\partial T} \right) - \left(\gamma^{SG} - T\frac{\partial \gamma^{SG}}{\partial T} \right) = -q_{imm} \qquad (2.1)$$

The equation sums up the Gibbs energies difference between a solid-liquid (γ^{SL}) and a solid-gas (γ^{SG}) interface, where q_{imm} and q_W stands for immersion and wetting energies.

As a result, the entropy of wetting can be shown with the following format.

$$\Delta_W S = \Delta_{imm} S = \frac{q_{imm}}{T} \tag{2.2}$$

At 25 °C, the entropy of wetting ranges between 40-120 kJ/mol, depending on the types of subtract material.[56] In general, the entropy of wetting is 40 kJ/mol for physical adsorption, 50-70 kJ/mol from hydrogen bonds and from 70-120 kJ/mol or higher for chemisorptions.[55] Silicon oxides, for example, have three times higher wetting entropy than amorphous silicon because of the presence of dehydrated silanol groups. In general, the wetting process can be considered irreversible for most materials.

After the wetting process, due to the mixed effect from dipole interaction and surface functional group disassociation, the surface will spontaneously carry charges (often by unprotonation of surface chemical groups). As a consequence, a compensation charge layer, composed by counter-ions, will form and diffusively distributed. Alternatively, the double layers form spontaneously by adsorption of charged species during the wetting process. The surface double layer structure will be influenced greatly by the electrolyte concentration around the colloid surface. [55]

With a given ion concentration in the solution and charge density on the surface, an exponential decay can be usually seen, as shown in Figure 2-1. However, the detailed structure of the DL varies a lot depending on different assumptions made. For example, Helmholtz model assums electrical neutrality is achieved in a fixed length away from the surface (mathematically simple), while Gouy-Chapman theory allows diffusive, dispersive distribution of counterions. In this thesis, the effective thickness of the DL is

more important than the detailed structure, therefore, the difference between these models will not be discussed.

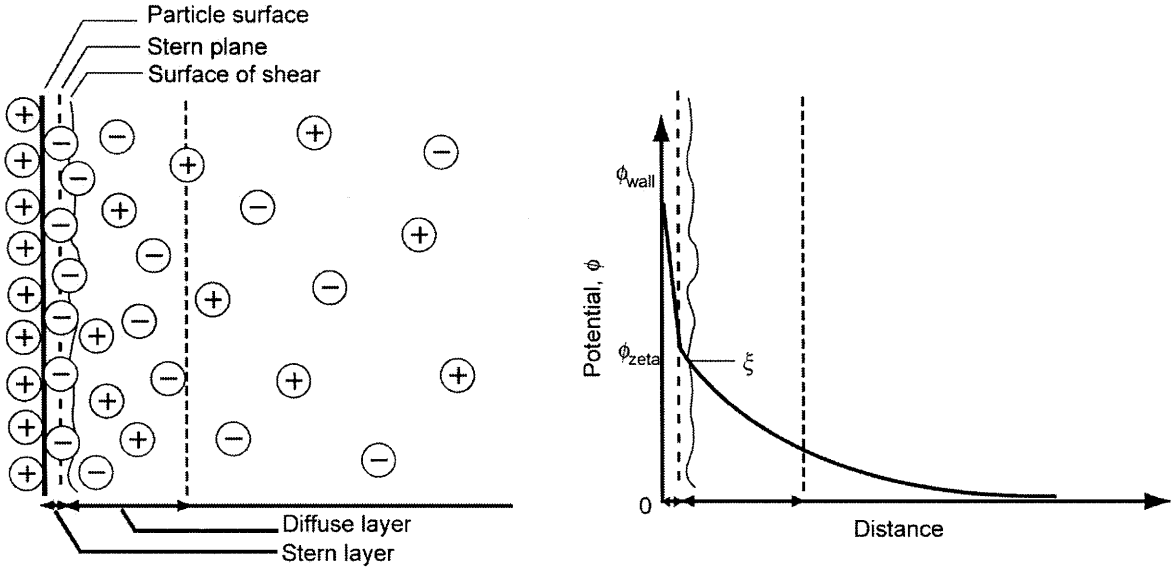

Figure 2-1 Surface charge layer distribution with inner Stern layer

The plot shows the identification of the particle surface charge, the specifically adsorbed charge, and the diffuse charge in a flat double layer. The plot to the right shows the potential distribution of the surface. Adapted from reference [57].

In the case of simple non-porous, non-reactive surface, the thickness of the DL can be considered a direct function of buffer concentration and can be characterized by measure the surface zeta (ζ) potential. The zeta potential is defined as the potential at the shear surface between the charge surface and the buffer and therefore can be measured by probing the electroosmotic velocity on a given surface.

2.2 Large Double Layer Effects in Nanofluidic Channels

As we have discussed, the inherent surface charges generate unique charge transport characteristics in nanofluidic channels. Charged species transport differently in

nanoscale, because the DL thickness becomes comparable to channel height. In these circumstances, the electric field inherent to the DL affects the transverse molecular transport of species with different charges. This phenomena is somewhat similar to the field-flow fractionation (FFF), a well-established method by Giddings *et al.*,[58] where an external field is applied perpendicularly to a pressure-driven flow to separate charged or neutral species apart. The separation technique was referred as ElectroKinetic Separation by Ion Valence (EKSIV) by Pennathur and Santiago, who been using nanoscale channels to separation molecule either by ion valances or ion mobilities.[59] As the field is provided by the naturally presented in the DL from the surface of the nanochannel, this technique is also referred as Autogenous Electrical Field-Flow Fractionation (AEFFF), as named by Griffiths *et al.*[60]

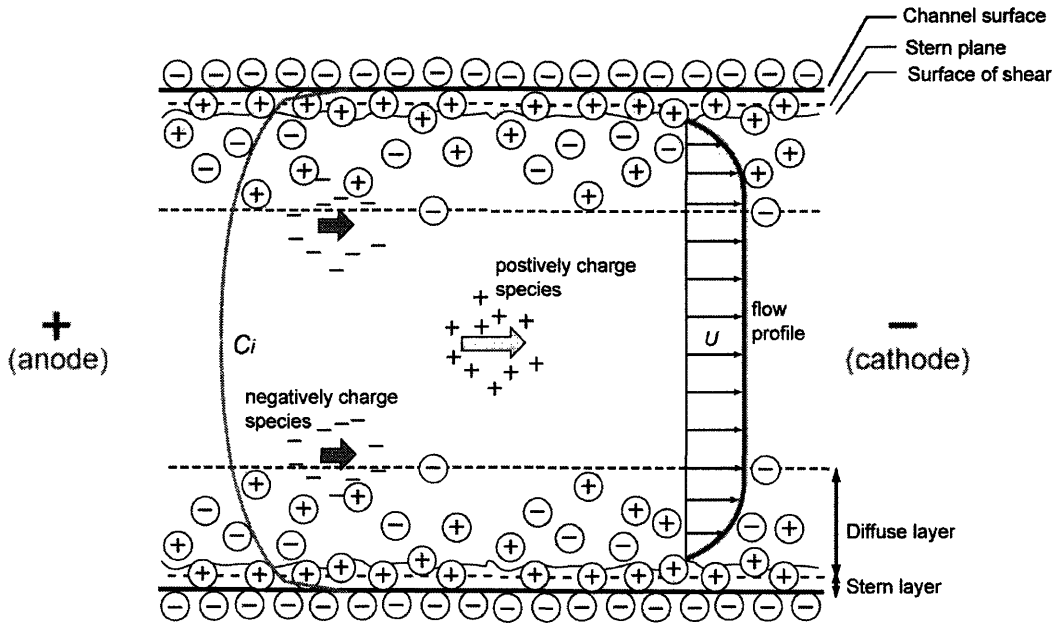

Figure 2-2 Schematic of a nanochannel with significant electrical double layer overlapping Given species concentration, C_i ,and velocity profiles *U*. Species concentrated near the centerline (+) travel faster along the channel than do those near the walls (-), enabling separation. Adapted from reference [60]

The following section will discuss more details about the interaction between the surface, ions, and external field inside the well confined infinite nanochannel.

2.3 Electric Field Distribution within Nanochannels

Considering nanochannels as planar plates with electrolyte filled between the surfaces, the net effect of the surface double layer can be viewed as an electric potential (ϕ) at the boundaries of the liquid-solid junction. When a uniform electric field E_x is applied along the channel axis using electrodes in the reservoirs at a long distance away from the surface of interest, a fluid flow will be induced, originating from the charged DL motion. This flow is called electroosmotic flow (EOF) and can be often seen in microchannels ranging from several μm to a few hundred μm. Depending on the fluid properties (viscosity) and surface electric zeta (ζ) potential, the EOF velocity field profile will varies. A detail discussion about these patterns can be found in earlier publications.[61, 62] The semi-uniform pattern of the EOF will translate into parabolic ones when the channels become thinner.

In order to analyze the field distribution within the nanochannel, Poisson-Nernst-Planck (PNP) equations shall be used to describe charge diffusion in the solution, within and outside of DL near the surface. Given a fixed permittivity ε, the Poisson equation governs the electric potential across the nanochannel

$$\varepsilon \nabla^2 \phi = -\rho_e \tag{2.3}$$

where the net local charge density ρ_e. If a symmetric electrolyte is assumed, this can be written as

$$\rho_e = -2zFc_0 \sinh(\frac{zF\phi}{RT}) \tag{2.4}$$

Here, F is the Faraday constant, z is the valance number, c_0 is the bulk fluid ion concentration, R is the universal gas constant and T is the temperature.

Since most fluid in nanochannels can be considered incompressible and at very low Reynold's number regime, we can simplify the Navier-Stoke equation into

$$\nabla \cdot u = 0 \tag{2.5}$$

and

$$\mu \nabla^2 u = \nabla p - \rho_e E \tag{2.6}$$

In these equations, u represents the local fluid velocity, μ for the viscosity, p for the local pressure, and E for the applied electric field.

While the above equations define the field gradient in the nanofluidic channel, the transport of ions is driven by diffusion, conduction (drift) and convection all together. The flux of charged species is given by the Nernst-Planck equation as

$$j_i = -D_i \nabla c_i + v_i z_i c_i F(E - \nabla \phi) + u c_i \tag{2.7}$$

Given Di is the diffusivity of species, v_i is the mobility. Combing the setting with Nernst-Einstein equation

$$v_i = \frac{D_i}{RT} \tag{2.8}$$

It is also worth a mention that the species mobility used here is an interpretation for ions, solid objects, or small molecules such as peptides and proteins. However, when it comes to DNA or other flexible large molecules, only their mechanical mobility, rather than electrophoretic mobility, is described by the Einstein equation.

With these conditions, one can obtain an integrateable equation for small molecules which leads to a Boltzmann equation for concentration distribution.

$$\frac{d \ln c_i}{dx} = -\frac{z_i F}{RT} \frac{d\phi}{dx} \tag{2.9}$$

After average species concentration across nanochannel with height $2h$, these equations can be derive into i) normalized Debye length, ii) average axial fluid speed iii) average zone velocity of charged species and iv) normalized contribution of pure EOF when in pressure free condition

i) $$\lambda = \frac{\varepsilon RT}{2z^2F^2a^2c_0} \tag{2.10}$$

ii) $$\bar{u} = \frac{1}{h}\int_0^h u dy \tag{2.11}$$

iii) $$\bar{u}_i = \frac{1}{c_i h}\int_0^h (u + v_i z_i F E_x) c_i dy \tag{2.12}$$

iv) $$\bar{u}_{EOF} = \frac{\varepsilon \zeta E_x}{\mu}\int_0^h (h - \frac{\phi}{\zeta}) dy \tag{2.13}$$

with a system like this, the retention ratio $R_i = \bar{u}_i / \bar{u}$ can be obtained that defined the relative speed of charged species to the average speed of the fluid. When the retention ratio $\neq 1$, the nanochannel will have separation power against differently charged species similar to FFF. As a net effect of the overlapped Debye layer and pressure-driven or electroosmotic flow, the retention ratio will become 0 when $z_i\zeta$ gets small enough. In other word, the nanochannel will completely screen out co-ions once $\int_0^h (u + v_i z_i F E_x) c_i dy = 0$. (Note: the effect of zeta potential comes in the Nernst-Einstein relation in the form of ϕ where $c_i \in e^{-\phi}$).

2.4 Nanochannel-Induced Concentration Polarization

In the previous section, the charge selectivity of nanofluidic channels and membranes was calculated in the form of retention ratio. As these unique properties of nanochannel have been used to separate charged molecules.[16, 24, 59] A more complex phenomenon occurs when the charge selective nanochannel is used in the context of a micro-nano-micro junction. In fact, even though the fabrication of (perm-selective) nanofluidic channels has only been realized recently, similar phenomenon has been described before in permselective membranes.[63]

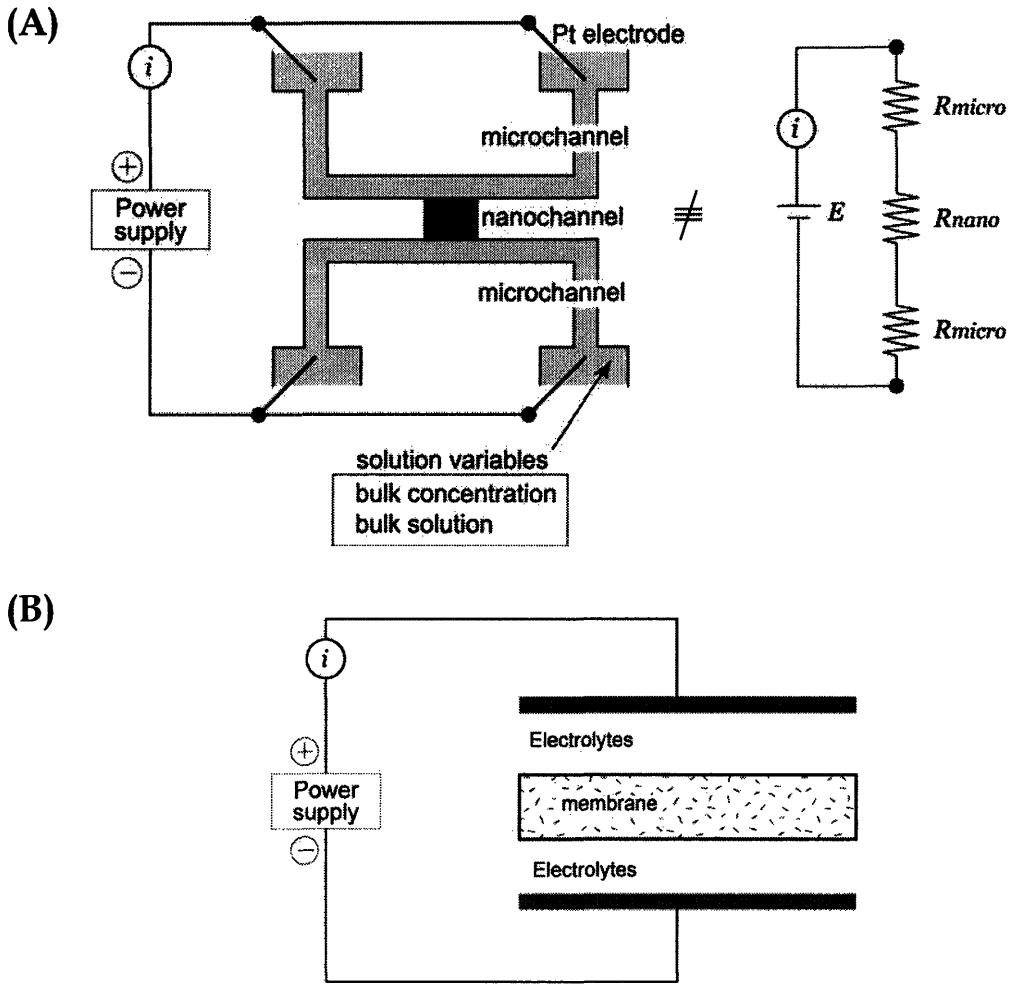

Figure 2-3 Comparison between nanofluidic device and charge selective membrane experimental setup

(A) Current measurement setup and equivalent circuit diagram of a nanofluidic channel connected to the reservoir by microchannels; (B) The same setup membrane scientist used to investigate electrical characteristic of ion-selective nanoporous membranes.

Randomly distributed, ion-selective nanoporous membranes can actually be regarded as a collection of nanochannels; therefore, a similar characteristic can be found between the membrane and nanochannels. These permselective (ion-exchange) membranes have been widely used for chromatographic separations, chemical synthesis, chemical

purification, and battery/fuel cell applications. The electrical characteristic of a micro-nano-micro junction can be quite different from standard resistor models (shown below), due to the "concentration polarization" effect, to be introduced in this session. However, this phenomenon has not been well-understood, due to the lack of experimental control in these nanoporous membranes. Due to the stochastic nature of polymerization reactions to make these membranes, it is not easy to engineer the pore size of these membranes as in the nanochannel systems in this thesis. As a result, the nanofluidic device presented here creates a valuable opportunity for us to have a closer look into these unique ion transport phenomena. Normal, the micro-nano-micro fluidic junction can be considered as a typical ion selective membrane as shown in Figure 2-4

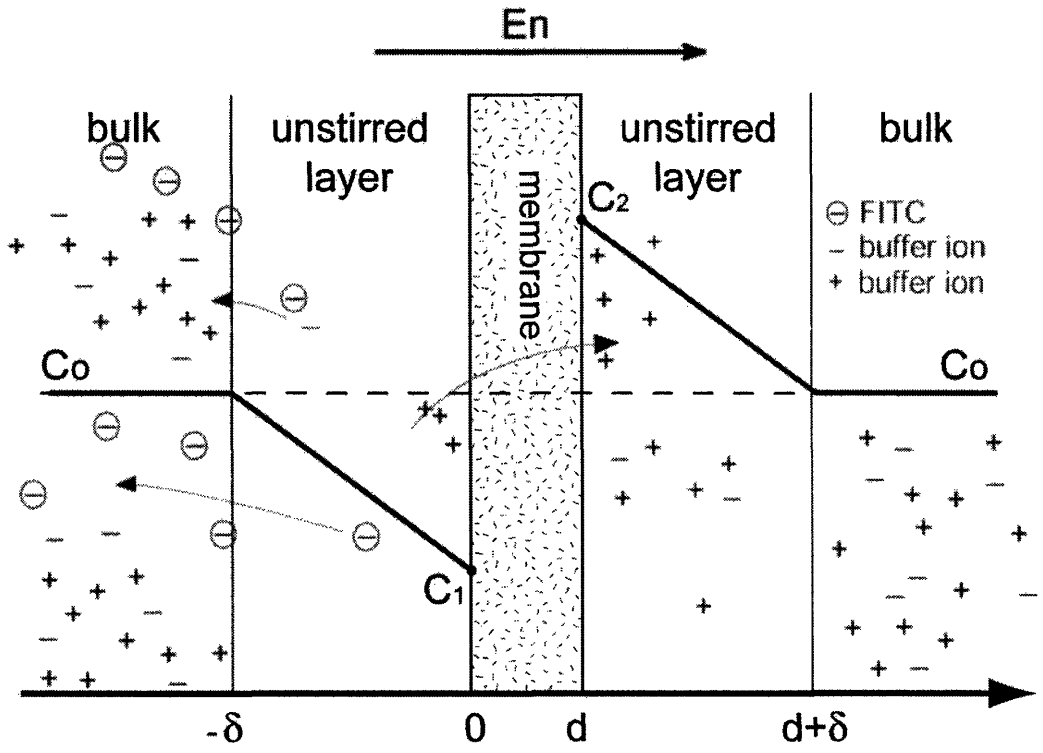

Figure 2-4 Concentration profile across charge selective nanoporous membrane with applied external electric field, based on classic concentration polarization theory

The potential distribution and ion drift/diffusion of the system is governed by Poisson-Nernst-Planck (PNP) equations:

$$\varepsilon\nabla(\vec{E}) = (C_p - C_n)\times F \tag{2.14}$$

$$\frac{\partial C_n}{\partial t} = \nabla\cdot(D_n\nabla C_n - u_n F C_n \nabla\phi) \tag{2.15}$$

$$\frac{\partial C_p}{\partial t} = \nabla\cdot(D_p\nabla C_p + u_p F C_p \nabla\phi) \tag{2.16}$$

From the above PNP equation, we can obtain the current density equation

$$I = \frac{FD(C_0 - C_1)}{\Delta t_i \delta} = \frac{FD(C_2 - C_0)}{\Delta t_i \delta} \tag{2.17}$$

As described by Nernst-Planck equations, when we have a charge selective membrane with preferential counter-ion transport Δt_i, and a fixed unstirred diffusive layer δ. In the previous section, local electroneutrality is not assumed when discussing the effect from the nanochannel DL overlapping. According to the classical theory of concentration polarization[64] where local charge neutrality is assumed to be well-preserved, once a counter-ion is transported through the membrane, its corresponding co-ions will be pushed away to keep a zero net charge condition. Given a constant current supply with sufficient external potential, the system can be pushed to the very extreme where the diffusion flux from bulk solution can no longer provide enough ions to compensate the depletion. When concentration at the membrane boundary (C_1) becomes zero, the current will reach a limiting value known as the limiting current (I_L).

$$I_L = 2Fj_D^{\lim} = \frac{2DC_0}{\Delta t_i \delta} \tag{2.18}$$

where $j_D^{\lim}$ is the highest diffusion flux one can have through the system.

When a system reaches this state, based on the classical theory, a quasi-equilibrium is assumed between the diffusion influx from the bulk into the stationary layer (also called

unstirred layer) and the drift out-flux through the membrane boundary. As a consequence, the concentration profile across the membrane can be illustrated by Figure 2-4. Take an anion selective membrane for example; the concentration of both positive and negative ions will go down at the anodic side of the membrane. On the contrary, ion concentration at the cathodic side of the membrane will go up, responding to the counter-ions transferred downstream by the field. The former is also referred as ion-depletion while the latter is called as ion-enrichment. When a system reaches a limiting current condition, based on the theory, there will be no further increase in the ion current regardless of the driving voltage.

2.5 Over-limiting Current in Nanofluidic Devices

As predicted by the classical theory of concentration polarization, when we perform a voltage sweep across the device using the setup shown in Figure 2-3, we can obtain a well recognized I-V characteristic shown in the PART I of Figure 2-5.

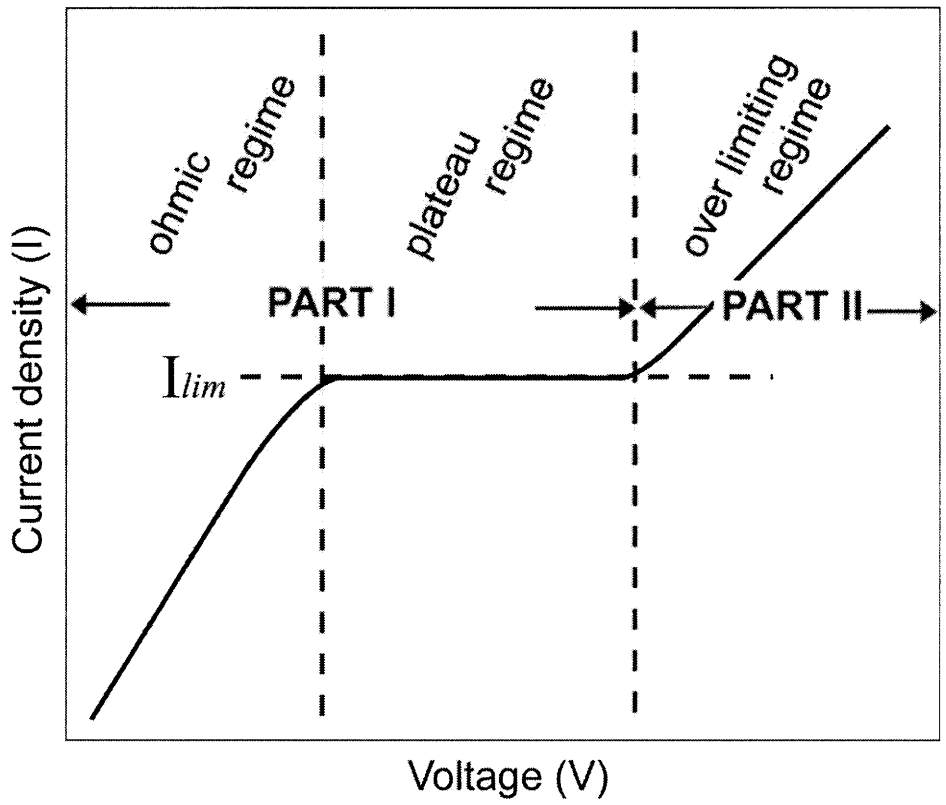

Figure 2-5 Current-voltage characteristic for an electrolytic cell with charge selective membrane

In Figure 2-5, even though the Ohmic and the plateau regimes can be explained readily by the limiting current equation derived above, a new regime (PART II), defined as the over-limiting current regime, is usually found in most experiments with perm-selective membranes. The formation of the subsequent over-limiting current was once considered coming from the electro-reaction or dissociation of the solvent and remained unexplained for many years.[57] One of the theory, as presented by Rubinstein *et al.*,[65]

attributes the over-limiting current to the hydrodynamic instability induced by the charge selective membranes. Such hydrodynamic instability (also called electroconvection) is often observed around charge selective membranes or electrodes. The onset of the flow has direct relation with the lateral non-uniformities of the electric potential at the membrane surface.[66]

These flows (referred as the electroosmotic flow of the second kind by Dukhin *et al.*) can presumably facilitate the mixing between the bulk fluid and the unstirred layer and therefore change the thickness of the diffusive boundary layer.[67] With our device, we can optically monitor the 'unstirred' layer that are not readily accessible in larger-scale membrane experiments, and possibly establish the relation between the dynamic nature of unstirred layer and the over-limiting current.

Since our 40 nm nanofluidic channel is comparable to the thickness of Debye layer, it's not too surprising that the same I-V profile found in ion selective membrane studies (Figure 2-5) can also be observed in our nanofluidic device. As shown in Figure 2-3, we have two microchannels bridged by a 100um long nanofluidic channel with 40 nm depth. At high ionic strength buffer conditions, the Debye layer is quenched, therefore, the system behaves like a standard Ohmic resistor, as shown in Figure 2-6. However, when we use buffers with lower concentrations such as 1~10 mM phosphate or KCl, the nanochannel becomes charge selective and three different current regions (Ohmic region, limiting current region and over-limiting current region as defined earlier) can be seen as we increase the voltage, shown in Figure 2-7. Also, to verify the presented effect is not coming from electrode reactions, a control experiment was done in 1mM buffer without cross the nanochannel. As shown in Figure 2-8, the result from this control experiment shows a perfect linear current-voltage response, as expected from Ohmic resistors.

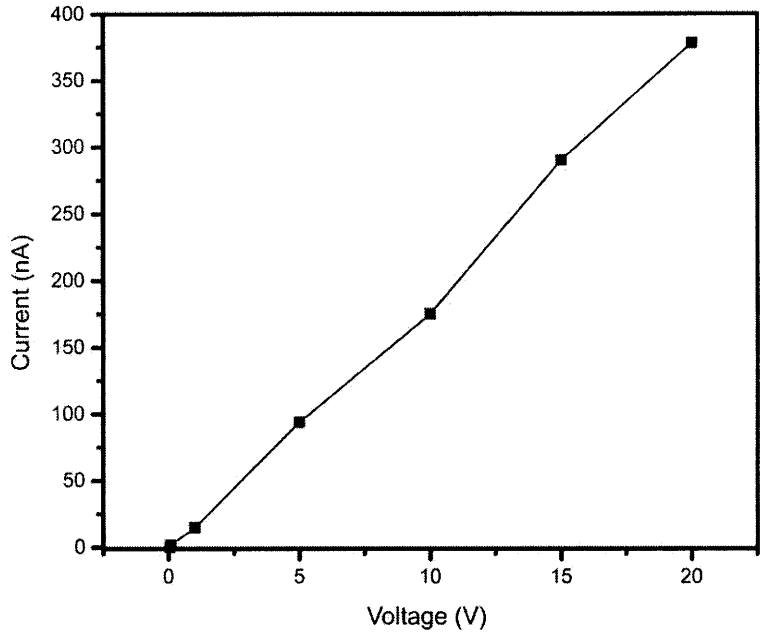

Figure 2-6 Current sweeping experiment across nanochannel filled with 50 mM Phosphate buffer

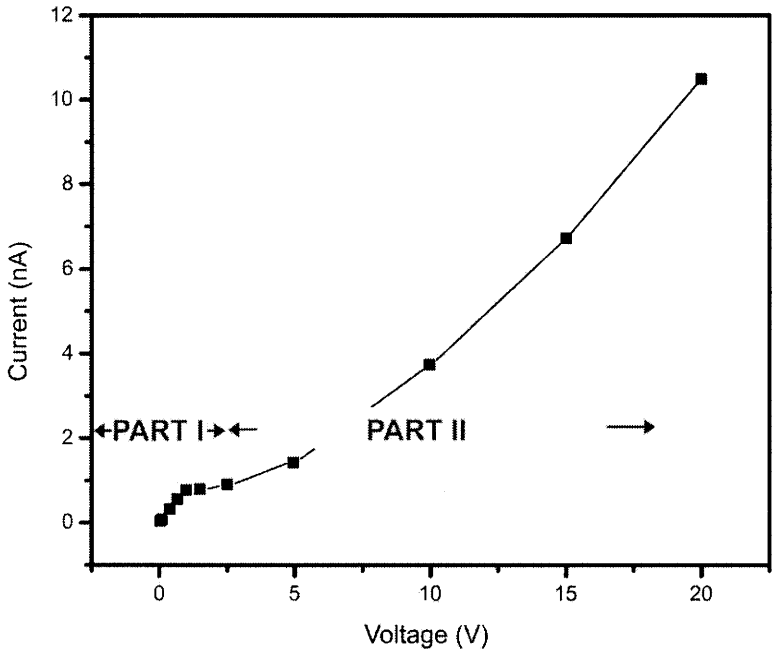

Figure 2-7 Current measurement across a micro-nano-micro junction filled with 1 mM buffer

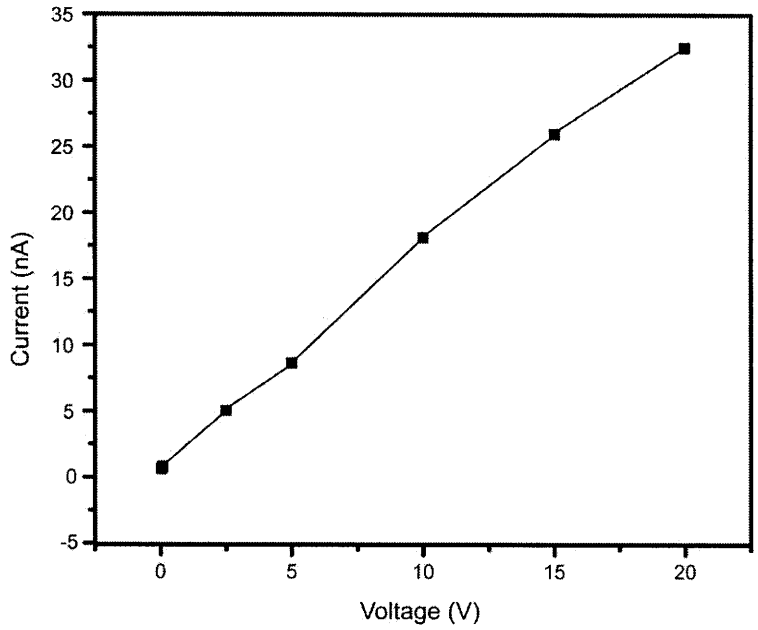

Figure 2-8 Control experiment, I-V sweep across micro channel only

To study the over-limiting current in greater details, we inject fluorescent tracer molecules (negatively-charged FITC dye) into the microchannel in the anodic side. With the combination of fluorescent tracer such as GFP or FITC dyes and fluorescent microscopy, we can study the depletion/concentration polarization mechanism in greater detail in situ. As shown in Figure 2-9, fluorescent molecules were loaded into the top microchannel (anodic side of the micro-nano-micro junction) and the distribution of tracers in the junction region was observed with microscopy and CCD camera.

When loaded with 33nM GFP and 10mM, pH 9 phosphate buffer, assuming the fluorescent molecule (minority ion carrier) is representing the background ion (majority ion carrier) concentration, we can plot the ion depletion along with the current measurement. As shown in Figure 2-9, one can see depletion starts around 5 V (applied voltage) and expands as the voltage increases. In addition, with the formation of the depletion region, one can read a significant conductivity drop in the microchannel.

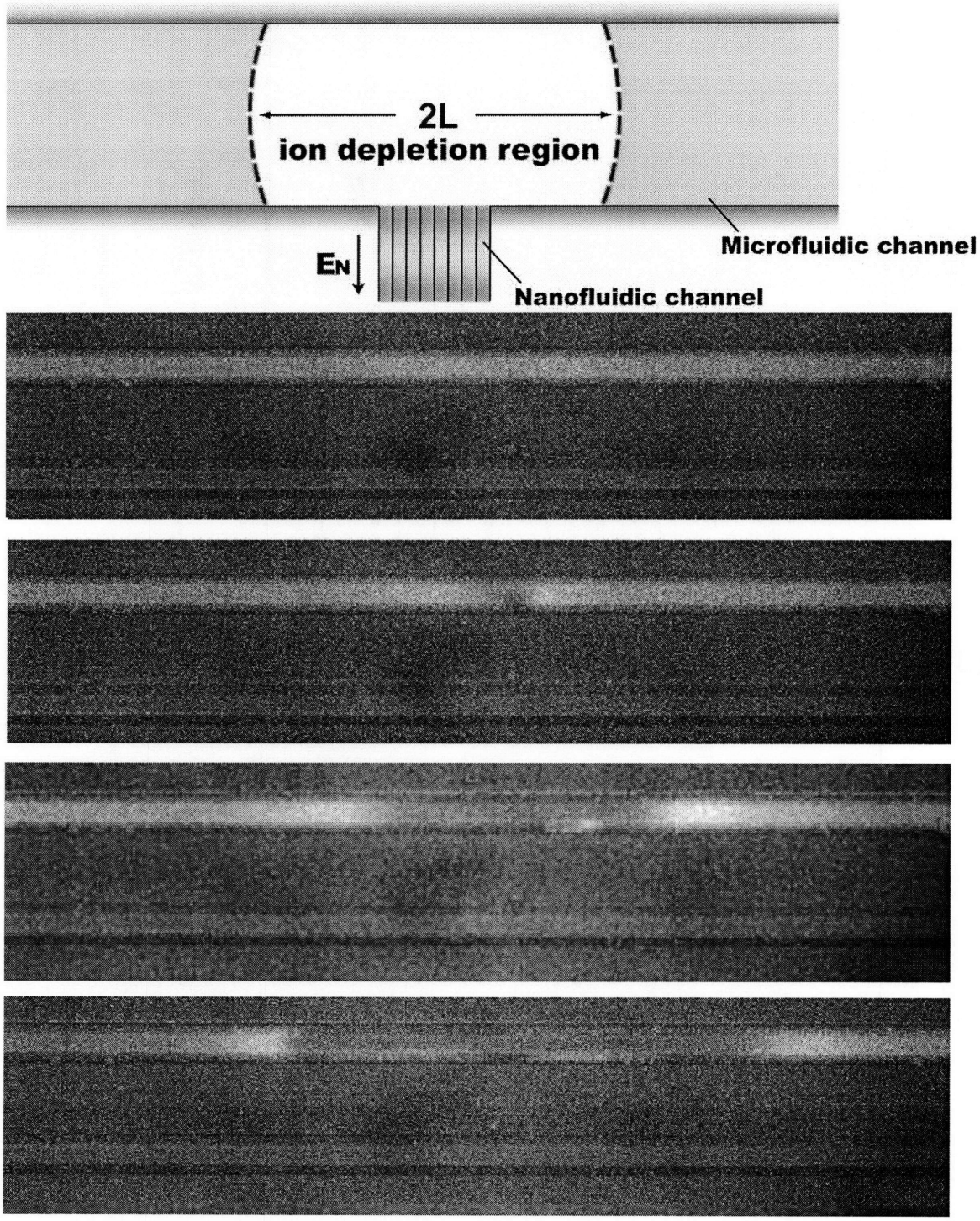

Figure 2-9 Images of microchannels injected with negatively charged tracer

The width ion depletion region increases responding to higher applied voltage (applied V=0, 5, 9, 25 V).

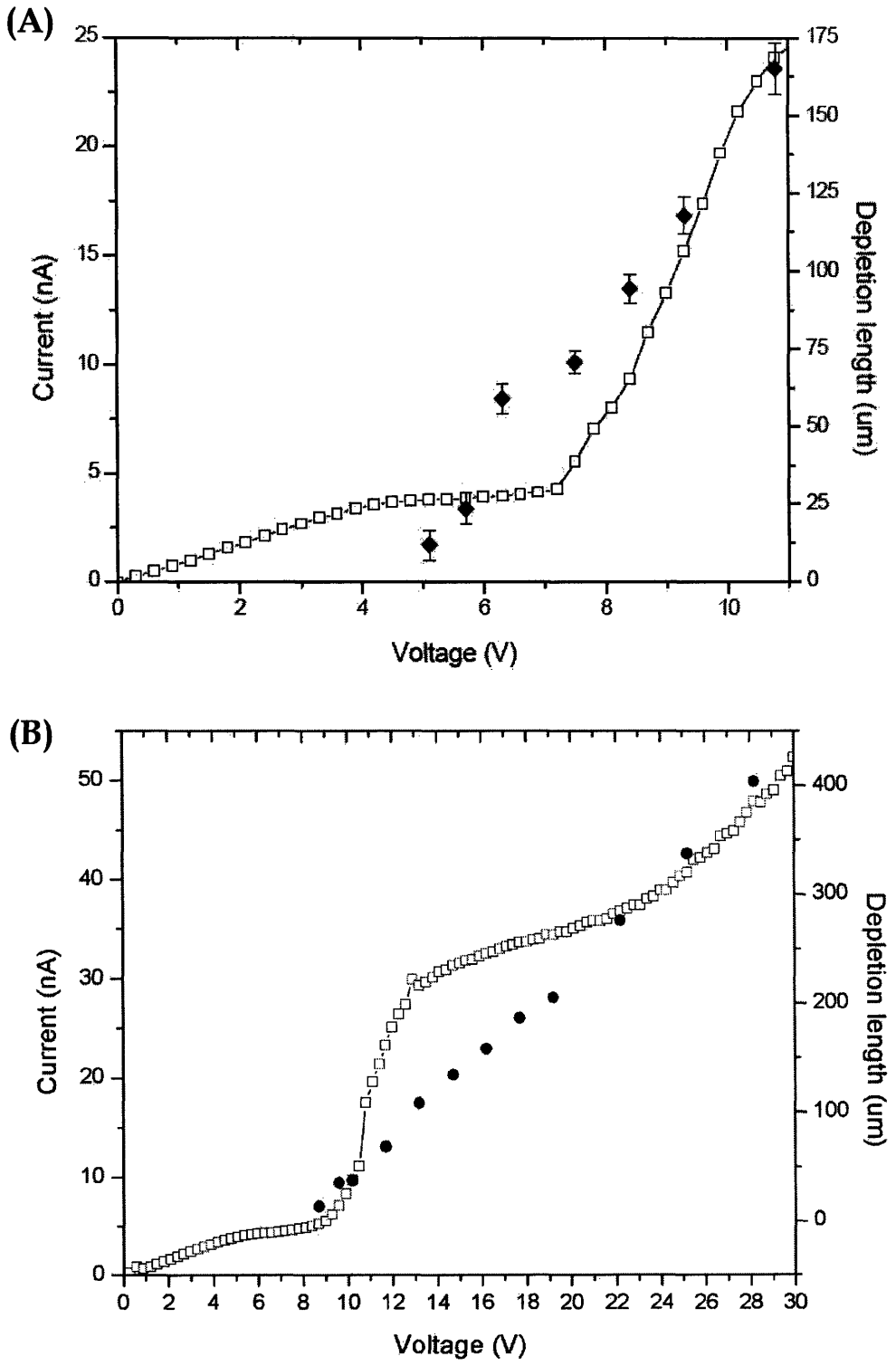

Figure 2-10 Voltage sweeping across 40 nm nanochannel

[A] Plots demonstrate the relation between limiting current and ion depletion [B] the over-limiting current region fluctuation pattern

The voltage sweep in this experiment was done by a programmed voltage source with current-tracking capability (current-source measurement unit 236, Keithley Instruments, Inc., OH). The voltage was ramped from 0 to 30 V in 100 sec. In Figure 2-10 (A), we can observe the depletion starts when current sweeping reach the limiting current and exp and almost linearly as the voltage increases. Besides, a significant conductivity drop can be detected in the microchannel when depletion happens. However, as the depletion region extends across the channel, the conductivity starts to increase again with applied potential. The unstable over-limiting current pattern shown in Figure 2-10 (B) can presumably be explained by the existence of the nonlinear electrokinetic flow as we discussed above. Due to the nonlinear nature of these flows, the exact pattern of these over-limiting current can vary slightly from run to run. Furthermore, the depletion length, L, shown in this experiment indicates only the detectable boundary of fluorescent GFP protein.

With the ability to track molecules, flows, and current measurements all together, the nanofluidic device introduced in this thesis is a valuable platform to study selective ion transfer. More details about the relation between the over-limiting current and a nonlinear electrokinetic flow can be found in the next chapter where we have used nanofluidic devices to perform flow experiments to further explore this phenomenon. There are clear experimental evidences showing that the limiting current and over-limiting current behavior has a strong correlation with the ion depletion and nonlinear electrokinetic mixing. These results can be used to confirm the viewpoints presented by Rubinstein *et al.* as introduced earlier in this Chapter. The nonlinear convection can provide an efficient mixing mechanism for the diffusion layer, which is capable of introducing the over-limiting current.[65, 66]

Chapter 3

Electroosmotic Flow of the Second Kind at the Micro/Nano-Fluidic Junctions

3.1 Electroosmosis of the Second Kind

The primary EOF is the electro-hydrodynamic flow driven by the electrokinetic slip at the surface of charged objects (stationary objects and moving fluid). It is also known as the counterpart of electrophoresis, in which the force was used to transport charged objects (stationary fluid and moving objects). According to the Helmholtz-Smoluchowski equation (Eq 2.13), the velocity of primary EOF is a linear function to the strength of the external electric field and surface (zeta) potential. While the hydraulic fluid resistance increases dramatically with decrease in channel size, the flow velocity of EOF is not a function of channel thickness in most situations. Therefore, EOF became an important fluid delivery technique in the world of micro and nanofluidics.

In addition to this well known linear electroosmotic flow, a new phenomenon, called the electrokinetic phenomena of the second kind was first reported by Dukhin *et al.* in early 90s.[67] The existence of a non-conventional electroosmosis was suggested, from direct

experimental observation of rapid EOF slip around ion-selective surface. These flows usually are much stronger than those predicted by standard EOF, and therefore they were named as the electroosmosis of the second kind to emphasize the difference between the ordinary EOF. The other notable characteristics of this nonlinear electroosmotic flow is that the flow velocity is a nonlinear function (in this case $\sim E_T E_n$) of the electric field. Compared with primary EOF driven by charges in the double layer, we can characterize the secondary electroosmosis as flows driven by the induced space charge layer (SCL). The space charge layer is not the equilibrium space charge layer (characterized by zeta potential), but will be proportional to the applied electric field (which is the source of the nonlinearity). By this definition, we can distinguish primary and secondary EOF as illustrated in Figure 3-1. The details about the SCL will be introduced in the following section. As a consequence, these flows can generate much stronger electroosmotic flow velocity than the normal electroosmotic flow.[68] In previous experiments using charged membrane beads, electroosmosis of the second kind was found to generate strong but uncontrollable flow vortices near the membrane, leading to a rapid mixing.[68-73]

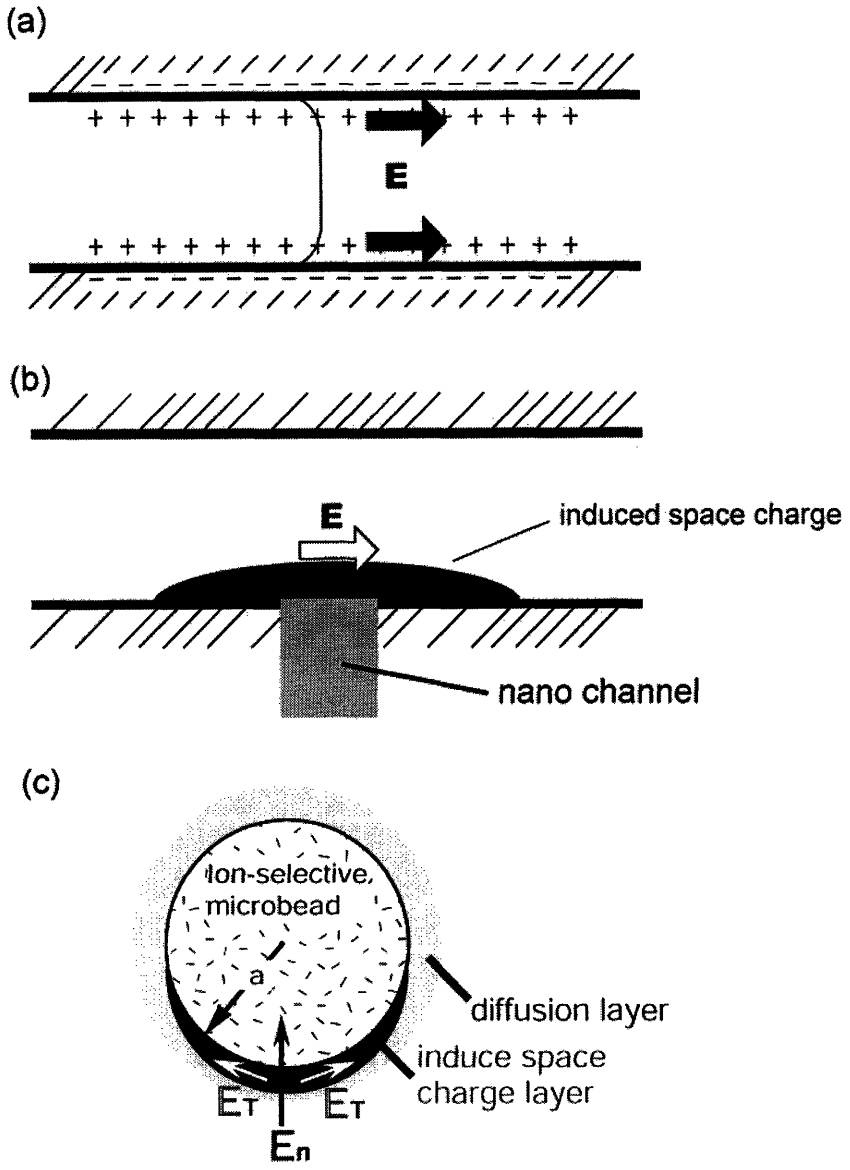

Figure 3-1 Schematic figures demonstrate differences between classical and the second kind of electroosmosis

(a) Classical Electrokinetic flow induced by surface Debye layer. (b)(c) New genre of electrokinetic flow induced by space charge (not to scale).

3.2 Over-limiting Current Induced by Electrokinetic Mixing

Due to the concentration polarization discussed in the previous chapter, the growth of the electric field will drive the current up to a limiting value (I_L), as shown in Figure 2-5.

$$I_L = \frac{2FDC_0}{\Delta t_i \delta} \tag{3.1}$$

In this state, the potential drop $\tilde{\phi}(x) = \frac{F\phi(x)}{RT}$ and charge density $\widetilde{\rho_e}(x) = \frac{\rho_e(x)}{C_0}$ in the concentration polarization zone (feature length L on each side) can be expressed in terms of limiting current density:

$$\phi = \frac{RT}{zF} \ln\left(\frac{C_0}{C(x_\infty)}\right) \tag{3.2}$$

$$\tilde{\phi}(x) = \ln\frac{C(x)}{C_0} = \ln(1 - \frac{i}{i_L}\frac{(L-x)}{L}) \tag{3.3}$$

$$\widetilde{\rho_e}(x) = \frac{\left(\frac{i}{i_L}\right)^2}{\left(1 - \frac{i}{i_L}\frac{L-x}{L}\right)^2}\left(\frac{\kappa^{-1}}{L}\right)^4 \tag{3.4}$$

where κ^{-1} presents the thickness of Debye layer.

These above equations have mathematical exceptions when $i \to i_L$ and $x \to 0$. In this limit, the potential drop and current density approaches infinity, which is clearly not feasible. The main problem with this calculation is in the assumption of local electroneutrality, as pointed out by Levich in his paper.[74, 75]

To address this problem, a new theory for strong concentration polarization was presented by Rubinstein *et al.* taking into consideration the individual ion fluxes coming

into the DL.[65] Instead of assuming the net ion flux being equal to zero (local electroneutrality), one should use $\nabla j^{\pm} = 0$ as the new conservation condition. The new theory defines a secondary double layer, which arises in strong electric field behind the quasi-equilibrium primary double layer and contains an induced space charge.[68]

To begin with, we shall first define the structure of an ion-selective membrane under the influence of an external electric field. Illustrated in Figure 3-2, when a higher electric field is applied, three distinguishable regions can be identified. In the figure, a bulk region (with a fixed ion concentration) is first identified where the fluid is well mixed by the convection and maintains a constant concentration. There is the diffusion layer, which is very similar to the diffusion layer of classical concentration polarization with thickness δ. The third region, the induced space charge layer, is absent at low voltages and has constant low electrolyte concentration C_0 and thickness S_0. This layer is of special interest because the counter-ion concentration is much higher than that of co-ions. It is defined as induced space charge layer because it has excess counter-ions while not connected with the membrane surface. The existence of the space charge layer is believed to be the source of the electro-osmosis of the second kind based on the limited experimental evidence.[68] The DL of the membrane is not defined in the figure.

At the other side of the membrane, the electroneutrality is preserved, corresponding to the electrolyte concentration increase (a.k.a. ion enrichment). As a result, the space charge region is not presented there. Considering that the SCL has conductivity much lower than the bulk electrolyte, most of the potential drop across the system is located in the SCL.[76] As the stronger field further enhances the concentration polarization, the thickness of S_0 further increases and creates a positive loop to solidify the assumption. Therefore, the potential drop across the SCL can be assumed a fix parameter.

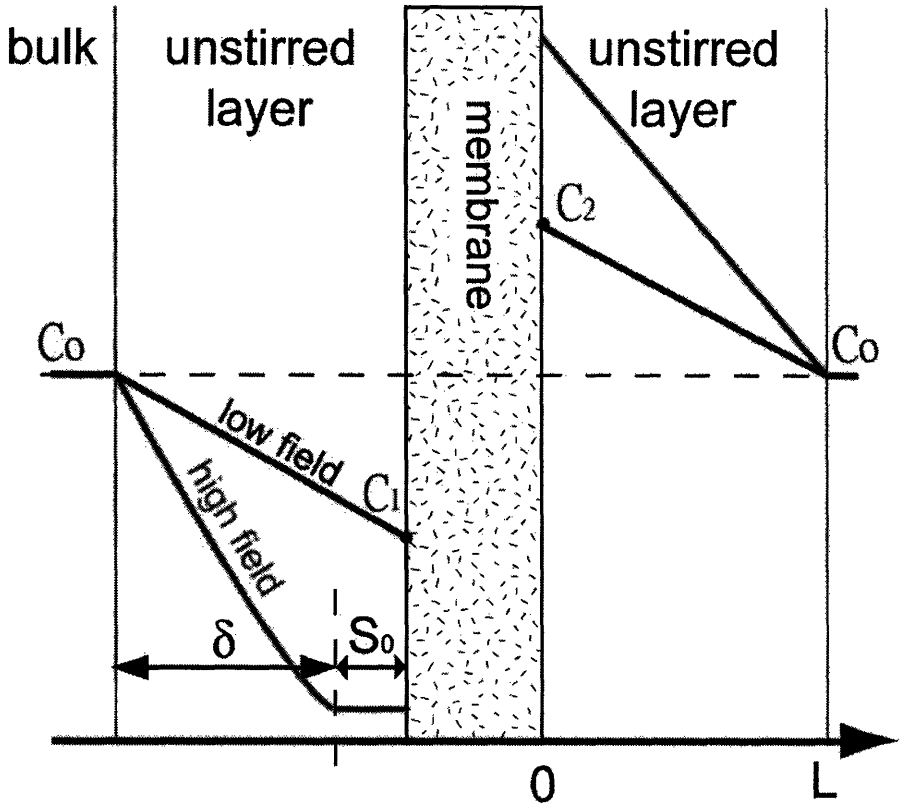

Figure 3-2 Polarization of an ion-selective membrane at different electric field strength (not to scale) adapted from works of Mishchuk *et al.*, the electrical double layer on the membrane surface is not illustrated.[68]

Following the assumption of concentration polarization and limiting current theory, the thickness of the unstirred layer is assumed to be a fixed value and the current density can be rewritten as

$$i = \frac{2FDC_0}{\delta} \tag{3.5}$$

Given an ideal ion-selective membrane ($\Delta t_i = 1$), since $L = \delta + S_0$, at low field condition, Equation (3.6) holds the same value as the limiting current obtain in Equation (3.7). However, when S_0 expends at high filed condition, the current density will reach over-limiting regime ($i > i_L$). However, the emergence of the SCL along can only increases the

current by several tens of percents. Therefore, it cannot fully explain the continues growing of the over-limiting current.[68]

Explained in their experiments, Mishchuk and Dukhin recorded the second kind electroosmosis around the charge-selective particle as shown in Figure 3-3. The circulating flow has three stages of development when field was applied across dispersed particles with sizes ranging from 2-5 μm. In the beginning, a closed whirls start to build up and due to the considerable difference between the primary and secondary electroosmotic velocities. A few minutes after the field is introduced, the flow developed to its maximum strength while the whirls can be as big as three-quarter the size of the particle. In the end, as the non-stationarity of polarization and hydrodynamic resistance balanced with the sedimentation of these small particles, the whirl flow velocity and size was damped to a smaller number. However, it is still considerably higher than the velocity calculated from primary EOF according to the Smoluchowski theory.

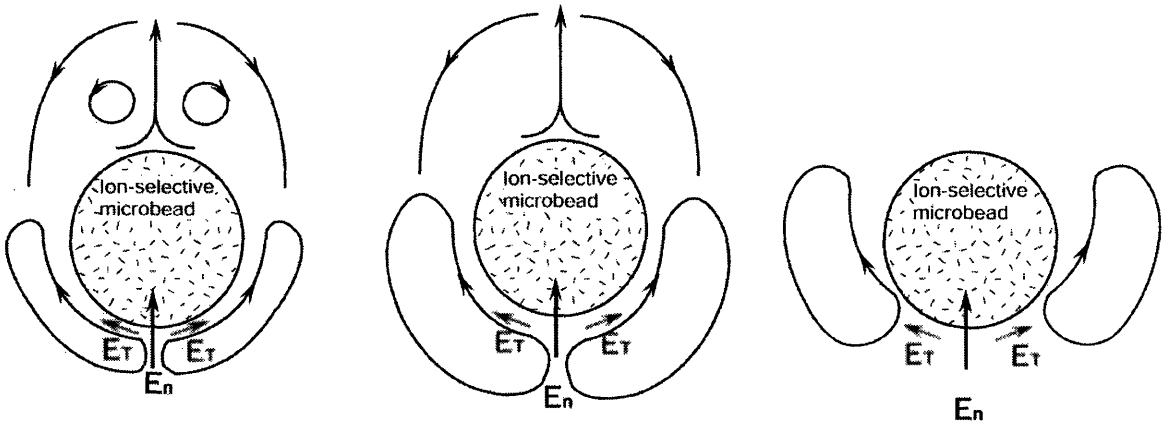

Figure 3-3 Nonlinear electrokinetic slip around porous silica beads
Figures show the there-stages development of electroosmotic slips near a cation-exchange particle. Adapted from Ref.[77]

To fully understand the over-limiting current, one has to take into consideration the changes in conductivity, electric field, fluid flow and pressure gradient under the

influence of extensive concentration polarization. It is extremely difficult if not impossible to obtain a comprehensive analytical of even numerical solution without simplification.

To simplify the problem, as discussed above, it is first assumed that the potential drop across the SCL is a fixed number due to the considerable lower conductivity in this region. While zeta potential (ζ) defines the electric potential that exists at the slip plane and governs the electrokinetic potential of the primary EOF, similar concept can be introduced with an effective electrokinetic potential, ζ_{eff}. This effective zeta potential then was estimated to have the same order of magnitude with the maximum potential drop in the induced space charge region. In this circumstance, effective electrokinetic potential has direct relationship with the maximum potential drop as $\zeta_{eff} \sim E$. To make a direct comparison with primary EOF (from Smoluchowski equation), the secondary EOF velocity can be expressed by $\upsilon'' \sim \zeta_{eff} E$. Therefore, as an indication to the scale, the velocity of electroosmosis of the second kind can be related to E field as:[65]

$$\upsilon'' \propto E^2 \tag{3.8}$$

We also observed similar, vortex like flow near the depletion region. The experiment was performed using the above mentioned devices (Figure2-3) with two different microchannel depths, 1.5 μm and 12 μm. To measure the nonlinear flow velocity, fluorescence particles were added in the main buffer solution, 1 mM phosphate (dibasic sodium phosphate) at pH = 8.7. The beads can either be 40 nm (Duke Scientific Corp.) or 500 nm (Invitrogen) carboxyl-terminated polystyrene beads, depending on the geometrical properties of the chip. The fluid development in this nanofluidic device, as shown in Figure 3-4, has a similar pattern compared with ones reported in charge selective porous silica studies (Figure 3-3). Initially, several small vortices were initiated and eventually merged into large vortices. The electric field versus flow velocity relationship observed in the flow experiment is plotted in Figure 3-5.

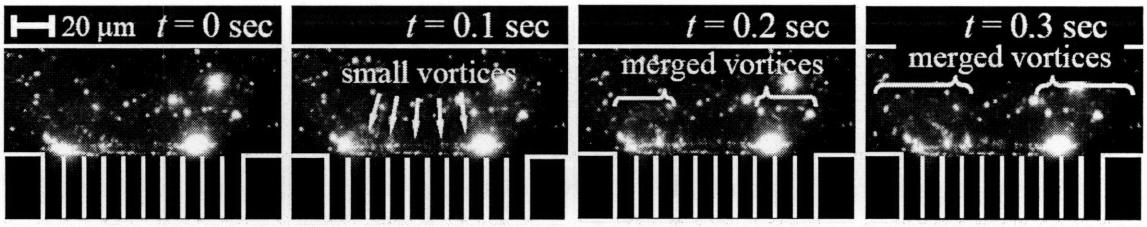

Figure 3-4 Time-dependent change of ion-depletion generation in the nanofluidic device
Strong vortices were generated to mix fluids inside the depletion region and caused a backflow outside of the depletion region. [76]

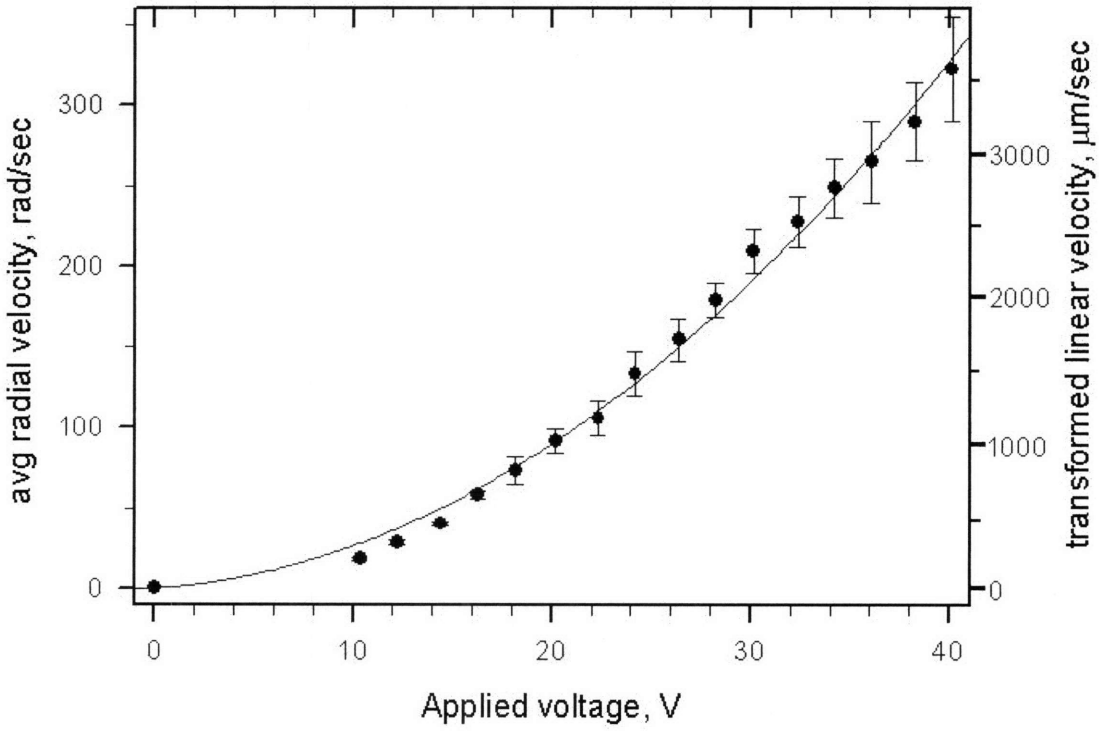

Figure 3-5 Electrokinetic slip of the second kind in nanofluidic devices.
Flow velocity versus applied field strength. (From Kim, *et al.* to be published.)

This experimental data (collaboration with Dr. Sung Jae Kim) shows non-linear flow velocity – voltage relationship, as predicted by Equation 4.8.[76] Since the nonlinear

electrokinetic flow is much faster than primary EOF, it is possible that this device can potentially lead to novel electrokinetic pumping mechanism.

As we have seen from Chapter 3, the continuous current growth above its "limiting" value can be explained by the variance in the diffusion layer thickness. Affected by both the growth of the space charge layer and the nonlinear electrokinetic mixing, the diffusion layer thickness decreases along with the scale of the electric field. Both factors contribute positively to each other and further intensify the current growth through the ion-selective membrane.

As the thickness of the diffusion layer is the inverse function of the Peclet number, the thickness of diffusion layer can be written as the following equation at high Peclet number condition:[77, 78]

$$\delta = \sqrt{\frac{xD}{\upsilon''}} \tag{3.9}$$

where x is the characteristic length of the system.
While the flow velocity (υ'') is proportional to the square of the electric field strength, we can have the relationship between δ and E as:

$$\delta \propto \frac{1}{E} \tag{3.10}$$

Plug this into the current density function Equation (4.4), we can see the current density above limiting current will again become a linear function of the applied field as

$$i' = \frac{2FDC_0}{\delta} \propto E \tag{3.11}$$

The result complies with the experimental observation we have in Figure 2-10. However, the over-limiting current is not perfectly linear due to the instability of these flows. Even though the pattern shows a certain degree of linearity, the exact shape of them varies from run to run depends on the flow and ion depletion zone development.

3.3 Nonlinear Electrokinetic in Nanofluidic Devices

In this thesis work, nanochannel systems were fabricated with microfabrication techniques, including standard photolithography and reactive ion etching, to produce nanofluidic channels as small as 40 nm. Because of the fidelity that contact/projection lithography processes deliver, we can engineer nanochannels with varies geometry in silicon. Unlike most previous membrane studies, the pore size (refers to nanochannel thickness in our system) is not randomly distributed and will not change during the experiment. As a result, the presented nanofluidic system is a better candidate for us to study these nonlinear electrokinetic phenomena. Furthermore, the planar layout of microfluidic structure enables direct observation of the micro-nano junction by high magnification microscopy.

By manipulating the electric field, the device can generate an extended space charge region, lasting for several hours, within a microchannel as a mean to collect and trap biomolecules and when applied a higher potential, the presented device can be used to study the chaotic flow adjacent to nanochannels described in the previous section.

As the conclusion from Mishchuk's paper suggested, the size of the whirl strongly depend on the particle size (a) because the filed ($\phi \approx 2aE$) is associated with it.[68] In our system the characteristic length is the microchannel thickness. As shown in the experimental result, the development and vortex flow radius does convey to the same three steps converging and the final size of the flow can also be directly related to the device characteristic length.

A direct relation between the over-limiting current and the nonlinear flow mixing can be observed in our nanofluidic flow experiments. By comparing the initiation voltage of the over-limiting current and the flow in Figure 2-10A and Figure 3-4, it can be clearly identified that the over-limiting current starts roughly the moment the convective flow

has been observed (around 10V). The result can further confirm the over-limiting behavior of charge selective membrane is indeed associated with the convective mixing that develops spontaneously in the depleted diffusion layer at the advanced stage of concentration polarization. Other group has also tried to confirm this scenario by an opposite approach. Conducted by Maletzki *et al.*, an experiment using C-membranes (known to be cation selective) was design to confirm the relationship between the over-limiting current and the nonlinear electrokinetic mixing. In this experiment, the surface of the cation exchange membrane was coated by agarose gel to eliminate possible electroconvection. As a result, the over-limiting current originally observed in the system can be successfully suppressed[66, 79] Considering the agarose gel experiment conducted by Maletzki provides an indirect evidence that the over-limiting current can be suppressed by eliminating the electroconvection, our experimental observation presented in this thesis actually support the idea directly that fluid instability near perm-selective membrane or nanochannel plays an important role in the over-limiting current behavior. With the nanofluidic device we presented, we can study not only these novel nanofluidic phenomena, but also its implications for biosample preconcentration, desalting and potentially novel electrokinetic pumping devices.

Chapter 4

Electrokinetic Trapping Phenomena at the Micro-Nano-Micro Fluidic Junction

Introduced in Chapter 1, proteomic studies require purification and separation steps to reduce the shear sample complexity. These purification processes are critical to most pharmaceutical and biotechnological research. In many circumstances, sample preparations can even be considered the most time consuming and major part of the process. However, after these preparations, the identification of biomarkers becomes extremely difficult, due to inherent sample loss. The problem becomes exacerbated by the fact that markers of developing diseases are presented only in trace amounts. To address this problem, an efficient sample concentrator that can condense samples into smaller volumes is critically needed. Because most existing microchip preconcentration schemes require either introducing complex reagents or dedicated physical constraints, the coupling with other integrated micro systems is difficult.

Presented in this chapter is the author's effort to apply the knowledge we learned from sub-60 nm nanochannels and the associated concentration polarization toward protein sample preconcentration. This work was first published in 2005 as the first robust and highly efficient protein preconcentration device, which implemented charge depletion phenomena, occurring at the micro-nano-micro interface.[40, 80] The nanofluidic

preconcentrator we built has various advantages over most current preconcentration techniques that will be discussed in the following section.

Based on electrokinetic trapping mechanism, the device is fabricated using the standard microfabrication techniques, not requiring any special reagents or membrane materials. Instead of charge-selective nanoporous membranes, regular, flat nanofluidic channels filled with buffer solution are used as the ion-selective membrane to generate an ion-depletion region for electrokinetic trapping. The concentration polarization phenomenon, which is often undesirable to membrane engineering, was utilized in our device to provide biomolecule trapping forces. The charge selectivity in the device can be controlled by adjusting both channel thickness and buffer concentration. Without any physical barriers or reagents, preconcentration experiments of proteins and peptides show that the preconcentration operation can last over several hours for up to million-folds in concentration, which allows for extremely high preconcentration factors.

4.1 The Dynamic Charge Depletion Pattern in Nanofluidic Devices

Recent studies in nanofluidics with critical dimension smaller than 100 nm have found a puzzling conductivity drop when voltages are applied to the system. As a quote from Dr. Brian Kirby of Cornell University:[15] "It's pretty common to turn on one of these [devices] and watch the current go to zero just because everything works for a while and then it stops!" Such behavior makes the device unable to perform its desired functionalities because one cannot sustain a consistent current flow through the device.[23] This is often caused by concentration polarization, which was introduced in the previous chapter. Unlike microfluidic devices, nanofluidic systems have fundamentally different transport phenomena, which originated from the unique size dimensions. As shown in Figure 4-1, for example, at a low enough buffer concentration, the Debye layer overlap will dramatically change the ion transport property of sub 100nm nanofluidic channels. Several experimental results were explained by concentration polarization and ion depletion phenomena, including fast protein concentration, ultra fast mixing, ion-depletions, ion-enrichments and so on.[23, 39, 81] Theoretical study of ion transport around nanofluidic channels has been quite challenging however, due to multi-scale and coupled (fluid-diffusion-field) nature of the problem. Therefore, our current understanding of the charge depletion phenomena is still limited. While the theoretical model relating charge depletion phenomena and ion-selective membranes has been suggested, it is still not widely recognized or accepted [70, 82], probably due to the lack of controlled experimental proof. Responding to this situation, one major goal of this thesis study is to arrive at a more comprehensive understanding about the relation between the Debye layer overlapping and the ion depletion phenomena.

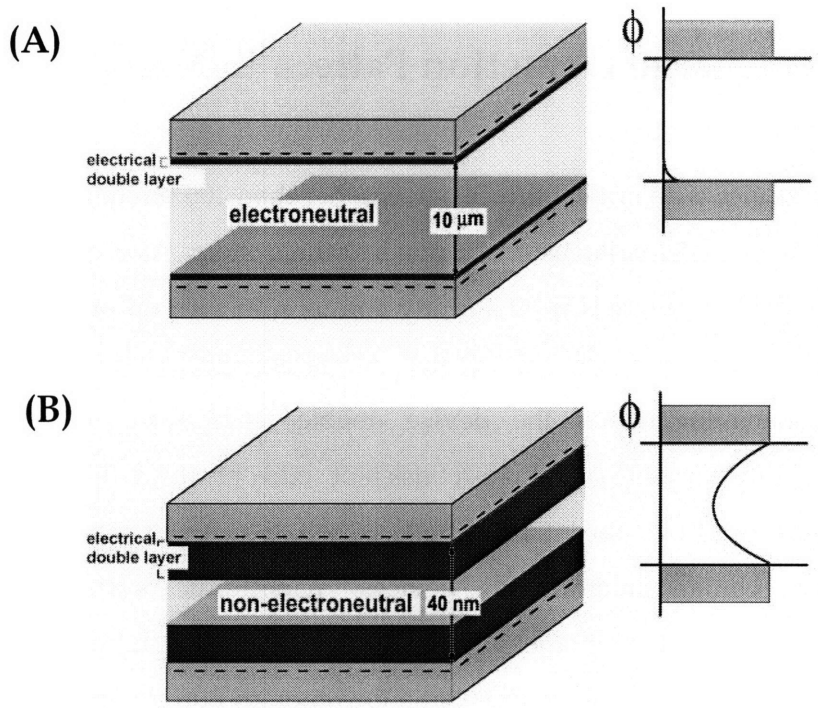

(C)

Characteristic Debye layer thickness

buffer (M) concentration	1	10^{-1}	10^{-2}	10^{-3}	10^{-4}
Debye layer (nm)	0.3	0.96	3.04	9.62	30.4

Allen, Bard "*Electrochemical Methods*"

Figure 4-1 The scale of the surface double layer in micro and nanofluidic channels
[A] Shown in the potential scheme, the core of a 10μm microchannel is electro-neutral.
[B] the scale of surface double layer in a 40nm nanofluidic channel. As the channel dimension becomes comparable to the thickness of the electrical double layer, the core of the nanochannel no longer maintains its electroneutrality. [C] Chart adapted from previous electrochemistry studies indicates the relationship between buffer concentration and Debye layer thickness.

It has been previously reported that nanofluidic channels (~50 nm in thickness) can support selective ion current transports similar to the way ion-exchange membranes behave.[83] When an electric field is applied across nanofluidic channels with charge

selectivity, more counter-ions (from the Debye layer) than co-ions will migrate across the nanofluidic channels. This results in a net transfer of charges (counter-ions) from the anodic side to the cathodic side, and the overall ion concentration will be decreased on the cathodic side due to the concentration polarization effect.[57, 84] Concentration polarization is a direct response to the difficult permselective transport of ions in the nanochannel.

It is important to note that such concentration polarization and ion depletion phenomena can occur at moderate buffer ionic strength (1~10 mM), even when the calculated λ_D is an order of magnitude smaller than the nanochannel depth. In fact, a significant Debye layer overlap can be 'initiated' from a slight overlap by a dynamic depletion process. Once the concentration polarization is initiated, the depletion zone on the anodic side shows similar behavior (expanding depletion zone over time), regardless of the initial buffer ionic strength. However, the time required to initiate similar level of concentration polarization depends on the ionic strength. Figure 4-2 is a recent experiment conducted by Dr. Kim in the device presented in this thesis. The plot shows the time required for the initial depletion boundary to reach the opposite wall of the main microchannel, against buffer concentration and applied voltages. As shown in the equilibrium Debye layer thickness chart in Figure 4-1, in order to significantly overlap the electrical double layer inside the nanochannel (40 nm deep), buffer concentration as low as ~1mM would be required. However, the graph clearly showed that the ion depletion was obtained at even higher than 10mM buffer concentration, which corresponds to only ~3nm double layer thickness. At higher buffer ionic strength, however, it takes longer to reach concentration polarization. This clearly demonstrates that the concentration polarization (ion depletion) is a dynamic process, and the equilibrium Debye length, λ_D, alone cannot adequately describe the phenomena properly. Even when the Debye layer is not thick enough to cover the entire nanochannel depth, ion current through such channel could induce small amount of additional counterions transported. Once a weak concentration polarization can be

induced, it will decrease ion concentration on the anodic side of the nanochannel and further increase the degree of Debye layer overlapping.

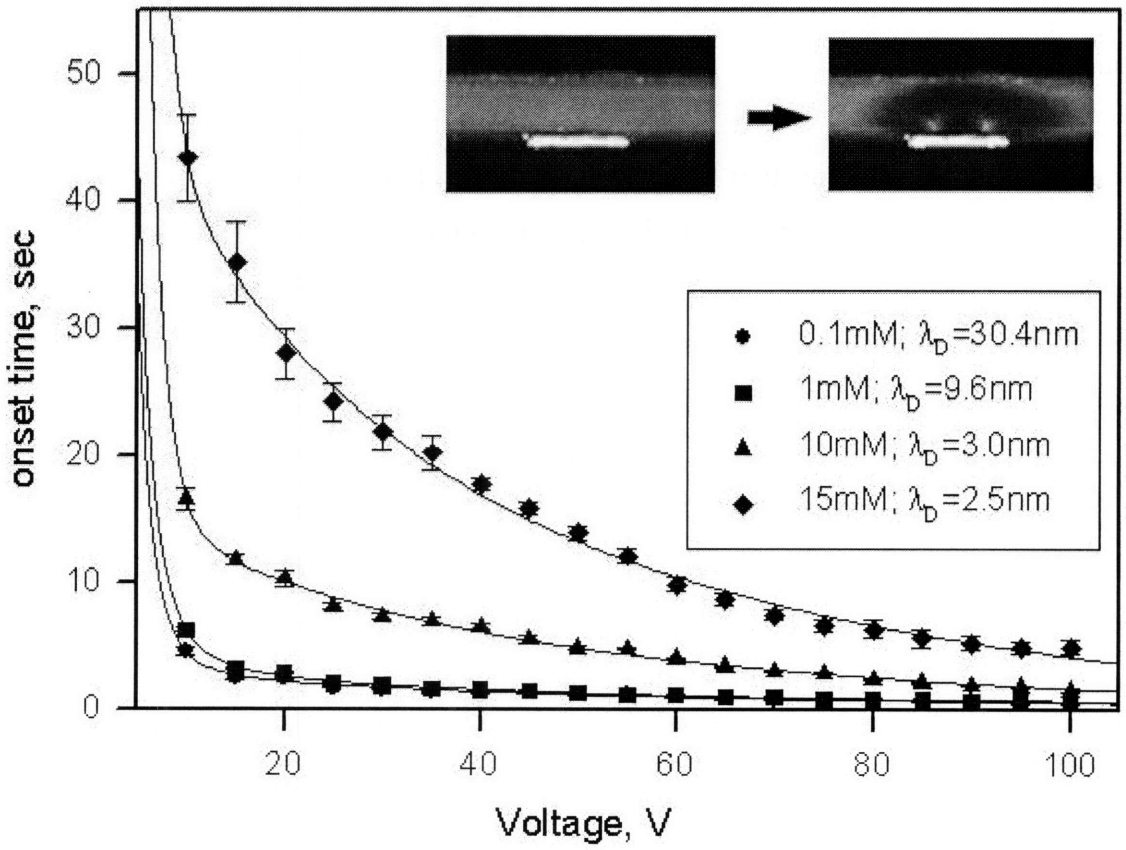

Figure 4-2 Onset time required for the depletion boundary to reach opposite microchannel wall
The figure illustrate the time as functions of applied voltage at anodic side (depletion voltage condition) and buffer concentrations. (From Kim et al. to be published.)

As a result, the perm-selectivity of nanochannel can be enhanced (via larger local Debye length) and eventually leads to even faster concentration polarization. Demonstrated in this experiment, the concentration polarization process in nanochannel is indeed a positive feedback process, with ever decreasing local ion concentration (anodic side) and increasing permselectivity (thicker local Debye layer thickness).

4.2 Fabrication and Experimental Setup

To study the selective ion transfer and its implication, we used a three-photomask microfabrication process to build the micro-nano-micro fluidic junction and a fluorescence detection method to observe the migration and concentration distribution of fluorescently-labeled biomolecules. The two microfluidic channels shown in Figure 4-3 are bridged by a nanofluidic array with a depth of 40 nm. The width of the array goes from 10 μm to 200 μm depends on the size of the microfluidic channel. Depending on different design requirements, the cross-section of the microchannel varies from 1 μm by 10 μm to 50 μm by 75 μm.

Figure 4-4 shows the schematics of the device fabrication process. Using the combination of photolithography and reactive-ion etching (RIE) techniques, both nanochannel array and microchannels can be etched into a 6-inch silicon wafer with desired thickness. As for the photolithography tools, both contact lithography (EV620, Electronic Visions Group, AZ) and projection lithography (Nikon NSR2005i9, Nikon Precision Inc., CA) were used depending on the target pitch size. Since chlorine (Cl_2) and hydrogen bromide (HBr) etching chemistry can be well-controlled for a sub-3 nm/sec etch rate of the silicon substrate during, the RIE step (AME P5000, Applied Materials Inc., CA) can be used to determine the depth of both nanochannels and microchannels precisely.

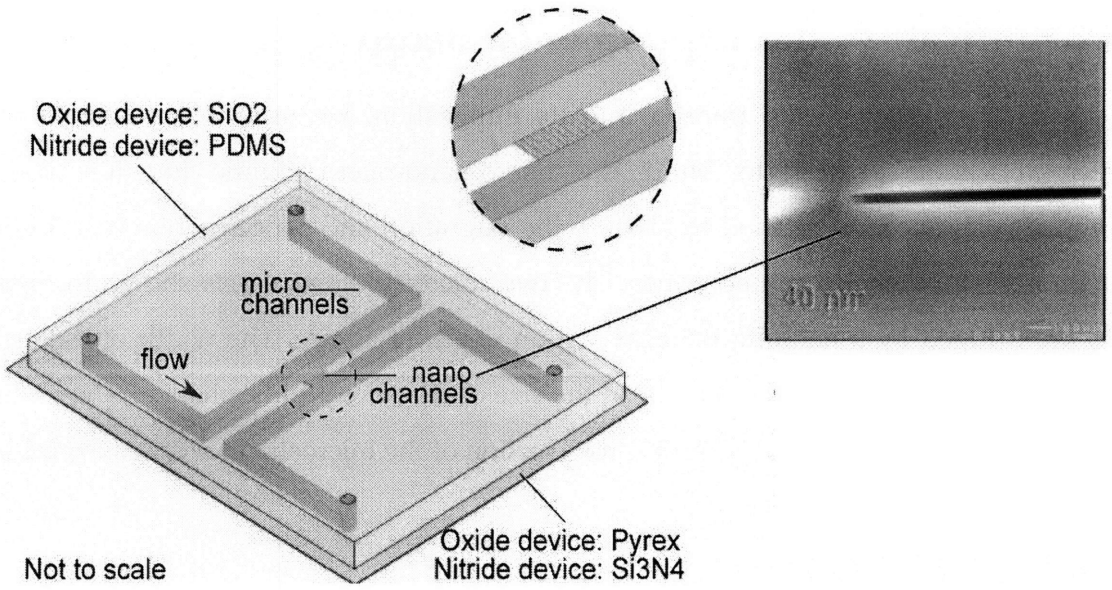

Figure 4-3 Schematic drawing of the biomolecule preconcentration device

After nanochannel and microchannel patterning, the wafers were first deposited a low-stress silicon nitride (Si_3N_4) layer on both sides of the Si wafer using the low-pressure chemical vapor deposition method (LPCVD) to a thickness of 400 nm. Following the deposition, through holes are patterned with another photolithography and RIE etching steps before performing the potassium hydroxide (KOH) etching to etch through the whole <1 0 0> Si wafer to create buffer access holes. Once all features and access hole are formed, a thick thermal oxide layer (500 nm) was then grown on the silicon wafer using LPCVD furnaces to provide an electrical isolation between the conductive Si substrate and buffer solution. In the end, the channels were sealed between the silicon wafer and a Pyrex wafer in an anodic bonding machine. The bonded wafers were then cut by diesaw into individual devices for experiments. The depth and surface uniformity of the nanofluidic array was further checked by either scanning with a surface profilometer (Prometrix P-10, KLA-Tenco Co., CA) or cross-section imaging with a scanning electron microscopy before and after the bonding.

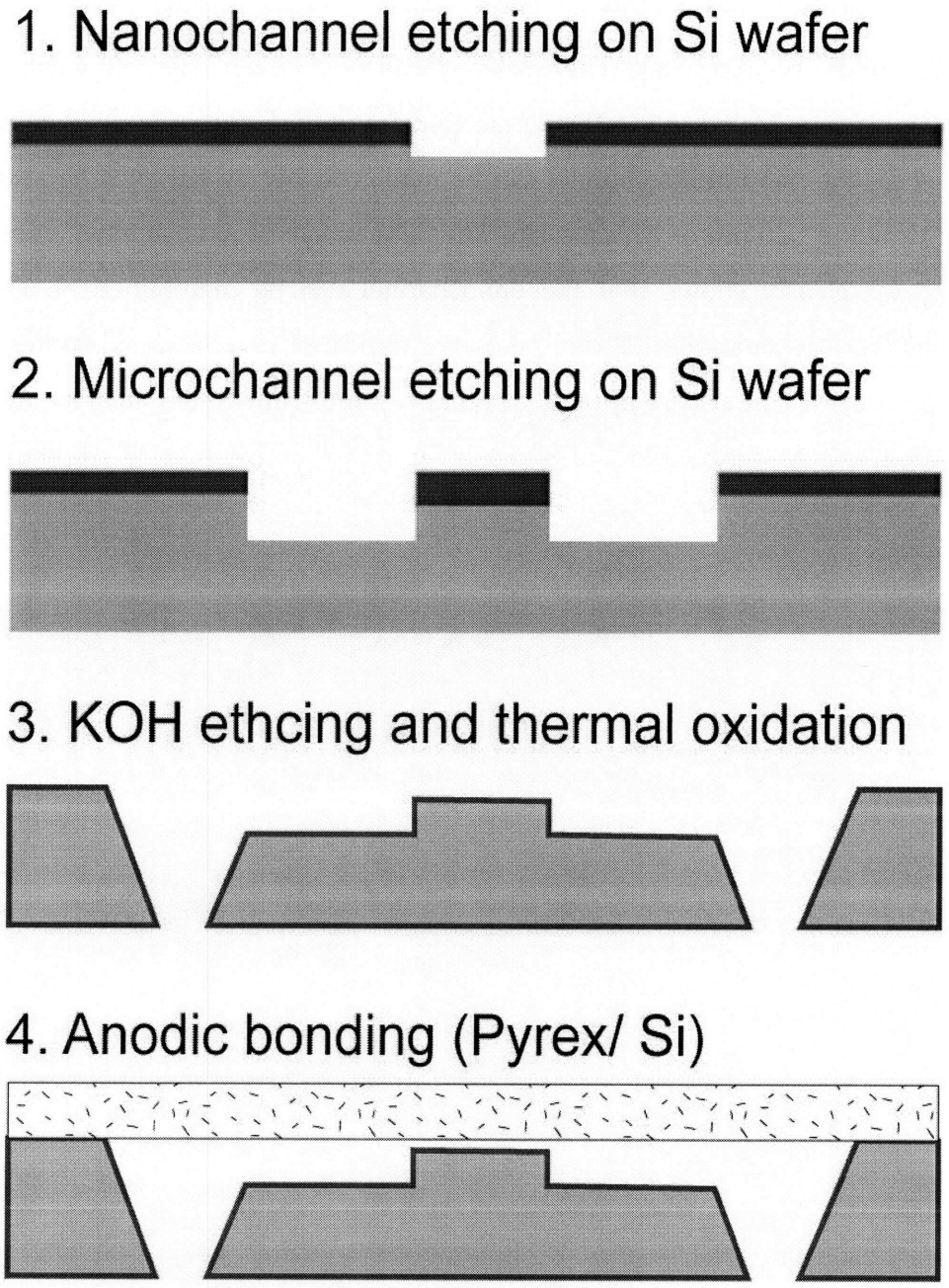

Figure 4-4 Fabrication process of nanofluidic preconcentration device

Figure 4-5 shows the cross-sectional SEM images of the nano/micro-fluidic junction before the anodic bonding step. The relative location between a nanofluidic array and microchannels is indicated in the 3D perspective drawing (Figure 4-3). As demonstrated by Mao *et al.*, the nanofluidic channel can be made reliably by RIE etching and anodic bonding down to ~20 nm or thinner.[85] The SEM image of nanochannel cross section in Figure 4-3 clearly shows that the nanochannel can be maintained at a uniform thickness. Since the nanofluidic devices were fabricated on silicon substrates, similar fabrication process can also be applied to other common substrates, such as quartz and Pyrex wafers.

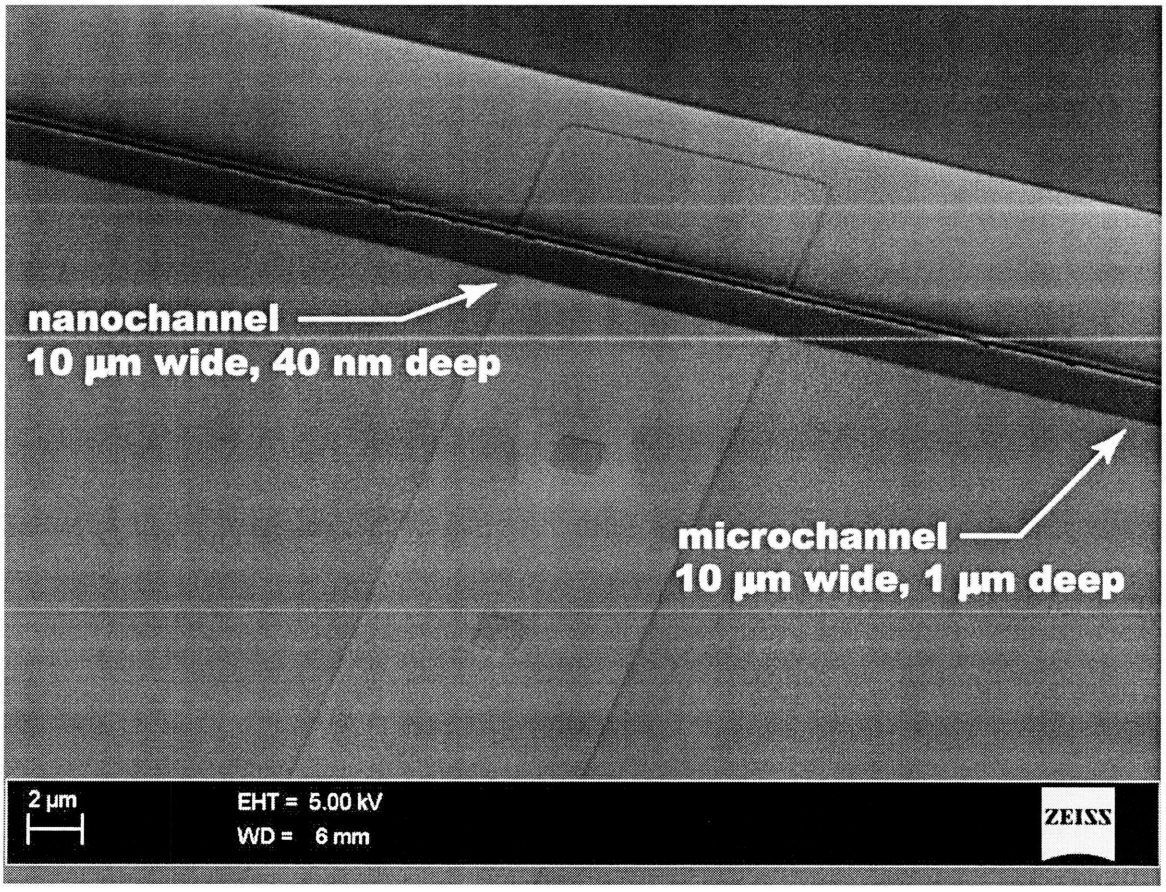

Figure 4-5 SEM image of the nano/micro-fluidic junction before anodic bonding The image is taken after the first two photolithography and RIE etching steps.

Because the microfluidic channels are connected to reservoirs through four access holes across the silicon wafer, etched by KOH etching, further connections can be made either by attaching plastic reservoirs directly onto the device or by bridging tubing with custom made clamps. Once the connection is made, sample fluids are first injected into both microchannels and nanochannels by pressure. After flushing out remaining gas residues in the device, EOF can then be induced by applying voltages to the reservoirs using hydrogen electrodes (Pt electrodes). For the observation, the device are mounted on an inverted microscope with fluorescence capability as shown in Figure 4-7 and samples are usually loaded only into the upper channel for easier fluorescent signal tracking. All the experiments in this Chapter were set up this way. Various sample including GFP (Clontech, CA), fluorescent labeled BSA (Sigma, MO), FITC (Sigma, MO), positively charge Rhodamine 6G (Fluka, MO), synthesized peptide (MIT Biopolymers Lab, MA), DNA (Beverly, MA), and fluorescent beads (Invitrogen, OR), were used.

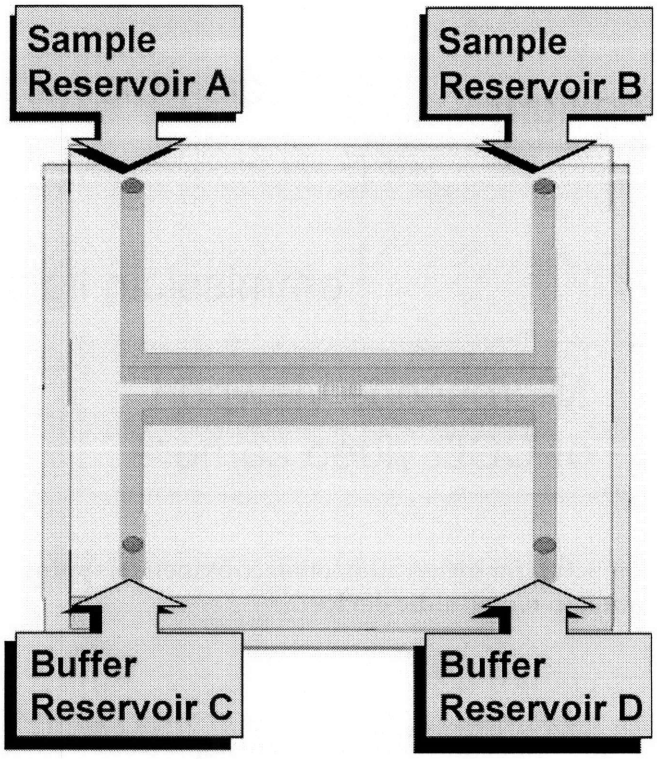

Figure 4-6 Schematic showing one nanofluidic array, two microchannels, and four access holes to the channels
Samples are usually loaded only into the upper channel. (not to scale)

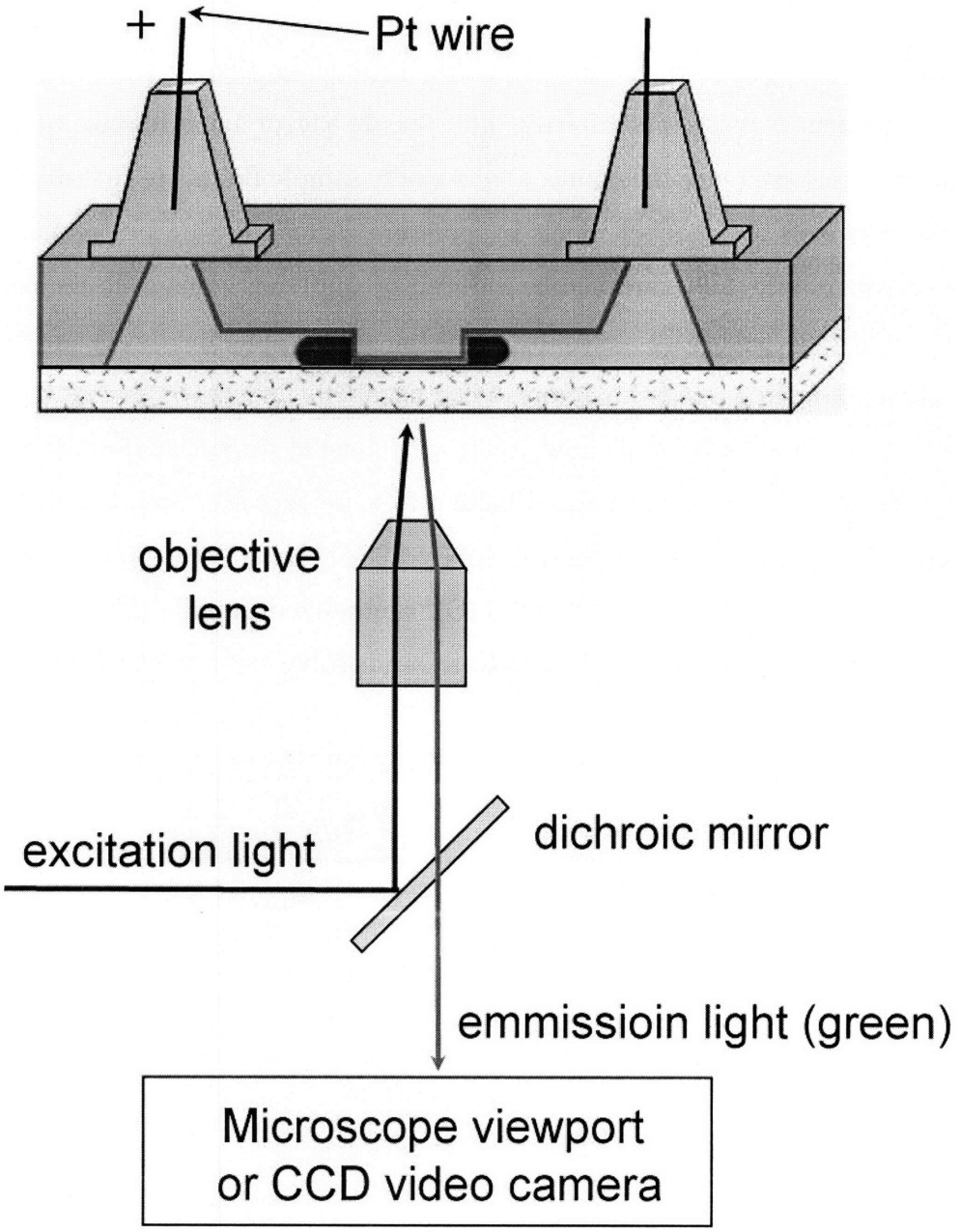

Figure 4-7 Experimental Setup for observation of electrokinetic trapping induced by concentration polarization in nanofluidic device

Currently, because fluid connections are made through KOH etched reservoirs, each of them has a pyramid shape with 1x1 mm^2 bottom, 0.7x0.7 mm^2 top, and a height of 675 μm. As a result, a dead volume of 0.49 μL is directly associated with any buffer

switching, which can be a problem when timely sequential injections are necessary. This problem can be solved in the future by either drilling smaller diameter holes through a Pyrex wafer or incorporating deeper side flushing channels.

4.3 Mechanism of Preconcentration in the Nanofluidic Device

With the device we built using microfabrication techniques, when a moderate Debye layer overlap is established inside the 40 nm nanofluidic channel, the selective ion transfer will generate concentration polarization as discussed in section 4.1. The concentration polarization phenomenon can be triggered even if the Debye layer only covers roughly 12% of the nanochannel (the 15 mM buffer). The first stage of the selective ion transfer can be shown in Figure 4-8A. Once an external voltage is being applied to the system (symmetrically), counter-ions will be preferentially transferred across the nanochannel. To maintain the charge neutrality in the adjacent region, both negatively and positively charged species will be dispelled away. However, under a small electric field, chemical diffusion dominates, therefore, the concentration distribution remains the same as can be seen in the fluorescent image. By increasing the applied field, shown in Figure 4-8B, concentration polarization can be observed as the resulting effect of the selective charge transfer. At this stage, the ion depletion (caused by concentration polarization) near the nanofluidic channel will consequentially make the Debye layer thicker and overlap more significantly in the nanofluidic channel, which will speed up the concentration polarization. Above a certain threshold value of E_n, the ion transport across the channel enters a new, non-linear regime (electrokinetics of the second kind), which has been previously reported in the ion-exchange membranes.[68, 82] In this regime, shown in Figure 4-8C, the counter-ions are depleted from the nanofluidic channel, and an extended space charge layer (induced electrical double layer) is formed in the bulk solution nearby, in this case, within the microfluidic channel.[82]

Within this induced electrical double layer, electroneutrality is locally broken (these charges are screening the fixed surface charges within the nanochannel), and co-ions (biomolecules) are prohibited from this region because of their negative potential, just as in the Debye layer. Currently, the length scale of the extended space charge layer is still under investigation. Whether or not the space charge layer can extend across the 20 μm wide microfluidic channels is still not clear. However, it has been demonstrated that the presence of the extended space charge layer induces a very strong flow in the presented device.[76] Such an induced mobile ion layer can generate a strong electroosmotic flow when a tangential component of electric field (E_T) is applied (Figure 4-8D). When the flow carries molecules in the preconcentrated plug toward the nanofluidic channel, molecules will encounter a much stronger depletion force. As a result, a much stronger signal can be detected due to the secondary sieving.

With the established depletion region, both charged (negatively and positively) species can only have limited transfer across the stacking boundary. By using positively charge Rhodamine dye, the preconcentration of positively charged molecules was usefully demonstrated in the device. The rate of the preconcentration, however, has yet to be characterized because positive charged molecules are prone to nonspecific binding onto the silica surface (negatively charged). By carefully controlling the electric fields (E_n and E_T), one can balance the two forces (static repulsion force from ion depletion vs. electroosmotic flow from the reservoir), stabilizing the interface. At the interface, biomolecules coming from the sample reservoir can be continuously trapped and collected. [40]

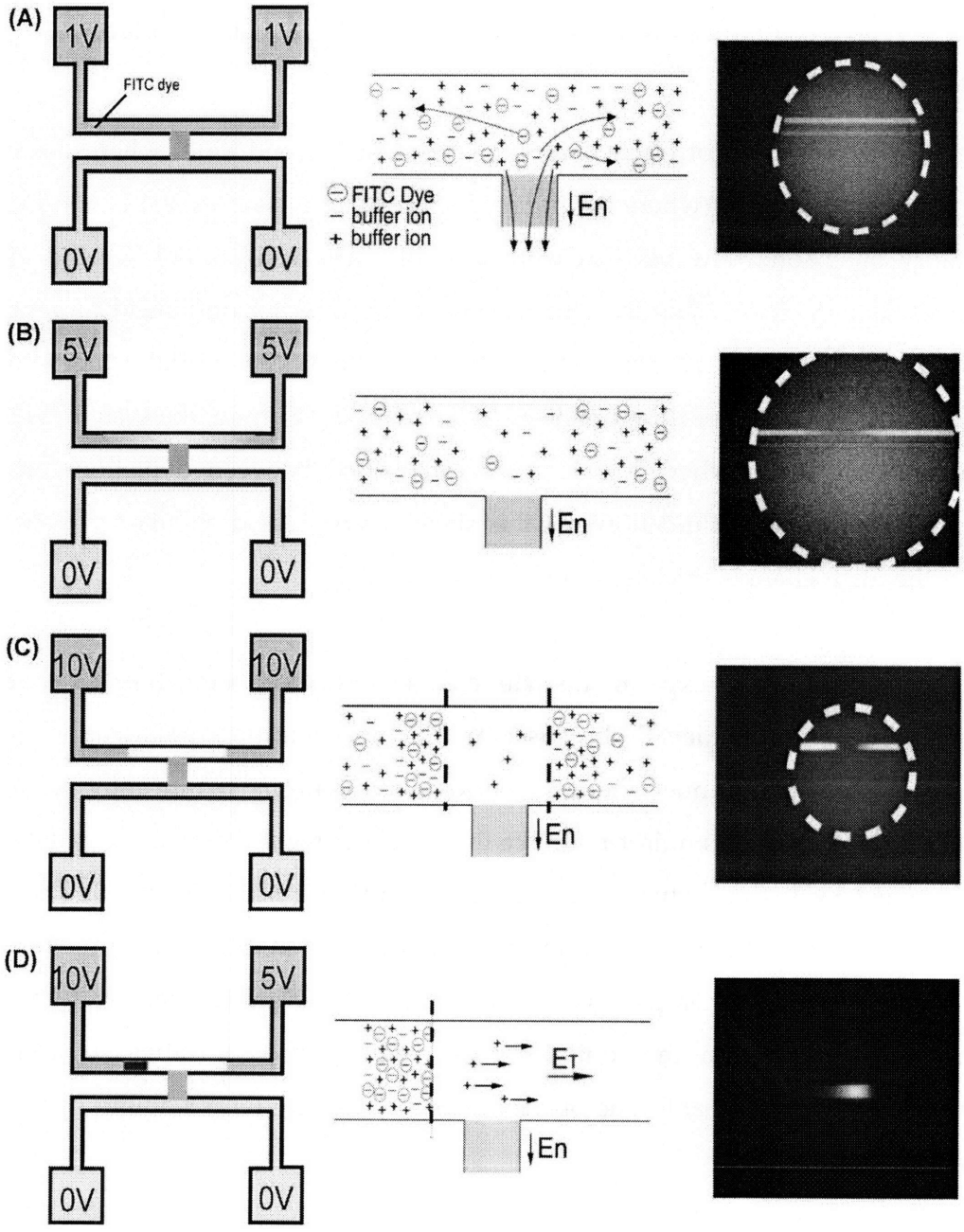

Figure 4-8 Mechanism of preconcentration in the nanofluidic device

(A) No concentration polarization was observed when a small electric field is applied across the nanofluidic channel. (B) As the En increases, the transport of ions becomes diffusion-limited and generates an ion depletion zone. (C) When a stronger field (En) was applied, a strong depletion boundary will be formed, which enables the trapping of charged molecules. (D) By applying an additional field along the microfluidic channel, the trapping scheme, also illustrated in Figure 4-9, can be created.

4.4 Continuous Preconcentration Using Electrokinetic Trapping

In previous experiments of electroomsotic flow of the second kind, where the electric field near the gel surface (where the induced space charge layer exists) is non-uniform, circulatory or chaotic flow vortices were typically observed.[68, 86] We did observe similar oscillatory flow, when the electric field values are not optimized to generate a stable boundary. This is especially evident during the initial stages of the preconcentration. Once the flow stabilized at a certain E_T/E_n ratio, the system will reach a (semi) steady state, where a balance is established between depletion force and tangential electrokinetic fluid flow. At this stage, a suppressed circulatory flow to the scale of the microchannel thickness can be observed.[76]

Compared with previous experiments with charged gel beads, a much better control on this phenomenon is achieved, because; 1) The concentration polarization zone is confined in the microchannel, therefore convective mixing is significantly reduced. 2) The tangential field (E_T) is uniform, unlike the gel experiment where the tangential field is determined by the curvature of the gel bead and very non-uniform. 3) Due to the small amount of current required and fast heat dissipation in the device, joule heating is not a concern. 4) Unlike charged gels or membranes, nanofluidic channels do not swell or shrink depending on the ionic strength, temperature, or other environmental conditions, which is probably one of the reasons for a long-term stability operation of the device.

The concentration behavior in this system is different from that of FAS or most electrokinetic manipulation, since both anions and cations are collected in the concentration polarization zone. Demonstrated in Figure 4-10, this device can preconcentrate samples for longer than three hours. In the beginning of the experiment, (Figure 4-10), 33pM GFP (green fluorescent protein) sample solution was loaded into the sample reservoir, and the resulting trapped protein peaks were monitored by

fluorescence microscopy. The preconcentration of proteins can be stably maintained up to several hours, which allows for preconcentration factors of more than a million fold (measured by the peak intensity). Figure 3 (D and E) shows the preconcentration of results of dilute GFP protein solutions of 33nM, 33pM, and 33fM monitored over ~3 hours. The concentrations of collected GFP protein plugs were estimated by measuring the fluorescence signal from the molecules. The result shows that preconcentration factors of 10^6~10^8 have been achieved. The measured collection speed is decreased when the plug concentration became high (around μM to mM level). The cause of this is not yet clear, and it is likely due to excessive non-specific binding of the protein on the channel surface (Wall-bound GFPs lose fluorescence activity). Recently, in the experiment conducted by Kim *et al.*, similar phenomenon that higher concentration samples exhibit slower collections and lower enhancement factors were also reported.[41]

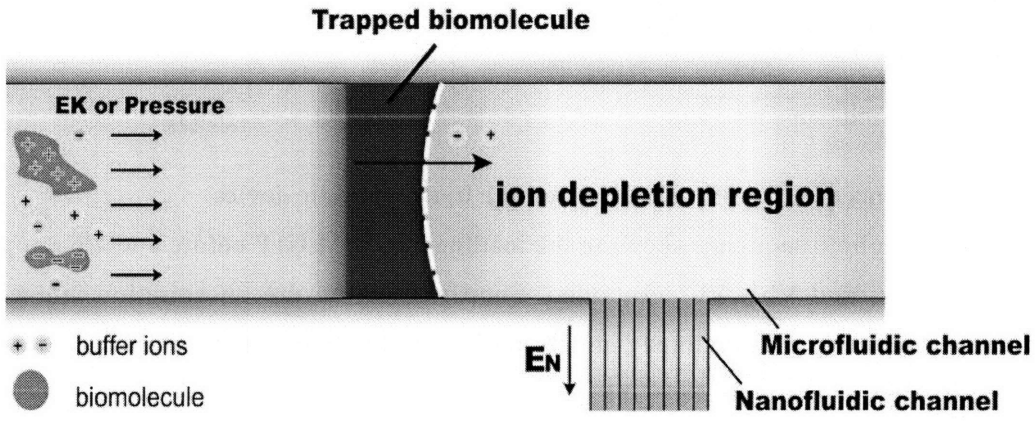

Figure 4-9 Device setup up and a summary of the preconcentration mechanism
During the experiment, if both Et and En were applied, molecules would be brought into the trapping area by either electrokinetic flow or pressure driven flow. When passing through the ion depletion area, charged molecules will be trapped at the boundary until the depletion force is removed. With this scheme, we can enhance the fluorescence readout of 33 fM GFP molecule by more than a million fold within 40 minutes.

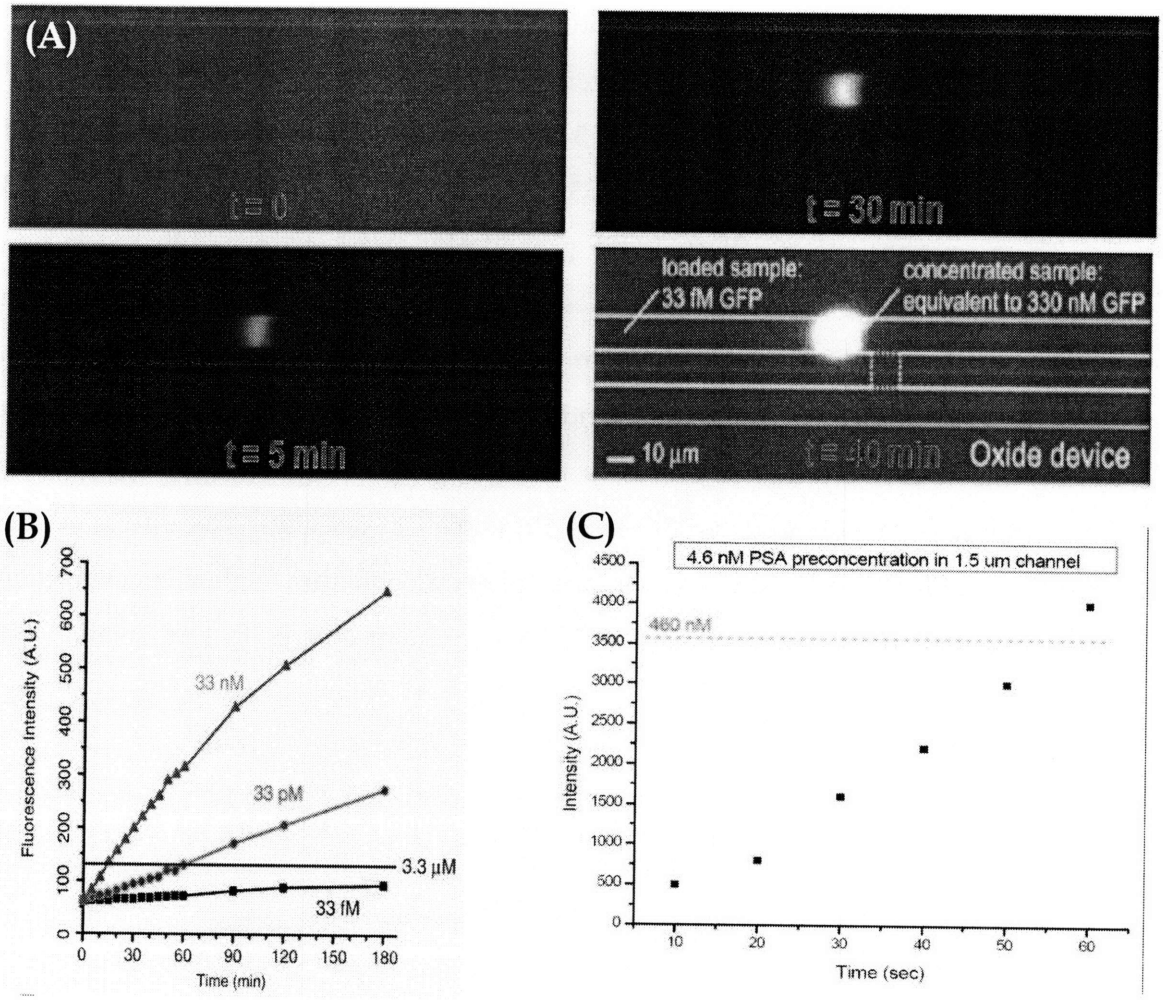

Figure 4-10 Preconcentration of various biosample in nanofluidic device

[A] A time lapse photo sequence showing the loading of 33 pM GFP before and after applying Vs=10 V, Vd=5V, and Vb1, Vb2 grounded. Shortly after the preconcentration voltage was applied, one can observe a previously undetectable sample plug forming in the microchannel. [B] Concentration of the collected GFP plug, starting from dilute GFP solutions with three different concentration (33 nM, 33 pM and 33 fM). The concentration was mapped by injected non-diluted sample into the device as the parallel line drawn in the plot. [C] Preconcentration of FITC labeled PSA (6.6 μM), approach 100x concentration enhancement within 1 min, the PSA proteins have estimated 87 dye molecules per protein molecule.

4.4.1 Channel Passivasion and Sample Delivery for Separation of Down Stream Identification or Free Solution CE

One major problem of protein analysis in untreated silica surfaces are the adsorption of samples. In this system, the adsorption can change the effective surface charge density and sometimes shift the optimal operating conditions. To eliminate this problem, a standard polyacrylamide coating was performed.[87] First, the device was coated with 3-(trimethoxysilyl)propylmethacrylate as an adhesion promoter. Then, 5% polyacrylamide solution was mixed with 0.2% VA-086 photo initiator (WAKO, Richmond, VA) and exposed under a UV-lamp for 5 min, to initiate polymerization. After the coating, there was no noticeable level of adsorption in the device. Even though the polyacrylamide coating process is expected to decrease surface potential and surface charge density, a similar charge polarization and sample trapping pattern can be observed (with a lower efficiency) by applying a higher operating potential. The lower efficiency can be overcome by adopting an even lower buffer ionic strength. One of the ongoing efforts is coating the channel with charged polymers that can reduce the amount of adsorption while maintaining the surface charge density.

Various nanofluidic channels with different thicknesses have been tested in this work, along with different buffer ionic strengths (Figure 4-2). Even a complex solution directly from the in-gel digestion of gel electrophoresis (which has high-ionic strength and contains some organic solvents) can be used as sample buffer. The complex solution described in the experimental section was used as a 'sample buffer' by adding labeled GFP molecules. For the preconcentration step, this simulated sample solution was diluted with 10 mM phosphate buffer (1:9 ratio) and loaded into the channel. In addition, various samples including proteins, synthesized peptide, fluorescent dye, fluorescent labeled proteins and fluorescent beads were tested. In all of these cases, the trapping mechanism shown in Figure 4-9 can be established, while the speed of the preconcentration at different conditions varied. The adaptability of this system opens up

the possibility of using samples directly from gel electrophoresis or other conventional purification techniques (using high ionic strength buffers) in the preconcentration device.

Because the trapping mechanism in this device comes from the depletion force induced by the externally applied En, one unique property of this presented nanofluidic preconcentrator is the ability to remove the trapping boundary at any given time by removing the applied field. As shown in Figure 4-11, we can define applying both E_T and E_n as the preconcentration (Precon) mode and applying only E_T as the capillary electrophoresis separation (CE) mode. When a preconcentration reaches a desired concentration level, one can switch from Precon mode to CE mode to release them for a downstream detection.

As the plug motion can be controlled real time remotely, we can monitor the above described operations closely by placing a detector down stream the depletion region. Shown in Figure 4-12(A) is the fluorescence readout of GFP signal, when the Precon voltage were initially applied, a depletion signal can be recorded after a short delay. It indicates GFP in the sample stream has been filtered out by the ion depletion force.

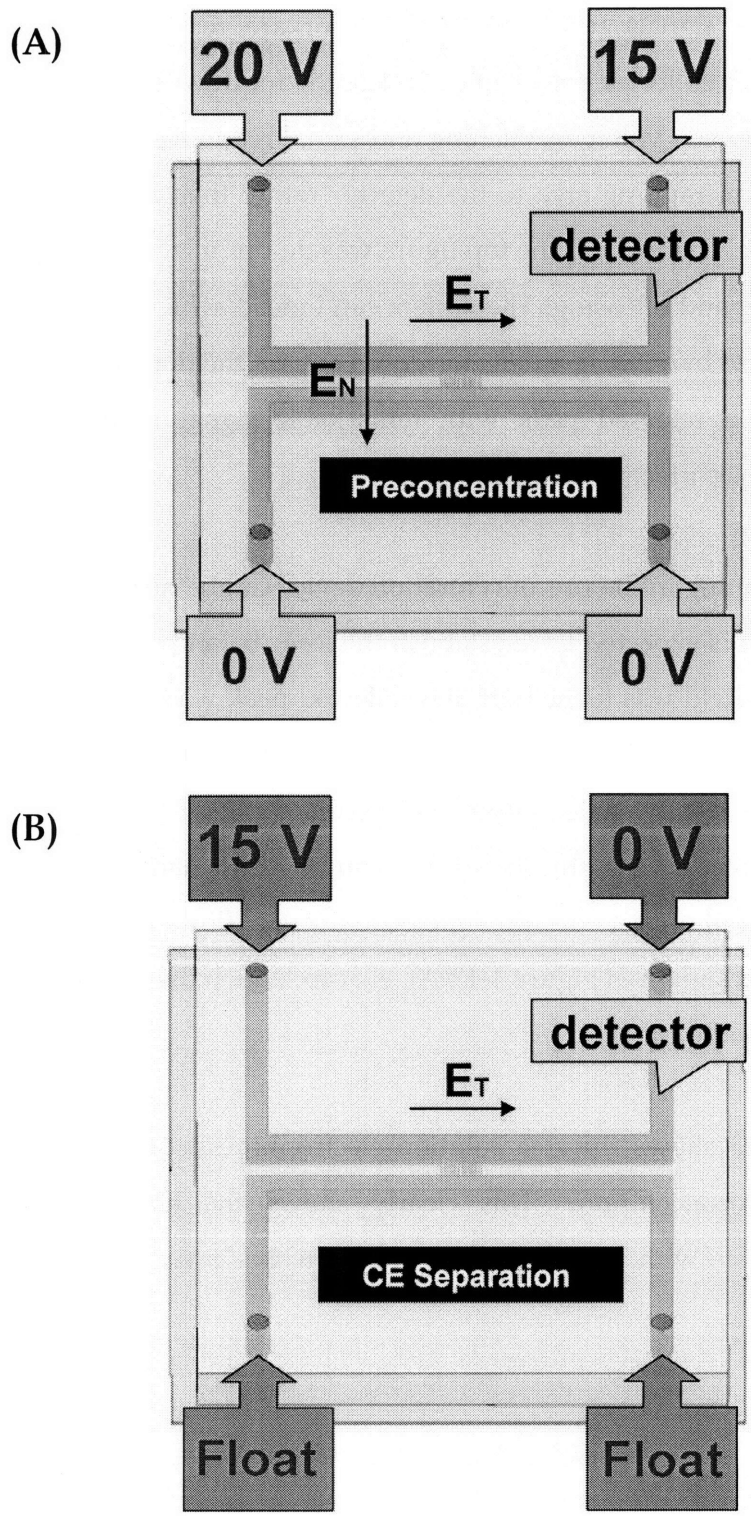

Figure 4-11 Experimental voltage scheme

[A] Preconcentration voltage scheme (apply both Et and En); [B] mobilize the preconcentration plug by removing the En across the nanofluidic array.

Therefore, only black signals from the CCD sensor are recorded. Likewise, when switched to CE mode, a collected peak can be "released" for downstream detections. The time delay we see between voltage switching and signal readout is the time it takes for samples to travel from trapping area to the detector rather than a delay in the system response. The experiment shown in the top figure was de-optimized on purpose to show details in the trapping and releasing. The system can indeed achieve preconcentration h much higher efficiency, by placing a detector down stream the depletion region. Shown in Figure 4-12(B) is a released peak with remarkable signal to noise ratio to the background after 500 sec preconcentration.

As the molecular trapping in the preconcentration device can be turned off by removing E_n, the buffer solution is expected to re-establish the ionic balance as soon as the field is turned off. When the field was turned off, the collected peak was instantly dispersed to about twice the original peak width, but there was no further dispersion observed. This dispersion reached a steady state within ~10 seconds time flame. As a result, the molecular plug generated by the preconcentrator can be easily manipulated either by the electric field (electrophoresis) or the pressure-driven flow. In our design, by manipulating the field shown in Figure 4-12(A), we can launch the molecular plug by E_T along the top microfluidic channel.

Moreover, Figure 4-13 shows the free solution electrophoresis of two protein species collected by the preconcentrator. This clearly shows the ability to couple this preconcentration device with downstream analysis, in this case, on-chip free solution electrophoresis.

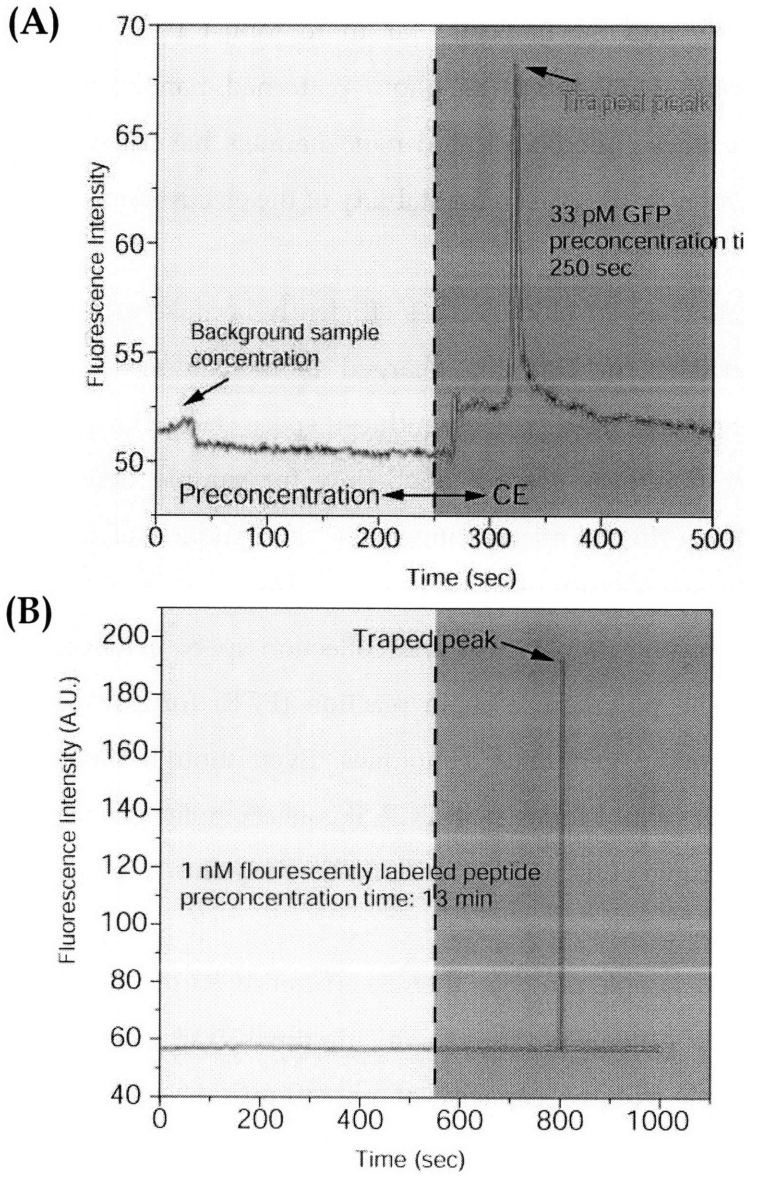

Figure 4-12 Fluorescence Electrophoregram under various operation schemes
[A] Electrophregram showing GFP preconcentration and release but switching on/off En [B] Electrophoregram of the same operation using peptide sample and longer preconcentration time.

This device can be fabricated with standard photolithography and etching techniques, without the need for high-resolution lithography or special fabrication tools. The ion-selective membrane in this device is the nanofluidic channel with the silica surface,

which is chemically and mechanically far more robust than any other nanoporous membrane materials. Unlike frits or photo patterned nanoporous membranes with random pore size, these microfabricated nanochannels have a uniform pore size and shape, which is probably the reason for stability of the electrokinetic trapping barrier.

This device collects charged biomolecules efficiently because of two main phenomena: (1) the energy barrier for trapping charged biomolecules, which is generated by concentration polarization and possibly induced space charge layer near the nanofluidic filter; (2) a faster nonlinear electrokinetic flow for sample deliveries driven by the induced space charge in the microchannel. The combination of these two phenomena results in a rapid preconcentration of proteins and peptides within the microfluidic channel. The preconcentration factors and collection speed achieved in this device are close to those of the polymerase chain reaction (PCR) for nucleic acid, which is an essential step for many genomics techniques. Even though this technique does not increase the number of molecules as in PCR, it collects molecules from a relatively large (~1 μL or larger) sample volume, and concentrates them into a small (1pL~1nL) volume.

Such a concentrated sample plug can then be efficiently sorted, separated or detected by various microfluidic systems without sacrificing the overall detection sensitivity caused by the small sample volume capacity of microfluidic biomolecule sorting/detection systems.

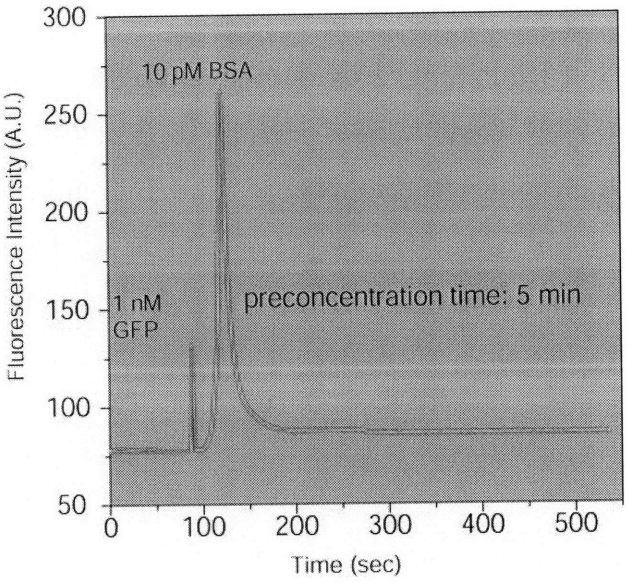

Figure 4-13 Preconcentration-CE separation of GFP and BSA mixture.

4.4.2 Optimization of the Nanofluidic Preconcentration Device

Except for increasing the sample capacity, increasing microchannel scale can also make pressure-driven operation a lot easier since fluid resistance has high correlation to the critical dimension (depth of the microchannel). Given μ as the fluid viscosity ($1.13\times10^{-3}\,Pa\cdot S$), L, w and h as the channel dimensions and p as the pressure drop, the fluid resistance and flow rate driven by pressure gradient can be written as:

Fluid resistance

$$R=\frac{8\mu L}{\pi h^4} \tag{4.1}$$

Flow rate

$$Q=\frac{h^3 w}{12\mu}\left(-\frac{dp}{dx}\right) \tag{4.2}$$

To hydraulically flush a 1 mm long, 100x10μm^2 microfluidic channel within 10 secs (a flow rate at 6 mm/min), it would takes a pressure drop of 19.7 psi. (Note: 1 atm=14.7 psi) However, if we would want to obtain 6mm/min flow rate across a 50nm nanofluidic channel, it will take ~786.7psi pressure to do so. As shown in Figure 4-14, the same preconcentration scheme can be carried out in channels much lager than the first approach (1.4μm x 10μm).

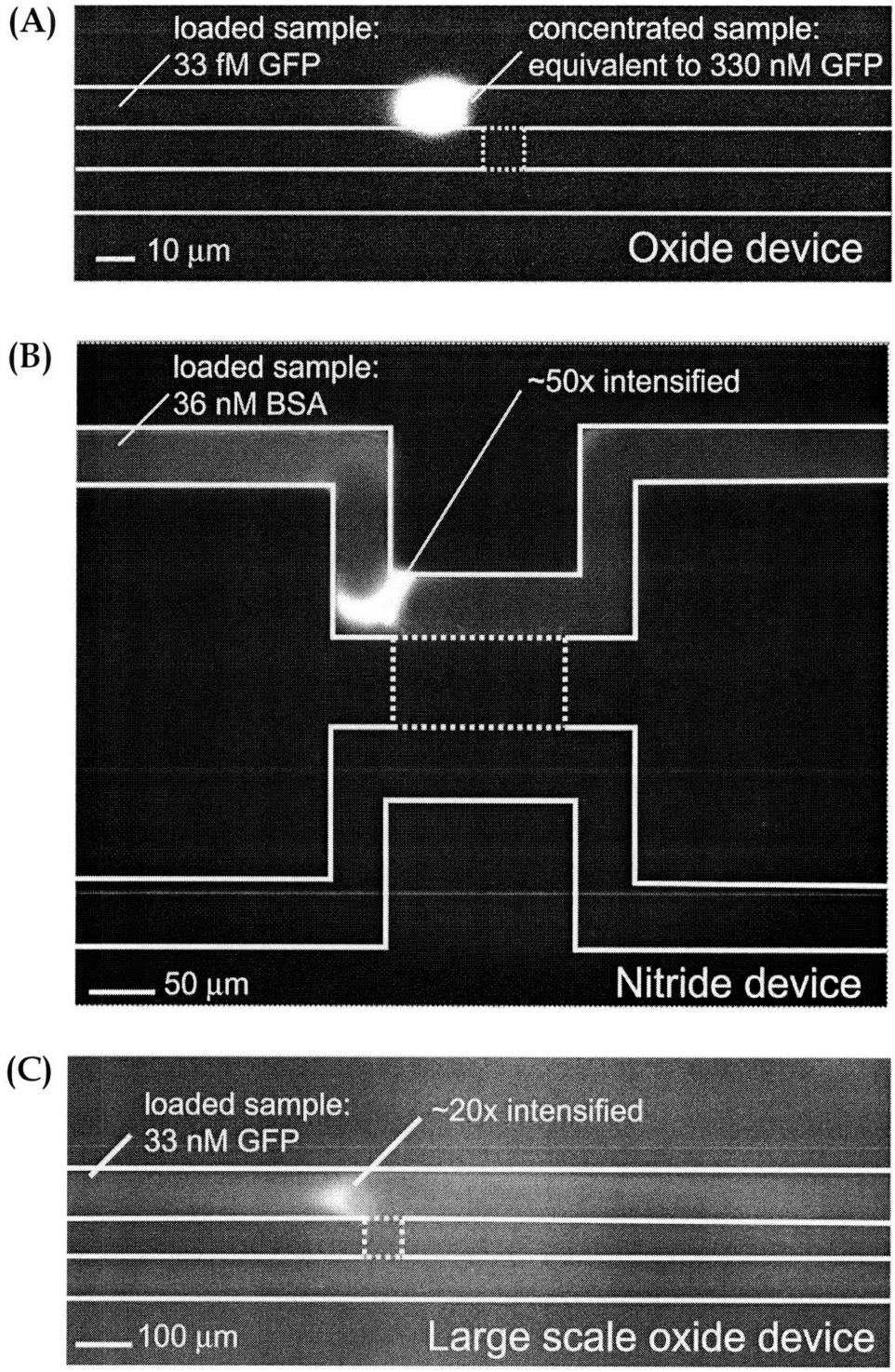

Figure 4-14 Preconcentration in large scale devices

(A) Collection of 33 fM GFP in silicon oxide based device. (B) Collection of 36 nM BSA in nitride-PDMS device. [C] Collection of 33 nM GFP in 50 μm deep wet-etched Pyrex device.

One major problem one would encounter after scaling up the device is the inefficient ion depletion across the microchannel to sustain a continuous biomolecule accumulation. As illustrated in Figure 4-15, when we increase the size of the microchannel, a much stronger En is usually needed to maintain a strong depletion across the span of the microchannel. However, as the second kind EOF mixing velocity increases to the square of the normal field, a stable concentration polarization can sometimes being impossible to maintain.

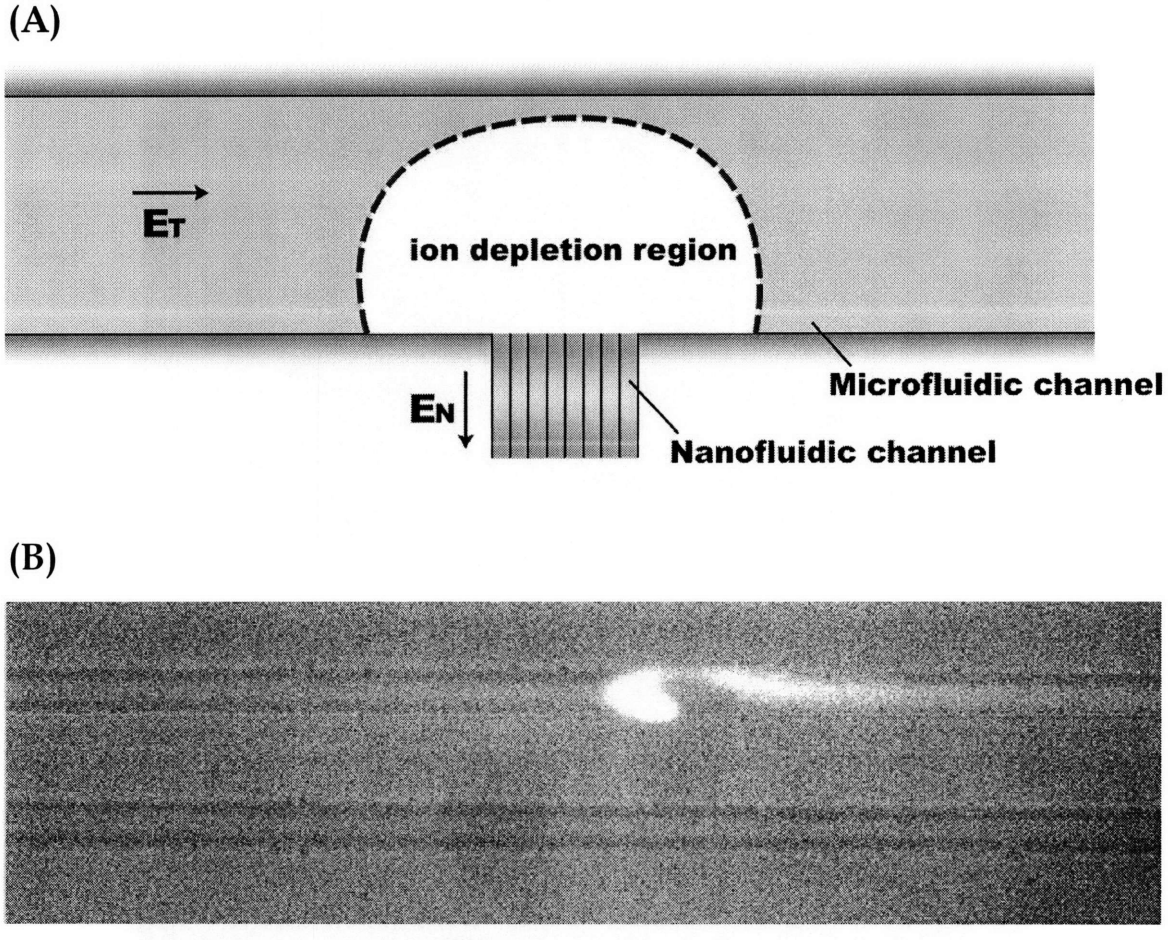

Figure 4-15 Inefficient ion depletion leads to breakdowns of the stacking boundary
(A) Drawing illustrates the compromised stacking boundary. (B) Fluorescent image of GFP samples leaking through the depletion area.

To address this problem, we modified the original design slightly to incorporate an additional set of nanofluidic channel array. While no additional reservoirs have to be introduced, the device can be operated with the original setup. With a device shown in Figure 4-16, maintaining a stable stacking boundary becomes less a daunting task.

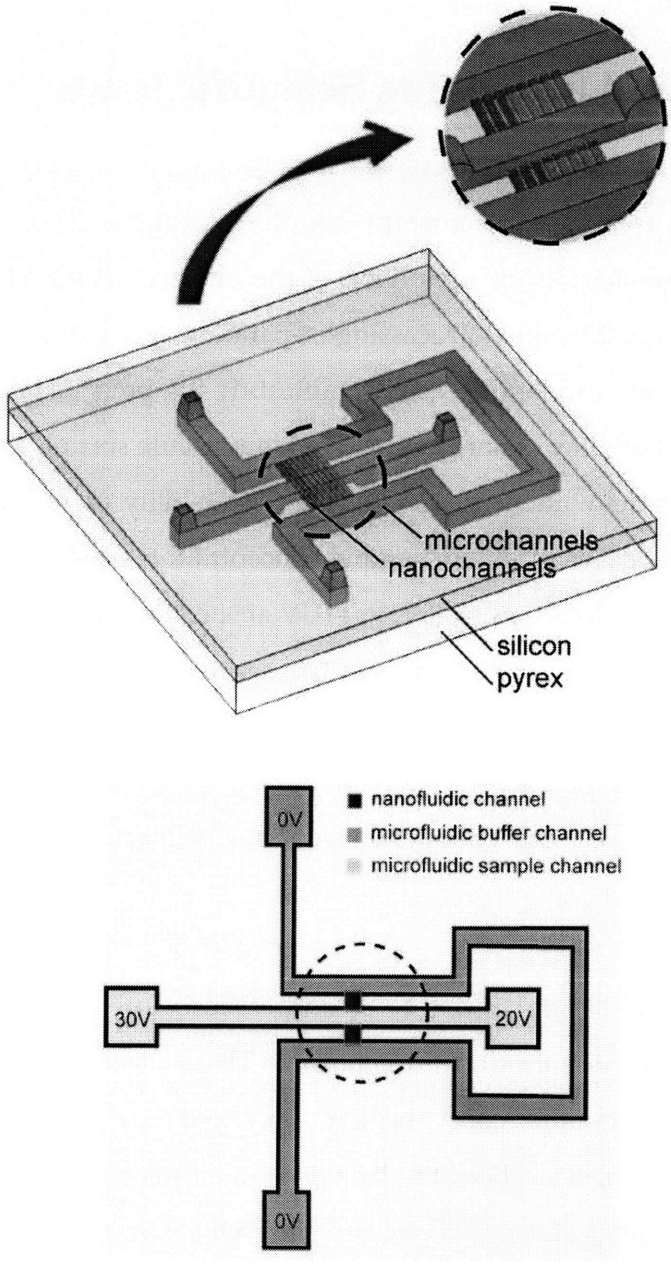

Figure 4-16 Perspective view of the double nanofluidic array device

As a result, an integrated device coupling the large scale preconcentrator to a bead-based sensor is made possible (Chapter 5). Besides, efforts are underway to incorporate this preconcentrator with other labeling-free detection techniques. Part of these ongoing efforts can be found in the following chapters.

4.5 Summary and Remaining Scientific Issues

As introduced in this chapter, the presented nanofluidic preconcentrator can act as an ideal world-to-chip (pipette-to-microchip) coupling adapter. This preconcentration device would be equivalent to the 'amplifier' of the (molecular) signal in the electronic circuits, which allows better signal processing (separation and purification, in this case). Since the signal intensity can be increased significantly (by preconcentrating molecules) just prior to detection, it allows more aggressive biomolecule sorting and/or removal of high-abundance proteins without sacrificing the detectability of the minor proteins or peptides. The availability of a protein sample concentration system will allow users to use several non-labeling detection techniques (UV absorption, for example) in the μTAS engineering, which was not possible due to the short path length and small internal volume of conventional microfluidic channels. Therefore, a combination of microfluidic biomolecule sorting and preconcentration would be an ideal platform for integrated microsystems for biomarker detection, environmental analysis, and chemical-biological agent detection.

However, there are still several issues to be addressed before one can understand the detailed trapping/preconcentration mechanism. These issues including the exact concentrated plug width and concentration, flow patterns around and inside the nanochannel array, effect from the cathodic side (ion enrichment), the relation between collection speed and plug concentration, and the exact size of extended space charge layer. One of the striking features of this preconcentration system is its speed. A 10^7-fold concentration has been achieved within an hour. Since the approximate volume of concentrated plug is about 0.5pL (~1.5 μm × 20 μm × 20 μm), this means the

preconcentrator pumped sample liquid volume as large as 1 μL through the channel and trapped the GFP within that volume. Given the concentration time of ~10^4 sec in this experiment, the average sample flow speed should be as high as 1mm/sec. This is not possible with normal electroosmotic flow (electroosmosis of the first kind), which only generates up to 10~100 μm/sec with the field used in this experiment (~10 V/cm). The fast collection (and fast sample fluid pumping) can be explained only by the electroosmotic flow of the second kind. Induced space charges are generated within the microchannel by the field (E_n), and the tangential field (E_T) mobilizes these induced space charges toward the cathodic reservoir. Such flows were also shown in the flow experiment we conducted in the other experiment.

As a result, the preconcentrator presented not only traps the molecules but also pumps the sample liquid very efficiently. In addition to the sample preconcentration, this device could be a novel, microfluidic fluid pumping device, which is much more efficient than electroosmotic (electrokinetic) pumping,[88] and simpler to implement than AC electrokinetic pumping.[89, 90]

The other yet to be proven reason of the fast collection, other then the fast electrokinetic flow, can be the net effect of nonlinear flows in the depletion region and the stacking boundary. However, due to the limited resolution we can have from a standard inverted fluorescent microscope, vertical and small flow patterns cannot be observed easily to verify this assumption. The scaling analysis basically assumed a linear collection of the target analyte from the fixed concentration in the bulk. This might not be accurate with the existence of the nonlinear flow around the stacking boundary. The combination for the repulsive force and a fast nonlinear flow can exponentially increase the local analyte concentration by a secondary screening from the concentrated plug and could lead to strong fluorescence readouts.

It is also suggested from the work published by Kim *et al.*, where a PDMS based preconcentration device has been built using a reversible bonding.[41] In this work, a

10^3-10^6 fold protein preconcentration in 30 min was reported. While the high rate of preconcentration is difficult to explain based on the flow rate they acquired, it is suggested that other signal enhancement mechanism yet to be identified might be involved. As a result, while the detectability was enhanced by 10^5 times, there is no conclusive evidence that the concentration has actually increased by factors of 10^5 in the device.

Because of these issues, further characterization of optimized preconcentration conditions is needed with either a quantitative tool or localized current measurements. Furthermore, the size and number of the nanochannel seem to affect the concentration efficiency of the device due to different electric field distributions in the system. With more understanding or the process, one can contribute both practically to the field of biomolecule preparation and academically to studies of nanofluidic electrokinetics.

Chapter 5

Enhancing Immunoassay Sensitivity and Kinetics Using Electrokinetic Preconcentrator

Presented in this chapter is the author's effort integrating a bead-based immunoassay with the novel nanofluidic sample preconcentrator. Its ability to immobilize or mobilize the preconcentrated plug enables the direct coupling between the preconcentrator and immunoassays or other detectors. With the flexibility and robustness provided by the preconcentration scheme, this device demonstrate the first on-chip integration of sample preconcentration and immunosensing and can increase the sensitivity by three orders of magnitude.

5.1 Immunological Biosensing

Immunological biosensing, also called immunosensing, is one of the most widely-used tools in recent medicine and fundamental life science research. An important aspect of this method is its ability to measure substances at small concentrations, even in complex matrices with little or no pretreatments. Due to this unique advantage, immunoassays

made many important and successful portable diagnostic systems possible. Examples such as pregnancy tests (measuring progesterone female hormone concentration) are well known and have a deep impact to our daily life. As a sensitive analytical tool, immunoassays were used frequently in either automated or semi-automated format with sensitivity in the sub-nanomolar (nM) range. They are also commonly used in microarrays for cancer and cardiovascular disease, diagnostic tests (detection/quantification), protein purifications, cellular proteins identification (localization) and drug development. Meanwhile, these biosensors also play a critical role in detecting emerging infectious diseases.[91]

Shown in Figure 5-1, biosensors can transfer ligand binding activities into electrical, optical, thermal or mass-based signals. One inherent downside of this method comes from the need to immobilize immunological materials on supporting structures (with the exception of some optical-based sensors), which renders biosensor's lifetime, reproducibility and stability limited.

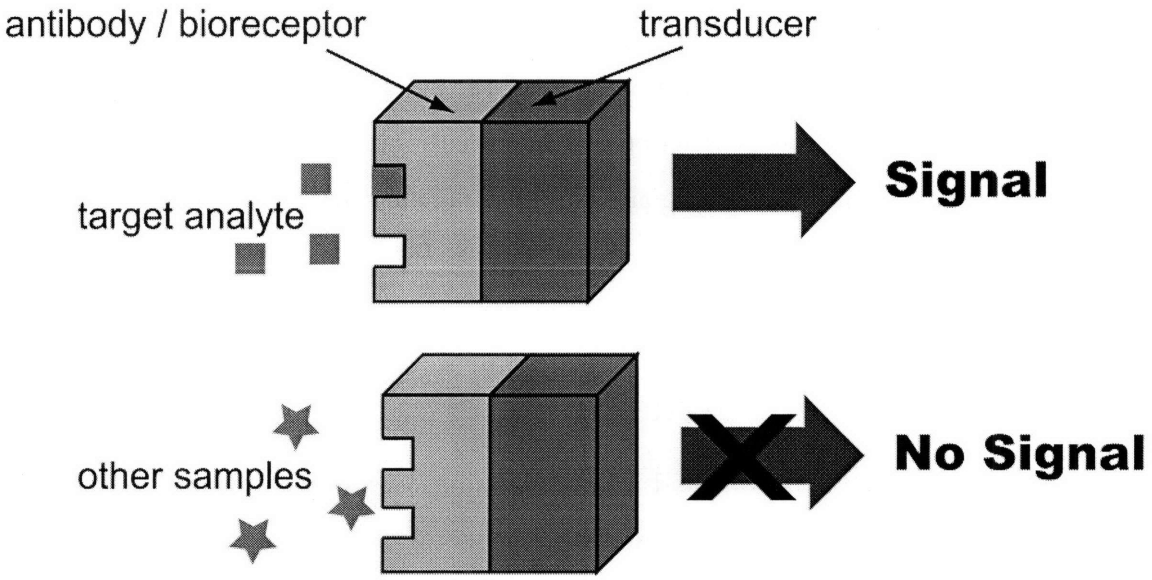

Figure 5-1 A schematic diagram of a typical biorecognition element.[91]

Unlike other biodetection tools such as mass spectrometry, immunological biosensors usually have excellent selectivity. However, low concentration analyte detection is practically very challenging because most transducers have higher noise level than these binding signals. In addition, most immunological biosensors are limited in detection dynamic range (typically ~10^3). As a result, it is highly desirable to have a large dynamic range, to accommodate the wide concentration ranges of typical biosample.

5.1.1 General Principle and Classification of Immunoassays

Antibodies are large Y-shaped proteins used by the immune system to identify and neutralize foreign objects. The other important function of these molecules is to serve as a linker of specific antigens to the immune system of the body. To serve these goals, their basic structure has two domains: one has highly flexible structure to interact with a vast diversity of antigens at their binding sites (epitope) and the other with relatively constant structure to interact with different immune cells and stimulus of the body. The former one has two branches and is also called the Fab fragment, while the later one represents the bottom rod of the "Y" and is often called the Fc fragment. Because of the presence of these distinct fragments, a chosen region can be modified without affecting the functionality of the other, therefore, enables complex multilayer applications. These domains play a critical role when developing sandwich assays such as enzyme-linked immunosorbent assay (ELISA) or other post amplification techniques, because they enable multiple layer binding and various chemical modification on their side chains. In order to visualize the binding activities, scientists have to modify the molecule with certain detectable objects. Modifications (labels) including radiology, fluorescence and so on have created vast number of opportunities.

Depending on the manufacturing methods, antibodies can be classified into two categories: monoclonal and polyclonal. Monoclonal antibodies are defined as uniform, homogeneous antibodies targeting single specific epitope, and are produced from single

cell clones. As a result, monoclonal antibodies have well-defined affinity and specificity. However, monoclonal antibodies are less resistant to changes in pH or salt concentrations, and could have lower binding affinity compared with polyclonal antibodies. On the other hand, polyclonal antibodies are obtained by immunizing animals and harvesting their antibodies produced. Even though polyclonal antibodies do not have the same batch to batch uniformity like monoclonal ones do, they still have advantages such as cheaper fabrication cost and higher binding affinity. Therefore, they are still valuable in certain applications. In general, when high selectivity is preferred, monoclonal antibodies are used.

The general antibody binding reaction is defined by the Law of Mass Action:
Binding equilibrium constant is given as,

$$K_{eq} = \frac{k_a}{k_d} = \frac{[Ag - Ab]}{[Ag] + [Ab]} \tag{5.1}$$

where $[Ag]$, $[Ab]$ and $[Ag - Ab]$ represent the concentration of antigen, antibody and antigent-antibody complex, respectively, and k_a, k_d represent the association and dissociation rate constants. With a given antigen-antibody complex, depending on the concentration of antigen and antibody, one can establish a sigmoid dose-response curve (as shown in Figure 5-6B), to be used to predict the signal response that depends on the concentration of target analyte. Direct binding assays are divided into Type I (excess antibody) and Type II (excess analyte). The assays to be used in the following chapter can be classified as Type I assay and is known to be less influenced by substances such as salt and urea.[92] As a general guideline, commonly used immunoassay buffer additives and their functions are listed in Table I. In addition, some common methods used for antibody purification/separation are listed in Table II.

Table 5-1. Buffer additives and usages[93]

Additive	Example	Reason
Proteins	Bovin serum albumin 0.1-0.5%	Reduce nonspecific binding of labeled tracer to various surfaces
Detergent	Triton X-100 0.01-0.1% Tween 20 0.05-0.5%	Reduce nonspecific binding to solid-phase reagents
Protease inhibitors	Trasylol	
Preservatives	Sodium azide 0.05-0.1%; Thiomersal 0.02%; Bronidox 0.1%	Useful to prolong shelf life of buffers and prevent growth of micro-organisms
Others	EDTA 0.01 M; PEG 1.4%	Optimize second antibody reaction and enhance visual precipitation (in turbidimetry)

Table 5-2. Methods of separation[93]

Method	Characteristics
Polymerization	Cross-linking of antibodies by polymerization using glutaraldehyde or ethylchloroformate. More effective using filtration rather than centrifugation. Partial loss of immunoreactivity likely following polymerization
Entrapping	Entrapment of antibodies within interstitial spaces of water insoluble polymer. The size of lattice may restrict access by larger molecules
Microencapsulation	Encapsulation of antibodies within a semi-permeable membrane. by forming a polymer at interface of an emulsion
Biotin-avidin	Usually couple avidin or streptavidin to solid-phase and biotinylated reagent. The vary high affinity of biotin for avidin will couple reagent to solid-phase during assay

For the developments of immunoassays, one has to integrate biomolecular recognition elements (binding reaction couple) with various types of transducers or detectors. Often, this signal transduction is achieved by either electrical or optical means, which makes biosensor development into a multi-disciplinary engineering. On the other hand, biosensors are trying to emulate the ultimate sensing model: our taste and olfaction. These natural sensing systems are both great standards and inspirations to anyone developing new sensors. The great interest in both academia and industry in this field is also reflected by the numbers of publications and patents per year. For the period of

1984-1990, there were roughly 300 scientific publications and 227 patents, compared to the period of 1998-2004, the number jumped to 6000 articles and 1100 patents.[91] In the context of this thesis, the discussion will be focused on heterogeneous assays (mostly surface-coated solid phases) for their abilities to accommodate various reagents' loading and washing process. Heterogeneous assays are more flexible when integrating with other fluidic systems and post amplification techniques.

5.2 Challenges in Biosensors with Immobilized Surface – Diffusion-limited Binding Kinetics

Currently, microarrays (biosensors for DNA and RNA) can achieve the detection of single molecule because molecular signals can be amplified by PCR techniques, before or after the microarray binding. However, protein equivalents (protein microarrays) still have several technical barriers to overcome before they can be implemented for rapid and accurate low abundant analyte detection.

Theoretically, based on the Law of Mass Action, antigen-antibody binding are solely governed by their concentration, association and dissociation rate constants. This assessment is generally valid when applied to liquid-phase assays. However, when it comes to solid-phase assays, different assumptions need to be made due to several complex issues. In solid-phase immunoassays, forward binding reactions usually takes longer to acquire a uniform amount of antigen bound to antibodies on the surface. The first reason is the development of the boundary layer, especially when analytes are present at low concentrations. Simply, the binding reaction quickly switches from a reaction-limited to diffusion-limited process when antigens are overwhelmed (depleted) by the numbers of capture antibodies near the surface. Because of slow diffusion transport in one dimensional case as shown in Figure 5-2, such kinetic constraint is the major factor limiting the rate of forward reaction, and therefore limits the possibility of rapid analyte binding at low target concentrations. [21, 94]

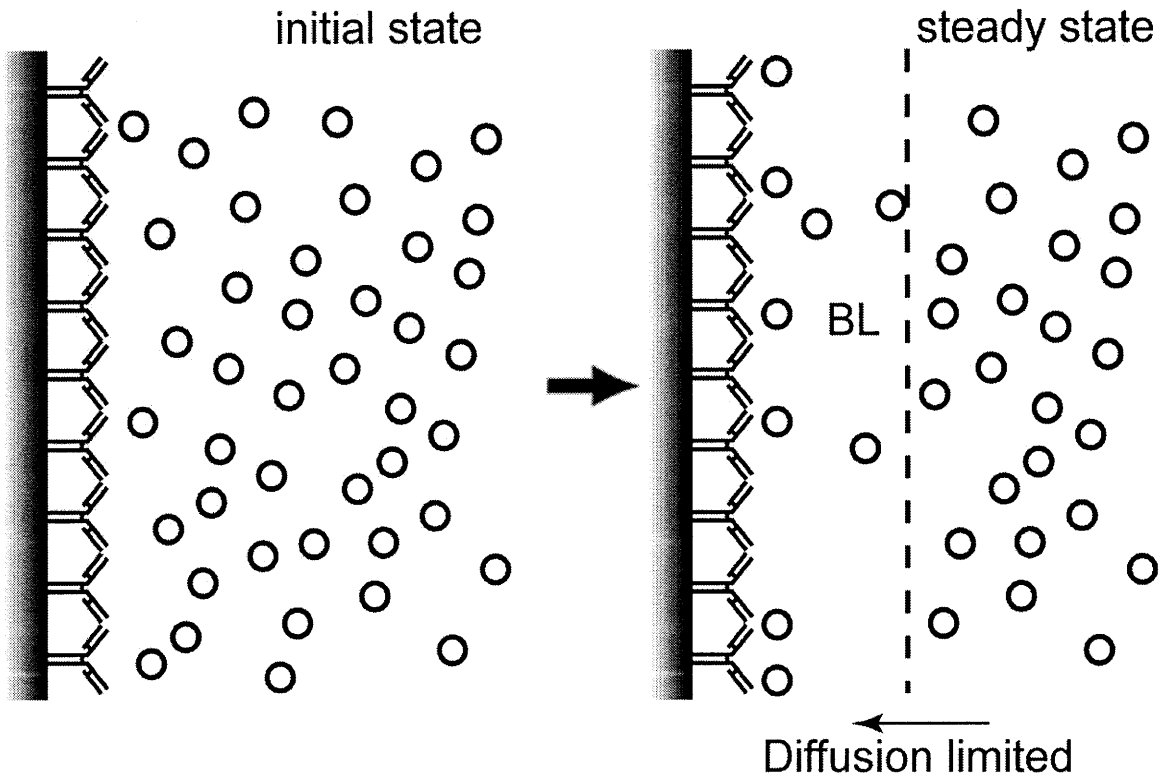

Figure 5-2 Formation of the boundary layer (BL) due to sample depletion

The other factor that can significantly lowers the association rate constant of solid phase assay is the sticking coefficient. Sticking coefficient reflects the lower association rate of surface-bonded antibodies due to the requirement for correct alignment between antibody and antigen. Unlike liquid-phase assays, antigen and antibody binding is only possible when both are in the correct orientation. Despite these unfavorable properties, solid-phase assays, however, have lower dissociation constant compared with free solution assays. It was suggested that the binding onto solid-phase adsorbed antibodies can essentially be considered as irreversible, because the possibility of a dissociated antigen being able to 'escape' from the boundary layer before recaptured by antibodies is extremely rare. [94]

Generally speaking, even though surface based immunoassays can provide higher sensitivity and ease of manipulation, the prolonged incubation time (from several hours to days) makes it difficult to be used in point of care systems. Aiming to fully exploit its potential, many strategies have been developed to provide better low concentration detection sensitivity and reliability, to be introduced in the following sections.

5.3 Current Progress in Biosensors and Post Amplification Techniques

Shown in Figure 5-3 is a typical scheme of a biosensing unit. Normally, when a more sensitive biomolecule detector is desired for low concentration analytes, one has to either find better antibodies, or make more antibodies available for a given number of targets, or build more sensitive transducers. With a fixed immobilized antibody concentration, a straightforward way to improve the assay is to decrease the K_D values of the antibody (by finding a better, more specific antibody). However, this approach can be challenging, time consuming and, most importantly, may not work for all target molecules.[95]

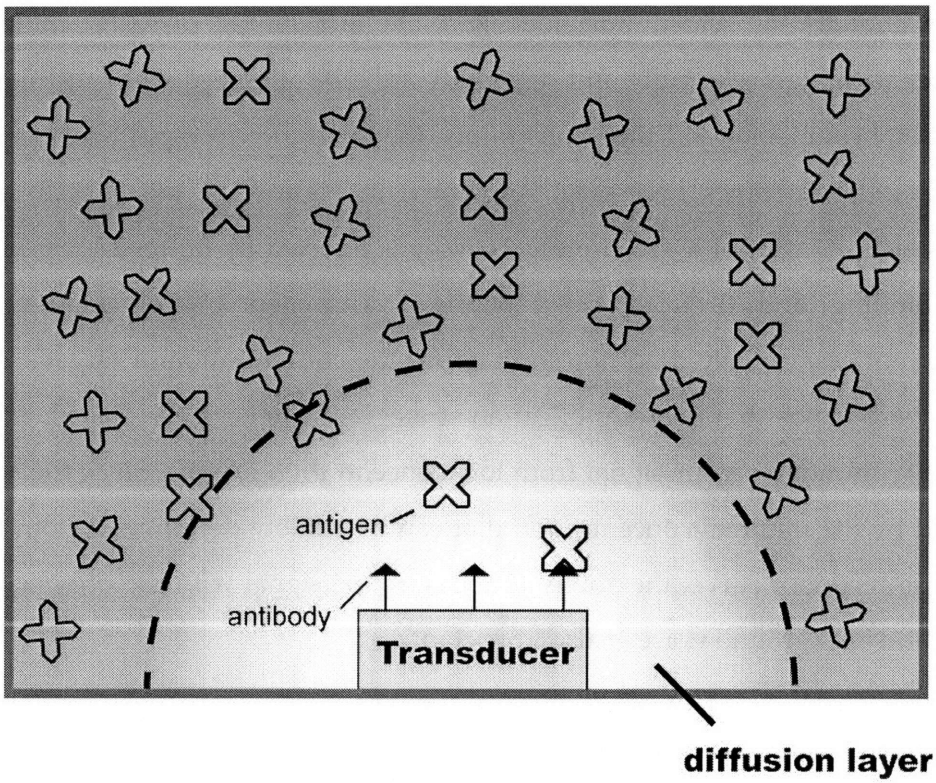

Figure 5-3 Standard biosensing scheme with immobilized primary antibody

Since detecting biomolecules from either bloodstream or environmental samples at low target concentration has been a major challenge in proteomic studies and emerging infectious disease monitoring, various forms of immunoassays, such as ELISA, are usually the method of choice. However, the detection at ultra low concentration is still a great challenge.[94]

To better monitor or screen infectious and life threatening diseases, multiplexable techniques with high selectivity and sensitivity are critically needed. In addition, due to the strict environmental and time constraints, the ability to do rapid analysis is highly favorable and sometimes necessary. As shown in Figure 5-4, the overall sensitivity (lower detection limit) of a given immunoassay is affected by buffer background, non-specific binding, and electronic noise of the measurement instrumentation. Because many current assays have detection limit above the concentration of target's biological activity, various post-binding amplification strategies have been developed, as a means to boost the immuno-sensor signal from low concentration sample. Since the sensitivity is defined by the minimal concentration that can be reliably determined from the slope of the dose-response curve, the ability to measure the signal with the presence of other analytes and background noise is also important.

To summarize recent efforts on improving biosensors, these efforts can be divided into two different sections: the improvement on biological recognition elements and the transducers (refer to Figure 5-1).

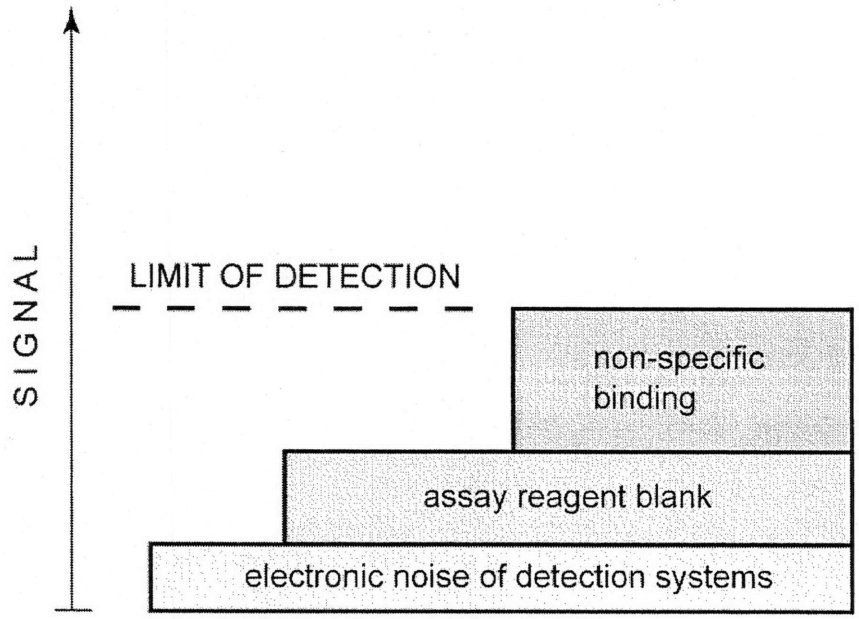

Figure 5-4 Sources of background signal in immunoassays[92]

5.3.1 Post-amplification Techniques

Immunoassays were brought into the biosensing community in 1959 in a liquid-phase radio tagged (isotopic) format.[96] Recent developments, however, have focused on nonradioisotopic labels in solid-phase assays in favor of their sensitivity, rapid reaction and automatability. A well recognized example is the use of enzyme amplification called ELISA as shown in Figure 5-5. The secondary enzyme can be readily replaced by chemiluminescent compound, cofactor such as ATP, electroactive compound or fluorophores. This is usually achieved by a sandwich assay, where a secondary antibody (specific to the target) labeled with enzyme is allowed to bind to the antibody-antigen pair. ELISA has become one of the most commonly used immunoassay because the "enzyme-linked" secondary antibody can elicit a chromogenic or fluorescent signal from the substrate via enzymatic reactions for multiple cycles. As a result, each enzyme molecule can produce many detectable molecules to give a better signal readout. After the reaction, the enzyme products can either be detected by color, fluorescence or luminescence. In addition, by attaching multiple enzyme labels to the secondary

antibody, the amount of detectable product can be increased without modifying other parameters.

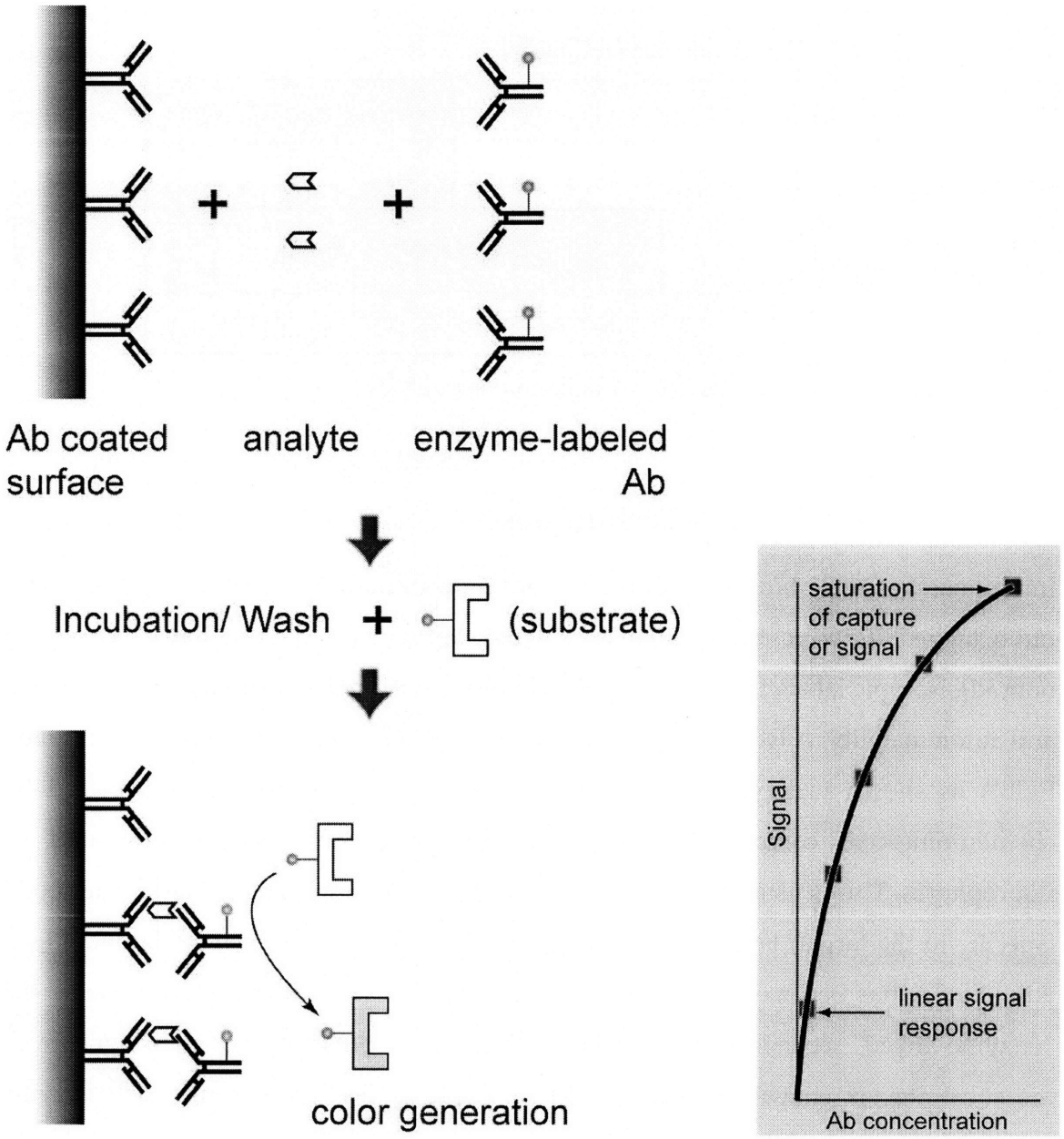

Figure 5-5 Enzyme Immunoassay for detection of antibodies (sandwich assay)

An inherent disadvantage of the ELISA and related immunoassays is that the fidelity is primarily governed by the dissociation constant (K_D), of the antibody-antigen complex. If the target antigen concentration is significantly below the K_D, then the binding kinetic is slow and readout precision of the antigen-antibody complex is degraded by noise. The K_D, depends on the properties of the antibody (e.g. monoclonal versus polyclonal) and typically ranges from 10^{-8} to 10^{-12} M. Sometimes protein-based biomarkers can be present at concentration levels that are significantly below the K_D of the antibody-antigen binding, which makes reliable detection challenging.

Another commercially available strategy is called cycle coupling, which is similar to EIA. During the first stage of the cycle coupling, the enzyme label catalyzes the conversion of substrate into product 1, however, not yet to be detected. Instead, product 1 is recycled to be converted into secondary or end product with other substrates in the reagent. By recycling product 1 for more reactions, one can have stronger signal and hence a more sensitive assay. This method also has been demonstrated with amplification factors as much as 100-fold.[97] It is also noticeable that some have used acetate kinase as the label to convert acetyl phosphate and ADP into ATP. While ATP can detected by highly efficient "firefly" luciferin, acetate kinase can be detected at concentration as low as 9 zeptomolar (less than 6000 molecules).[94]

One technique drive these sandwich assays to the extreme is the use of DNA tags on the antibody to replace the need for enzyme amplification. For example, by using a sequence of DNA as the label on the secondary antibodies, Sano *et al.* developed a new technique called Immuno-PCR. After undergoing approximately 25 PCR cycles, the DNA concentration can be increased by a million-fold.[98] The same strategy has been adapted to microscale immunoassay systems by Schweitzer *et al.*,[12] named the isothermal rolling-circle amplification (RCA) that can amplify the signal for multiple analytes by more than 1000 fold. Therefore, it can achieve sub femtomolar (fM) sensitivity with high specificity.[12] In this work, the authors attached the

oligonucleotide primer (5') on the primary antibody with biotin-avidin chemistry. Once the antibody-DNA conjugate binds to its specific target molecule, fluorescent oligonucleotides can be hybridized onto predetermined sequences using PCR-like techniques. Due to the specificity of hybridizations, RCA provides much better signal-to-noise ratio compared with general enzyme labeling. This method however can provide no better quantitative range than the original assay because the signal strength is determined by the number of bound antibody-DNA conjugates.

Magneto-immunosensor is also a newly developed method that provides a powerful alternative for enzyme labeling. In these approaches, magnetic beads are used either as an alternative label or the solid-phase for the following procedures. With the help of magnetic beads, researches can isolate antigen-magnetic bead conjugate from the sample solution with magnetic field. When the binding was accomplished, magnetic field was turned on to trap particles during intense washing cycles to eliminate background noise for post amplification. Following the isolation, different detections or amplifications can be achieved without interference with un-reacted species. The second analytical approach on these magnetic beads is to use them as a "weight" to mass-based sensing techniques such as microbalance, piezo-electric or cantilever-based sensors.

5.3.2 Novel Nanobiosensors for High-sensitivity Immuno-signal Transduction

The other approach one can take to lower the biosensors' detection limit is to reduce the electronic noise of detections systems.[92] Recently, significant advances have been reported using novel nanoscale sensors to improve the detection sensitivity of the immunoassay. These include surface plasmon resonance (SPR)[5], cantilever-based sensors[6-8, 52], carbon nanotube or nanowire-based sensors[9, 10, 99], and nanoparticle-based assays[11]. SPR was first introduced in early 90s and quickly became the gold standard to study ligand binding kinetics with high sensitivity. It is still widely used today even in the microfluidic format regardless its high cost, low throughput, and the

lack of quantitative measurements. Nanoscale sensors, on the other way, provide a unique opportunity for ultrahigh sensitivity sensing. By reducing the size of the electronic nanowire or nanotube devices, these sensors exhibit the ability to monitor the conductivity changes from extremely small numbers of binding events.

Even though these techniques achieve high sensitivity either by improving the detection of a small number of antibody-antigen binding events, they are still subject to some of the inherent limitations posed by primary binding of the antibody and the target antigen. Often, this primary binding is a diffusion-limited process.[21, 100, 101] Therefore sometimes it requires a long incubation time in order to achieve the necessary sensitivity.[102]

Therefore, despite these methods can possibly bring the electronic noise below a "single molecule" level, the reliability and detection quantitative (dynamic) range is still not satisfying. With the approach presented in this thesis, we can again solve this problem in a completely different approach. One specific goal of this thesis is to use the described nanofluidic preconcentrator to address the critical problem in proteomic sample preparation and identification. To better serve this goal, basics about the capabilities and limitations of immunological biosensors are also introduced in the following sections.

5.4 Preconcentration for Immunosensing

As introduced in the previous section, many post amplification techniques have been developed with remarkable detection sensitivity, however, none of them can address the problem that low concentration analyte binding is a mass diffusion limited process. Besides, since the signal amplification can work only based on the initial amount of captured antigens, these amplification methods often provide less dynamic range of detection compared to the original assay.

While the major goal of most signal amplification strategies is to provide low concentration reading with better fidelity, increasing the original sample concentration can be a straightforward yet hard to implement idea. With the strict incubation and buffer swapping requirements, most current sample preconcentration requirements cannot be applied directly to immunoassays. In certain biomarker detection applications, K_D can be 10- to 100-fold smaller than a saturated situation due to analyte depletion and/or the diffusive transport constraint.[101] Therefore, as the antigen concentration decreases, the time required for binding equilibrium will increase dramatically. Such kinetic behavior is clearly shown in Figure 5-6 [Top]. In this experiment, the equilibrium time of R-PE binding on primary antibodies (on beads) increases dramatically with decreasing target concentrations. More details about the experimental setup of this test are provided in the next section. As the consequence of sample depletion in the diffusive layer, when low concentration antigen diagnosis is needed, incubations from several hours to overnight are usually used.[102] Such a long incubation is a common problem in immuno-biosensing once the analyte concentration goes below the scaling limit:[7, 100, 101] The diffusion limited regime can be defined by the following equation presented by Nair *et al.*

$$t_c < \frac{N_m r}{D \times [Ag]} \tag{5.2}$$

Here, t_c is the characteristic reaction time, N_m is the minimum number of molecules to be captured for detection, D is the diffusion coefficient of the molecules and r is the radius of the sensor unit. The rate determining step is molecular diffusion of targets to antibodies, rather than the binding constant.[21, 100] Therefore, with the same binding pair (affinity constant) and the reaction time, the detection limit of the system is mainly governed by the K_D.

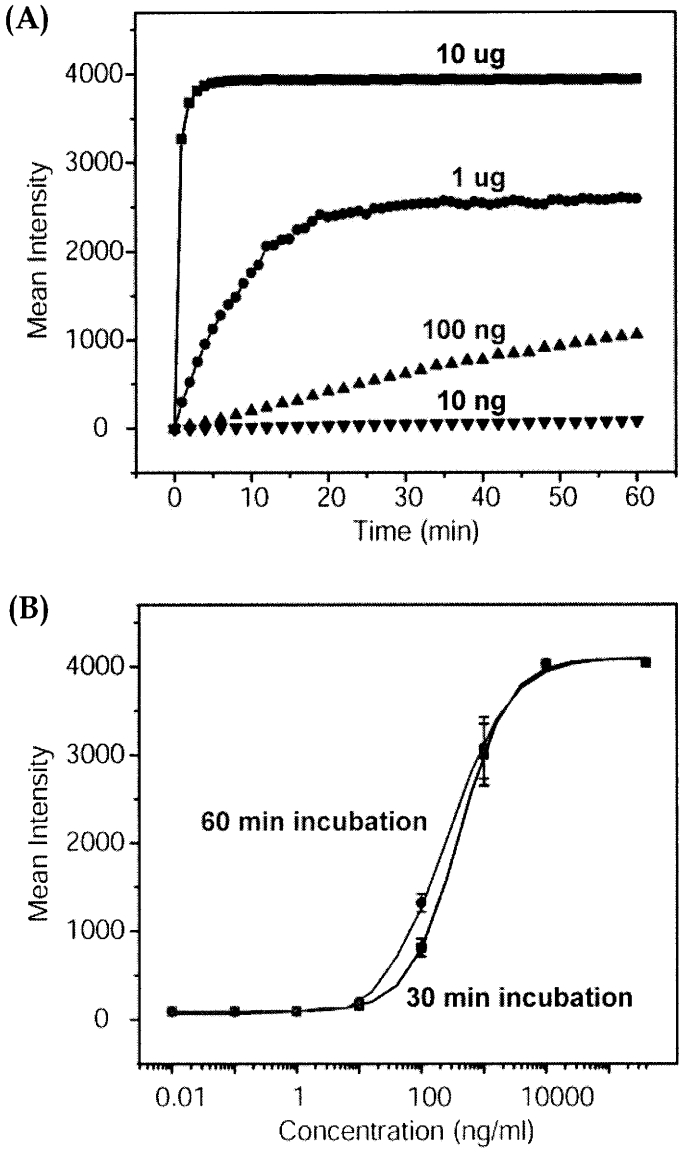

Figure 5-6 Kinetics and dose response of bead based R-PE immunoassay

[A] The plot shows the immunoassay binding kinetics of R-PE samples. Samples were loaded with various concentrations and the intensity represents the fluorescent signal from R-PE molecule captured on polystyrene beads. Due to the depletion of free analytes, the association rate decreases at lower analyte concentration. As a result, the detection of R-PE samples with concentration lower than 100 ng/ml takes more than one hour to reach equilibrium.

[B] Dose response curves of R-PE molecule on anti-R-PE beads. As shown in the plot, longer incubation time can only slightly increase the signal intensity. Comparing the responses between 30 min and 1 hr incubation, the detection limited (10 ng/ml) is not improved by 30 min longer incubations.

Based on these scaling arguments, integrating sample preconcentration with immunoassay can not only benefit low concentration analytes detection but also reduce the time of analysis dramatically. Moreover, unlike post-binding amplification techniques, sample preconcentration can broaden the dynamic range of detection based on its ability to adjust the amount of initial binding.

To address these issues, we are proposing a novel strategy: Instead of amplifying the signal after the primary immuno-reaction, we seek to enhance the concentration of the target molecule before the reaction using a molecular preconcentration device. In this way, the kinetics of primary immuno-reaction could be driven toward the bound state, improving both the sensitivity and the time required for detection. In this work, we demonstrate this by integrating a standard bead-based immunoassay with a nanofluidic preconcentrator in a microfluidic device format. There have been several preconcentration techniques available, for example, field amplified stacking,[33] membrane preconcentration,[31] chromatographic preconcentration,[103] and electrokinetic preconcentration.[39] Among these, electrokinetic concentration methods would be ideally suited for integration with downstream immunoassays, due to their material robustness, high efficiency, and flexibility for integration. Integration of membrane-based preconcentration systems with immunoassays has been achieved previously,[104, 105] although the signal enhancement factor was limited due to clogging of membranes. While microfluidic immunoassays have been developed for rapid diagnostics/identification[106, 107], advantages of microfluidic format cannot be fully realized primarily because detecting low concentration analytes requires longer incubation time. Unlike other preconcentration techniques, our recently developed nanofluidic preconcentrator[40] can precisely locate the collected molecule with high preconcentration factors at a predetermined spot. Moreover, because this technique requires no physical confinement and complex buffer reagents, it has no interfacing problem with other detectors, post amplification, and multiplexing techniques.

5.5 Bead-based Immunoassay

5.5.1 Device Fabrication

The devices were fabricated in a standard microfabrication facility (Microsystems Technology Laboratories of MIT). The nanofluidic channels and through-holes were defined and etched into a Si wafer using projective photolithography (Nikon Precision Inc., CA) and reactive-ion etching techniques to a depth of 40 nm. Following the through hole etching on silicon wafer in a 80 ^{0}C, 20% KOH solution and silicon nitride stripping, a 500 nm thermal oxide layer was grown to provide an electrical isolation between the conductive silicon substrate and buffer solution.

As for the microchannels and dam structure, a 200 nm a-Si layer was deposited on the Corning Pyrex wafer to work as the hard mask for isotropic BOE wet etching. The deep trench channels are first patterned and etched by contact photolithography and reactive-ion etching. Following the hard mask etching, a 6.5 μm wet etching was done in diluted HF solution buffered by Nitric acid. After the first step etching, the shallow dam structure was patterned and etched with the same procedure to a thickness of 5.5 μm. Microchannels were etched into Pyrex instead of silicon wafers because etching deep trenches on wafer is troublesome for both electrical isolation and further lithography. This two step etching, as a result, gives a 12 μm deep microchannel with a shallow dam region of 5.5 μm for bead process trapping at the predefined location.

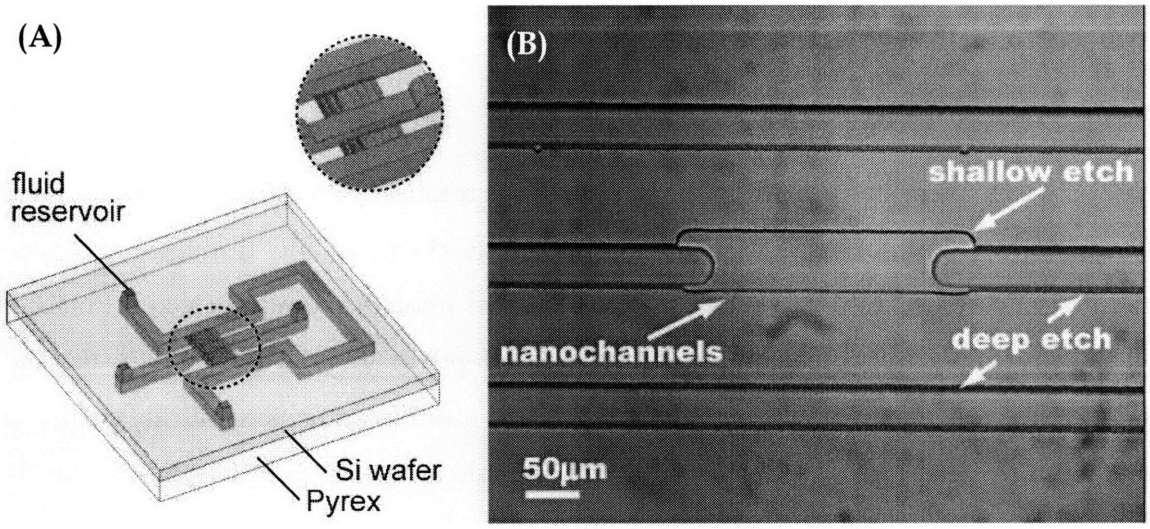

Figure 5-7 Device schematics and snapshot

[A] Schematics showing the nanofluidic preconcentration device. The center sample channel is connected to the U shaped buffer channel by nanochannel arrays. The close view shows the nanofluidic channels and bead trapping dam structure from the back side. [B] Bright field image of a nanofluidic preconcentrator with bead trapping structure

At the end of the process, the device was sealed by bonding the Pyrex wafer on the silicon wafer after backside alignment with lithography tools (Electronic Vision, Tempe, AZ). The bonded wafers were then cut into individual devices for experiments in a custom-made clamp. The depths and surface uniformity of the nanochannels and wet-etched microchannels were measured by imaging the cross-section of the nanofilter with scanning electron microscopy (JEOL USA, Inc., Peabody, MA) after anodic bonding. The final device is shown in Figure 5-7.

Compared with the device described in Chapter 4, this device has deeper microfluidic channels to accommodate the 7.5 μm diameter bead assays.[40] In the previous device, two 10 μm by 1.5 μm (cross-section) microchannels with a 50 μm wide, 20 μm long and 40 μm deep nanochannel array and a million-fold green fluorescent protein (GFP) preconcentration was achieved within 30 min. Aiming to have the higher throughput, easier fluid and bead delivery required for this work, we fabricated devices with scaled up microfluidic channels (cross-section 50 μm by 12 μm). As a consequence, the ion

depletion region was harder to generate and maintain. To solve this problem, the double nanochannel array shown in Figure 5-7 was proposed to provide a stronger ion depletion and more stable operation. With nanochannels only on one side, a considerably higher voltage is required to extend the ion depletion region across the channel. Meanwhile, wide microfluidic channels have less stable concentration polarization due to the rapid mixing driven by the nonlinear electroosmosis.[76] In this work, a sample buffer (10mM phosphate with 40pM R-phycoerythrin (R-PE) and 0.37 μM GFP was loaded into the middle microfluidic channel and the buffer was loaded into the channel. With the voltage scheme shown in Figure 5-7, a steady concentration enhancement of R-PE can be obtained as demonstrated in Figure 5-8. Currently, the R-PE can be concentrated by more than 1000 fold (average plug concentration) in 30 min within a 10,000X more concentrated GFP background.

Moreover, various samples have been tested in this device with a similar voltage scheme (including small peptides, proteins with different molecular weights, positive and negative charged dyes). Compared to the previous shallow microchannel works, the concentration factor is compromised in these large scale devices due to more rapid mixing in the less confined environment.[76] However, it could be further improved by tailoring the channel geometries in the future.

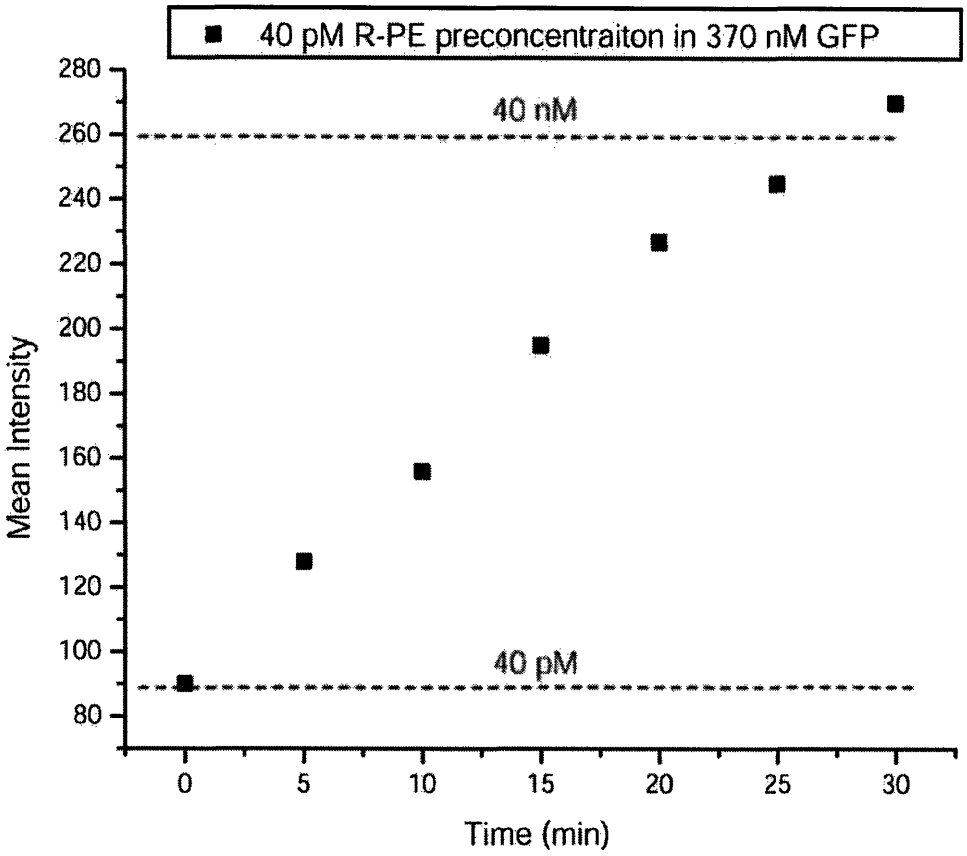

Figure 5-8 Plot showing continuous preconcentration of the R-PE and GFP mixture
In this experiment GFP is 10,000 fold more concentrated than the R-PE. The intensity represents the native fluorescence from R-PE molecule recorded by a CCD camera. In comparison, the R-PE preconcentration is not affected by the presence of high concentration GFP.

5.5.2 Sample Preparation and Surface Immobilization

R-PE (Invitrogen, Grand Island, NY), rGFP (BD Biosciences, Franklin Lakes, NJ), biotinylated anti-GFP (Fitzgerald Industry, Concrod, MA), biotinylated anti-R-PE (BD Biosciences, San Jose, CA) were purchased and used as received without further purification and diluted in the sample buffer (10 mM phosphate buffer with 0.02% sodium azide) prior to the experiment.

325 µl Streptavidin bead (Applied Biosystem, Foster city, CA) at concentration of 30×10^6 beads/ml concentration was mixed with 800 µl phosphate buffer with 8 µg anti-R-PE

and incubated 2 hrs with constant mixing at room temperature. After the incubation, the beads were isolated by a centrifugal molecular weight cut-off filter (Millipore, Billerica, MA) and resuspended in to 1 ml phosphate buffer. The same procedure was used with anti-GFP, a robust and versatile antibody immobilization method for other biotinylated antibodies. These beads were further diluted by 1000 times before loading into the device.

To immobilize these antibody labeled streptavidin beads, the device contains a dam structure. Because the gap was controlled between 5.5 to 6 μm, the 7.5 μm beads will be trapped as illustrated in Figure 5-9. Once the beads are trapped, the antigen binding (incubation) can be done by delivering a constant fluid flow with fixed antigen concentration through the device.

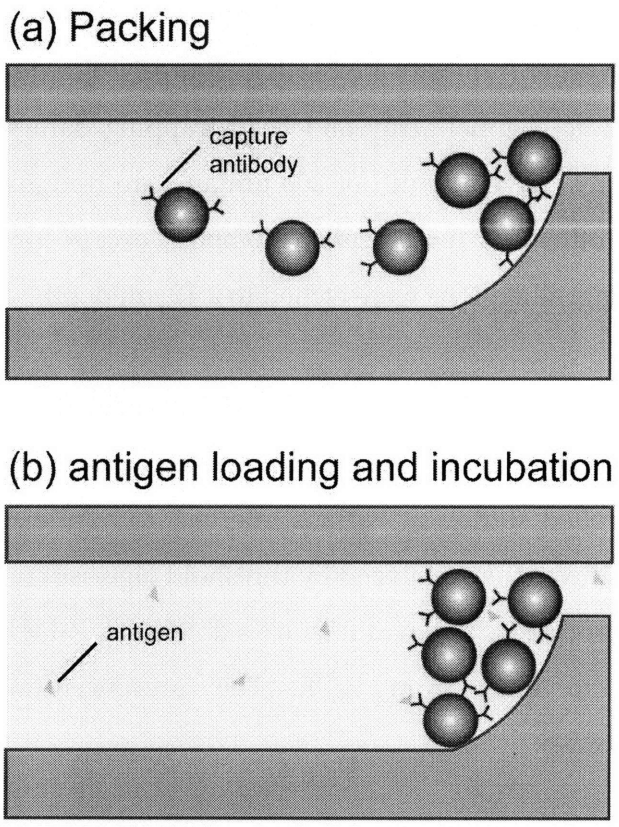

Figure 5-9 Bead loading and sample incubation relying on the bead trapping structure

All the experiments were imaged with an inverted epi-fluorescence microscope (IX-71, Olympus, Melville, NY) equipped with a thermoelectrically cooled CCD camera (Sensicam QE, Cooke Co., Auburn Hill, MI) and a 100W mercury lamp (Chiu Technical Corp., Kings Park, NY). Fluorescence imaging was visualized through either the TRITC filter set (exitation: 562 nm, emission: 624 nm, Semrock, Rochester, NY) or the FITC filter set (exitation: 482 nm, emission: 536 nm, Semrock, Rochester, NY). Sequences or images were analyzed with image processing software (IPLab 3.6, Scanalytics, BD Bioscience, Rockville, MD).

5.5.3 Immunoassay Response Measurement

To prevent nonspecific binding of samples, each of the new devices was first loaded with 1% BSA solution for 30 min. After coating, diluted beads labeled with anti-R-PE or anti-GFP were loaded into the channel, and only a few beads were controlled to prevent stacking between each other (typically 4-6 beads). Figure 5-10[top] shows the bright field image of the nanofluidic channel array and bead trapping dam structure. The 40 nm deep nanochannel arrays have a width of 200 μm and are bridging microchannels 100 μm away from each other. As for the microchannels, except for the 5.5 μm shallow etches for bead trapping, all regions were etched to a 12 μm depth.

After bead loading, sample buffer was introduced and incubated with pressure driven flow similar to flow injection analysis experiments. The fluorescent signal was recorded using computer controlled shutter at various intervals to minimize photobleaching on the samples. The signal was then analyzed by threshold algorism to average only signals from the beads. As reported by the manufacture's datasheet, R-PE has indistinguishable response compared to ones from B-PE. The preconcentration efficiency was demonstrated in Figure 5-8.

(A)

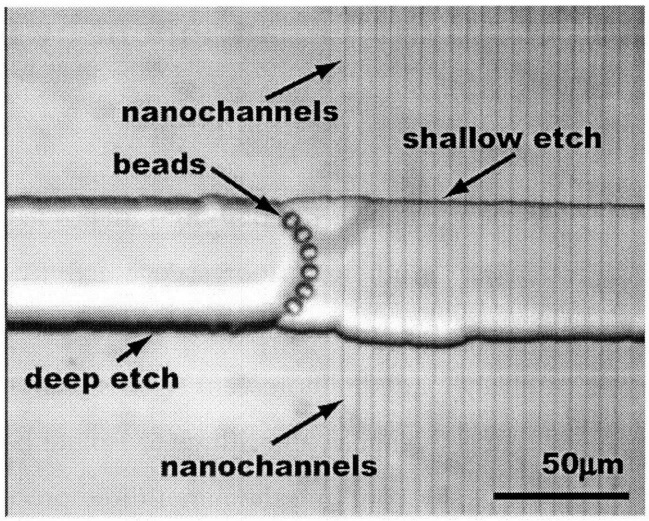

(B)

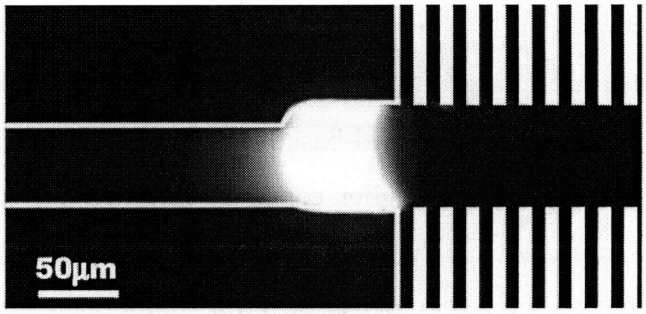

(C)

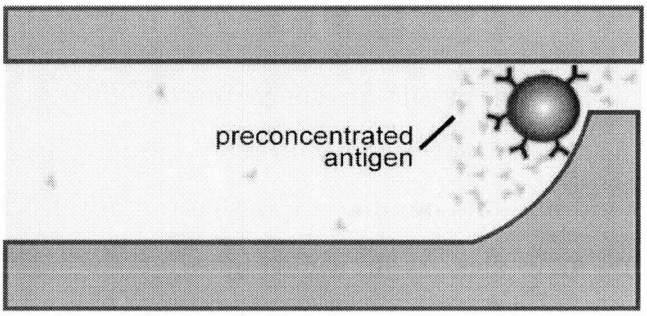

Figure 5-10 Preconcentration of better immunosensing

[A] Antibody labeled polystyrene beads trapped by the shallow etch (dam structure); the circular profile is the pattern of isotropic Pyrex wet etching. The numbers of the beads were controlled to prevent beads from overlapping with each other [B] Fluorescent image of preconcentrated R-PE (preconcentration time= 30 min with initial concentration= 40 pM) [C] Schematics showing the primary antibody labeled bead trapped by the dam structure etched in the microfluidic channel. The higher local antigen concentration represents the preconcentrated biomolecule plug (on-site preconcentration).

5.6 Kinetics and Sensitivity Enhancement by On-site Electrokinetic Trapping

In order to enable real time monitoring of the binding kinetics and primary immuno-reaction, we use two proteins with inherent fluorescence activity (R-PE and GFP) as model antigens. To avoid false signal increment from overlapped surfaces, only a few beads were counted and carefully loaded. Fluorescent signals were recorded by a cooled CCD camera and analyzed using threshold algorithms to isolate bead signals from the background. As described above, by coupling the nanofluidic preconcentrator with the bead-based assay, we can achieve a continuous on-site sample preconcentration on various charged biomolecules. Therefore, the presented strategy can be applied to different biomolecules with very little or no adaptation. Figure 6-3(b) shows the dose response (binding curve) of this bead-based immunoassay with the presence of background analytes (in this case, higher concentration of GFP). As we increase the reaction time from 30 min to 1 hr, the response signal is marginally improved, without the significant changes in the lower detection limit maintained at around ~10 ng/ml level for the given monoclonal antibody-antigen (R-PE) pair.

Nevertheless, with a 30 min on-site preconcentration, this system can lower the sensitivity limit by ~500 fold from the 50 pM to 100 fM range (Figure 5-11). In addition, the preconcentration and immuno-binding response is not affected by adding 10 μg/ml GFP as the background molecules. As shown in Figure 5-8, the enhanced signals (bound R-PE on the bead) were not affected by the additional washing/flushing step, clearly demonstrating the enhanced binding made available by the preconcentration step. Figure 5-12 is fluorescent images from the on-site preconcentration of a 10 ng/ml sample. While only a small signal can be acquired after a 30 min incubation of samples, the signal was enhanced to 10 μg/ml level after a 30 min on-site preconcentration and flushing. Because of the simplicity of the presented method, this preconcentrator can be widely applied to various detection and post amplification techniques.

(A)

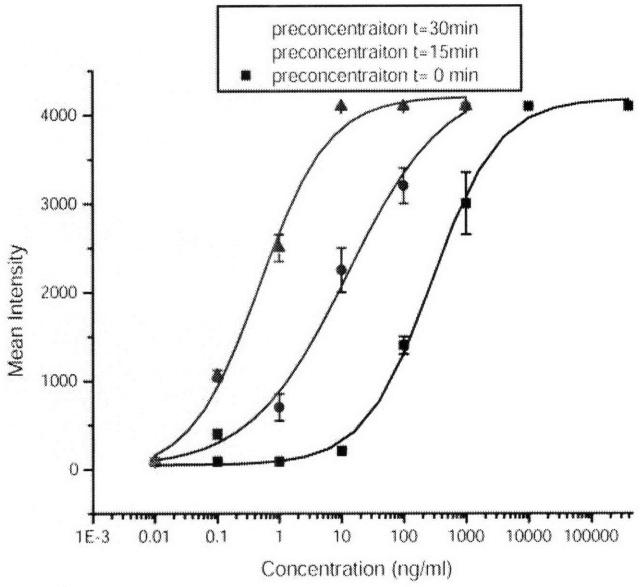

(B)

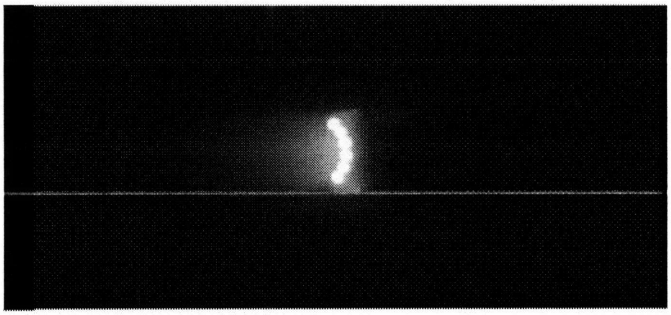

Figure 5-11 Dose response curves of R-PE sample with various preconcentration time

(A) The plot shows a 30 min incubation with no preconcentration (right), with 15 min preconcentration (middle) and 30 min incubation with 30 min preconcentration (left)

(B) Through maintaining a 30 min on-site preconcentration, this approach can lower the sensitivity limit by about 500 fold from 50 pM to sub 100 fM range. The fluorescent image shows preconcentration PE sample plug on top of trapped microbeads.

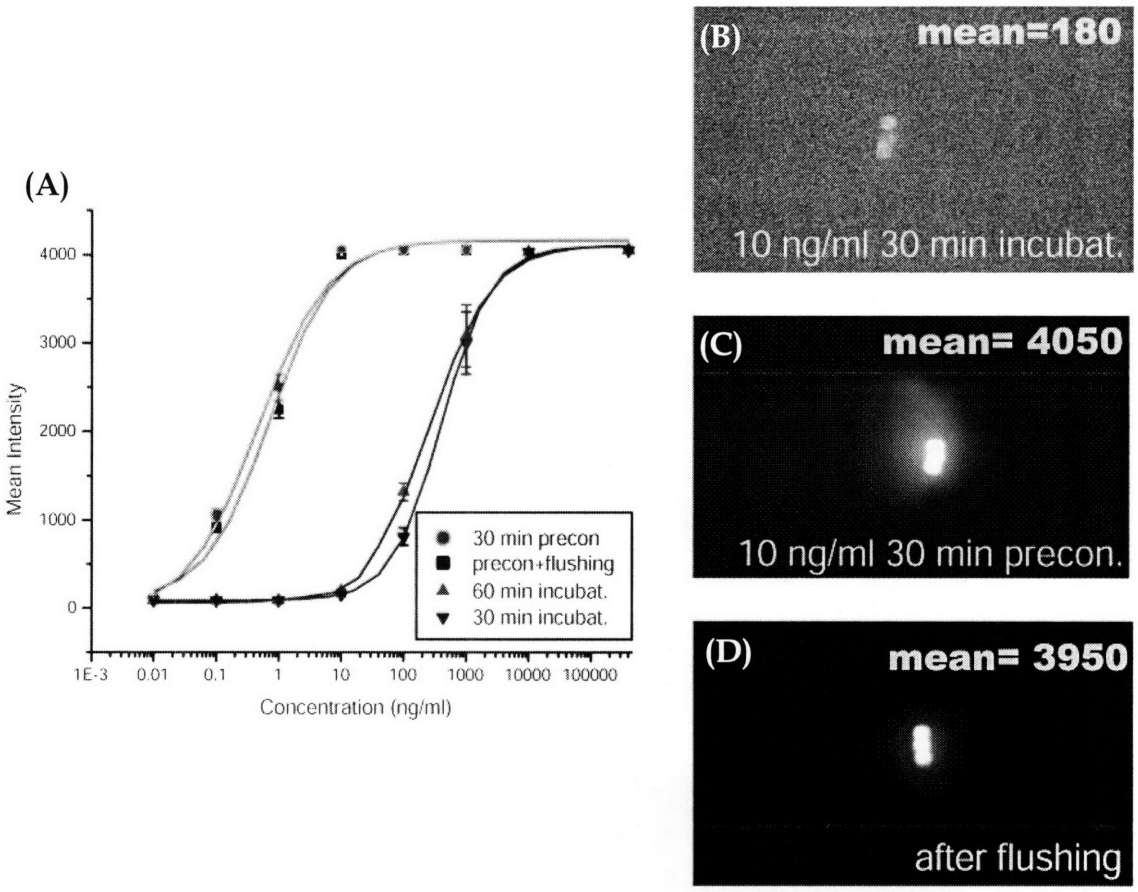

Figure 5-12 Dose responses and fluorescent images of anti-R-PE beads in 10 ng/ml PE sample Figure (A) Dose responses demonstrating different incubation and preconcentration condition as indicated by legends; Figure (B) The signal response after 30 min incubation; Figure (C) The fluorescent image of beads sitting in the preconcentrated R-PE plug (preconcentration time= 30min); Figure (D) The signal of bound R-PE does not decrease after flushing of the preconcentrated plug.

5.7 Remarks

In this chapter, we have demonstrated the development and validation of the nanofluidic electrokinetic preconcentrator for enhancing the detection limit and binding kinetics for general immunological biosensors. With a given antibody-antigen pair, the device can not only change the optimal detection range but also increase the sensitivity by at least ~500 fold. Furthermore, by increasing the concentration of target antigen

around the immunoassay, the binding kinetics is significantly improved. The assay is also tested with high concentration GFP as a background molecule, demonstrating that operation of the device was unaffected even with much higher concentration background molecules. Because the system is in a microfluidic platform, it requires only a small amount of sample and reagent for detection, therefore, is ideal for miniaturized, point-of-care biosensing applications. In addition, multiplexing for many different targets is highly feasible due to the possibility of massively parallelizing these assays on a chip.

Because the preconcentrator traps molecules based on electrostatic interaction at a specific location for various detectors, it can be used as a general tool addressing problems in detecting low concentration analytes, both small and large molecules. Furthermore, the chosen bead-based sensor has already been commercialized (flow cytometry assays such as Bio-Plex from BioRad or xMAP from Luminex).[108] Therefore, the integration and multi-analyte multiplexing can be easily achieved by labeling the beads with antibodies specific to different targets. Moreover, this device gives us the ability to tailor the sensitivity range (dynamic range) of immunosensing by changing the preconcentration time rather than increasing surface antibody density or decreasing antibody K_D, both of which are often very challenging and time-consuming. As a result, this approach can be used to identify multiple scarce markers at various concentrations. Adaptation of this strategy to sandwich assays (using both primary and secondary antibodies) could be done easily in the future. Most importantly, to further enhance detection sensitivity and selectivity, any existing and novel biosensing strategies that utilize post-binding amplification can be coupled with this strategy.

In conclusion, we have demonstrated a highly flexible sensitivity/kinetics enhancement method for immunological bioassays based on electrokinetic trapping of biomolecules. As the system has flexibilities to change either the sensitivity limit or the detection dynamic range, it can be used to identify multiple low-abundance markers at various concentrations. Thus, we believe the nanofluidic preconcentration-immunoassay

strategy can effectively address the critical detection issues in the early detection of common disease biomarkers.

Chapter 6

Conclusion

6.1 Summary of Contribution

Biosample purification (preparation) has long been the most demanding and expensive process in proteomics laboratories. Recent developments in micro Total Analysis Systems have shown promising solutions to address the problem, and have provided opportunities for mass production and automatable analysis. Thus, many proteomic researchers have moved their conventional analysis toward these microfluidic platforms. While various microfluidic systems have been developed to replace conventional technologies, identifying low abundance proteins in a complex mixture is still a great challenge.

Nanostructures (Nanofluidic channels) and nanomaterials have similar intrinsic scales as biomolecules, therefore they can be used to control and automate sample processing. So far, they have been largely used as molecular sieving infrastructures to build customized separation devices.[16, 17] Nevertheless, the comparable size scales between biologically-relevant molecules and nanostructures also promises exticitn opportunities in the field of biosensing.[9] With these recent developments of micro and

nanofabrication techniques, unique properties found in nanostructures have led to new inventions and have been demonstrated to be useful in areas of biomolecule separation, preconcentration, detection and other critical sample preparation elements.[13-15, 40, 109]

Inspired by these concepts, this thesis has focused on using micro/nano-fluidic technologies to address challenges in proteomic studies, for applications like sample preparation and biosensing. A novel electrokinetic trapping device was invented in 2005, which can achieve more than a million-fold preconcentration within 30 minutes.[40] In addition, coupling between the nanofluidic preconcentrator and immunological sensors has been achieved, and the integrated device successfully enhanced immunoassay sensitivity limits by more than 500 times. This is the first device that can couple the preconcentration method with immunological sensing tools. This is one of the examples of using nanotechnology to advance the sample preparation process.[4, 13-15, 110-113]

In addition to practical application to proteomics, nanofluidic systems described in this thesis provide an ideal experimental platform to study novel electrokinetic phenomena such as concentration polarization, nonlinear electrokinetics, and limiting current behavior. Progresses in these areas have been limited due to the critical lack of experimental tools, which this device can provide.

6.2 Directions for Future Research

It takes continual effort to develop integrated devices for biosample preparation and proteomic studies. With the experience and knowledge acquired in this thesis, various interesting proteomic projects can be suggested. In addition, since our understanding of various nanofluidic systems is still limited, studies on ion transport, flow patterns, and molecular dynamics associated with nanofluidic structures are still needed.

6.2.1 Integrated Systems for Disease Monitoring

With the success of DNA arrays and portable biosensing devices, such as glucose monitor, great attention has been focusing on probing biology activity markers (for example, enzymes and hormones) in lab-on-a-chip devices to achieve rapid and ultra-sensitive disease diagnosis and biomolecule identification. However, the detection of low-abundance biomarkers in complex biofluids is still challenging since there are more than 10,000 proteins with concentrations of 10 orders of magnitude in the human proteome. As a result, sample preparation has been a major challenge in proteomic studies. To solve this problem, a successful bioanalysis usually involves sample extraction, separation, amplification, and detection. For samples as complex as the human proteome, none of these steps can be omitted and granted a reliable readout.

Moreover, monitoring proteins is far more difficult than identifying DNA molecules, since there is no PCR-like amplification technique available. The nanofluidic preconcentrator can be an ideal technique to bridge this technical gap. By preconcentrating molecules, we can increase the signal intensity significantly prior to detection, therefore allowing more aggressive biomolecule sorting and the removal of high-abundance proteins without sacrificing the detectability of low abundance targets. Based on the integrated device presented in this thesis, we can design and fabricate integrated devices that are capable of processing complex samples and identifying target molecule, either with on-chip immunoassays or off-chip detectors such as mass spectrometry. In the meantime, since the bead labeling is a well-established technique, with all the reaction dynamic we obtain from this work, enhancing and detecting low concentration biomarkers should be feasible. This challenging research area has vast implications for proteomic studies and point-of-care system developments.

6.2.2 Nanofluidic Concentrators for Immunoassay and Enzyme Activity Studies

A major limiting factor in low concentration analyte detection is the prolonged incubation time to reach equilibrium due to the diffusion layers on the surface.[21] With the high preconcentration factor achieved by the nanofluidic preconcentrator, we can explore diverse applications that utilize concentration capability. For example, the preconcentrator can be used to build fluorimetric enzyme activity assays where subtracts are delivered with microfluidic integration downstream from the preconcentrator. While the preconcentrator can concentrate target enzymes rapidly, the device can be used to probe various biochemical activities associated with human physiology.

6.2.3 Exploring Novel Nanofluidic Phenomena

The unique ion transportation phenomena associated with nanofluidic channels can be apply to fields such as fuel cells, sample preconcentrations,[22, 23] and chromatographic separations.[24] Current studies suggest that the overlapping of Debye screening layers in nanofluidic channels can give them better proton conductivity than conventional media. These new proton exchange membranes could be used to develop next-generation micro fuel cells. Furthermore, because the surface screening layers have profound effects on biomolecules and ions, nanofluidic devices are the ideal platforms for us to study novel ion selective transfer. Because the study of ion transportation around these nanofluidic channels involves multiple disciplines and large spatial dimension differences, our current understanding of the charge depletion phenomena is still limited.

Using the experimental platform similar to our device, one can observe concentration polarization, charge depletion, and nonlinear electrokinetic flow in the adjacent microfluidic channel using fluorescent microscopy. By manipulating the electric field,

the device can be used to study extended space charge region. When a higher potential is applied, the presented device can be used to study the chaotic flow adjacent to nanochannels. The preliminary results from these experiments have been presented in both μTAS and APS conferences and received broad interests from various scientific communities. [75, 112] As demonstrated, the devices we developed in this thesis can help researchers understand more about novel nanoscale fluid science.

Appendix A

List of Symbols

Symbol	Definition
a	particle size
$[Ag]$	antigen concentration
$[Ab]$	antibody concentration
[C]/ C	concentration
Di	diffusivity
E	electric field
F	Faraday constant
H	enthalpy
I	current
I_L	limiting current
j_D	diffusion flux
K	Partition coefficient
k_a	association rate constants
k_d	dissociation rate constants
K_D	dissociation constant
L	length of ion depletion
p	local pressure
q	heat
R	universal gas constant
S_0	induced space charge layer
S	entropy
T	temperature
t_c	characteristic reaction time
u	velocity
V	voltage
x	characteristic length
z	valance number
δ	unstirred diffusive layer
ϕ	electric potential
γ	relative conductive
κ^{-1}	Debye layer
λ_D	Debye layer

μ	viscosity
ε	permittivity
ρ_e	charge density
σ_L	conductivity
v_i	mobility
ζ	zeta potential

Bibliography

1. Kornberg, A., *Ten Commandments: Lessons from the Enzymology of DNA Replication.* J. Bacteriol., 2000. **182**: p. 3613-3618.
2. Auroux, P.-A., et al., *Micro Total Analysis Systems. 2. Analytical Standard Operations and Applications.* Analytical Chemistry, 2002. **74**: p. 2637-2652.
3. Reyes, D.R., et al., *Micro Total Analysis Systems. 1. Introduction, Theory, and Technology.* Analytical Chemistry, 2002. **74**: p. 2623-2636.
4. Dittrich, P.S., K. Tachikawa, and A. Manz, *Micro Total Analysis Systems. Latest Advancements and Trends.* Analytical Chemistry, 2006. **78**: p. 3887-3098.
5. Kurita, R., et al., *On-Chip Enzyme Immunoassay of a Cardiac Marker Using a Microfluidic Device Combined with a Portable Surface Plasmon Resonance System.* Analytical Chemistry, 2006. **78**: p. 5525-5531.
6. Wu, G., et al., *Bioassay of prostate-specific antigen (PSA) using microcantilevers.* Nature Biotechnology, 2001. **19**: p. 856-860.
7. Hwang, K.S., et al., *In-situ quantitative analysis of a prostate-specific antigen (PSA) using a nanomechanical PZT cantilever.* Lab on a Chip, 2004. **4**: p. 547-552.
8. Burg, T.P. and S.R. Manalis, *Suspended microchannel resonators for biomolecular detection.* Applied Physics Letters, 2003. **83**: p. 2698-2700.
9. Zheng, G., et al., *Multiplexed electrical detection of cancer markers with nanowire sensor arrays.* Nature Biotechnology, 2005. **23**: p. 1294-1301.
10. Chen, R.J., et al., *Noncovalent functionalization of carbon nanotubes for highly specific electronic biosensors.* Natl Acad. Sci. USA, 2003. **100**: p. 4984-4989.
11. Georganopoulou, D.G., et al., *Nanoparticle-based detection in cerebral spinal fluid of a soluble pathogenic biomarker for Alzheimer's disease.* Proc. Natl Acad. Sci. USA, 2005. **102**: p. 2273-2276.
12. Schweitzer, B., et al., *Immunoassays with rolling circle DNA amplification: A versatile platform for ultrasensitive antigen detection.* Proc. Natl Acad. Sci. USA, 2000. **97**: p. 10113-10119.
13. Eijkel, J.C.T. and A.V.D. Berg, *The promise of nanotechnology for separation devices-from a top-down approach to nature-inspired separation devices.* Electrophoresis, 2006. **27**: p. 677-685.
14. Mohamadi, M.R., et al., *Nanotechnology for genomics & proteomics.* Nanotoday, 2006. **1**: p. 38-45.
15. Mukhopadhyay, R., *What Does Nanofluidics Have to Offer?* Analytical Chemistry, 2006. **78**: p. 7379-7382.

16. Fu, J., et al., *A patterned anisotropic nanofluidic sieving structure for continuous-flow separation of DNA and proteins.* Nature Nanotechnology, 2006. **2**: p. 121-128.
17. Han, J. and H.G. Craighead, *Separation of Long DNA Molecules in a Microfabricated Entropic Trap Array.* Science, 2000. **288**: p. 1026-1029.
18. Hu, J.T., T.W. Odom, and C.M. Lieber, *Chemistry and physics in one dimension: synthesis and properties of nanowires and nanotubes.* Acc. Chem. Res., 1999. **32**: p. 435-445.
19. Ebbesen, T.W., *Carbon nanotubes.* Annu. Rev. Mater. Sci., 1994. **24**: p. 235-264.
20. Alivisatos, P., *The use of nanocrystals in biological detection.* Nature Biotechnology, 2004. **22**: p. 47-52.
21. Nair, P.R. and M.A. Alam, *Performance limits of nanobiosensors.* Applied Physics Letters, 2006. **88**: p. 233120-233123.
22. Liu, S., et al., *From Nanochannel-Induced Proton Conduction Enhancement to a Nanochannel-Based Fuel Cell.* Nano Letters, 2005. **5**: p. 1389-1393.
23. Pu, Q., et al., *Ion-Enrichment and Ion-Depletion Effect of Nanochannel Structures.* Nano Letters, 2004. **4**: p. 1099-1103.
24. Pennathur, S. and J.G. Santiago, *Electrokinetic Transport in Nanochannels. 2. Experiments.* Analytical Chemistry, 2006. **78**: p. 972-973.
25. Anderson, N.L. and N.G. Anderson, *The Human Plasma Proteome.* Molecular & Cellular Proteomics, 2002. **1**: p. 845-867.
26. Man Ho Choi, Y.-C.W., John S. Wishnok, Steven R. Tannenbaum and a.J. Han, *On-chip Isoelectric Focusing Coupled to Micro Liquid Chromatography in Blood Proteomics.* Micro Total Analysis Systems, 2003. **1**: p. 955-958.
27. Yu, C., et al., *Monolithic Porous Polymer for On-Chip Solid-Phase Extraction and Preconcentration Prepared by Photoinitiated in Situ Polymerization within a Microfluidic Device.* Analytical Chemistry, 2001. **73**: p. 5088-5096.
28. Oleschuk, R.D., et al., *Trapping of Bead-Based Reagents within Microfluidic Systems: On-Chip Solid-Phase Extraction and Electrochromatography.* Analytical Chemistry, 2000. **72**: p. 585-590.
29. Ramsey, J.D. and G.E. Collins, *Integrated Microfluidic Device for Solid-Phase Extraction Coupled to Micellar Electrokinetic Chromatography Separation.* Analytical Chemistry, 2005. **77**: p. 6664-6670.
30. Song, S., A.K. Singh, and B.J. Kirby, *Electrophoretic Concentration of Proteins at Laser-Patterned Nanoporous Membranes in Microchips.* Analytical Chemistry, 2004. **76**: p. 4587-4592.
31. Khandurina, J., et al., *Microfabricated Porous Membrane Structure for Sample Concentration and Electrophoretic Analysis.* Analytical Chemistry, 1999. **71**: p. 1815-1819.
32. Foote, R.S., et al., *Preconcentration of Protein on Microfluidic Devices Using Porous Silica Membranes.* Analytical Chemistry, 2005. **77**: p. 57-63.
33. Burgi, D.S. and R.-L. Chien, *Optimization in Sample Stacking for High-Performance Capillary Electrophoresis.* Analytical Chemistry, 1991. **63**: p. 2042-2047.
34. Gebauer, P. and P. Bocek, *Recent Progress in Capillary Isotachophoresis.* Electrophoresis, 2002. **23**: p. 3858-3864.

35. Jung, B., R. Bharadwaj, and J.G. Santiago, *On-chip Millionfold Sample Stacking Using Transient Isotachophoresis.* Analytical Chemistry, 2006. **78**: p. 2319-2327.
36. Quirion, J.P. and S. Terabe, *Exceeding 5000-Fold Concentration of Dilute Analytes in Micellar Electrokinetic Chromatography.* Science, 1998. **282**: p. 465-468.
37. Quirion, J.P. and S. Terabe, *Approaching a Million-Fold Sensitivity Increase in Capillary Electrophoresis with Direct Ultraviolet Detection: Cation-Selective Exhaustive Injection and Sweeping.* Analytical Chemistry, 2000. **2000**: p. 1023-1030.
38. Astorga-Wells, J. and H. Swerdlow, *Fluidic Preconcentrator Device for Capillary Electrophoresis of Proteins.* Analytical Chemistry, 2003. **75**: p. 5207-5212.
39. Singh, A.K., et al., *A Novel Miniaturized Protein Preconcentrator Based on Electric Filedaddressable Retention and Release.* Micro Total Analysis Systems, 2002. **1**: p. 347-349.
40. Wang, Y.-C., A.L. Stevens, and J. Han, *Million-fold Preconcentration of Proteins and Peptides by Nanofluidic Filter.* Analytical Chemistry, 2005. **77**: p. 4293-4299.
41. Kim, S.M., M.A. Burns, and E.F. Hasselbrink, *Electrokinetic Protein Preconcentration Using a Simple Glass/Poly(dimethylsiloxane) Microfluidic Chip.* Analytical Chemistry, 2006. **78**: p. 4779-4785.
42. Dhopeshwarkar, R., L. Sun, and R.M. Crooks, *Electrokinetic Concentration Enrichment within a Microfluidic Device Using a Hydrogel Microplug.* Lab on a Chip, 2005. **5**: p. 1148-1154.
43. Mikkers, F.E.P., F.M. Everaerts, and T.P.E.M. Verheggen, *High-performance zone electrophoresis.* Journal of chromatography, 1979. **169**: p. 11-20.
44. Lichtenberg, J., E. Verpoorte, and N.F.d. Rooij, *Sample preconcentration by field amplification stacking for microchip-based capillary electrophoresis.* Electrophoresis, 2001. **22**: p. 258-271.
45. Jacobson, S.C., et al., *Effects of Injection Schemes and Column Geometry on the Performance of Microchip Electrophoresis Devices.* Analytical Chemistry, 1994. **66**: p. 1107-1113.
46. Ross, D. and L.E. Locascio, *Microfluidic Temperature Gradient Focusing.* Analytical Chemistry, 2002. **74**: p. 2556-2564.
47. O'FARRELL, P.H., *Separation Techniques Based on the Opposition of Two Counteracting Forces to Produce a Dynamic Equilibrium.* Science, 1985. **227**: p. 1586-1589.
48. Hatch, A.V., et al., *Integrated Preconcentration SDS-PAGE of Proteins in Microchips Using Photopatterned Cross-Linked Polyacrylamide Gels.* Analytical Chemistry, 2006. **78**: p. 4976-4984.
49. Dodge, A., et al., *Electrokinetically Driven Microfluidic Chips with Surface-Modified Chambers for Heterogeneous Immunoassays.* Analytical Chemistry, 2001. **73**: p. 3400-3409.
50. Sato, K., et al., *Integration of an Immunosorbent Assay System: Analysis of Secretory Human Immunoglobulin A on Polystyrene Beads in a Microchip.* Analytical Chemistry, 2000. **72**: p. 1144-1147.

51. Manz, A., N. Graber, and H.M. Widmer, *Miniaturized total chemical analysis systems: A novel concept for chemical sensing.* Sensors and Actuators B: Chemical, 1990. **1**: p. 244-248.
52. Karnik, R., et al., *Electrostatic Control of Ions and Molecules in Nanofluidic Transistors.* Nano Letters, 2005. **5**: p. 943-948.
53. Li, B., et al., *Separation of DNA with Different Configurations on Flat and Nanopatterned Surfaces.* Analytical Chemistry, 2006. **78**: p. 4743-4751.
54. Reuss, F.F., *Charge-induced flow.* Proceedings of the Imperial Society of Naturalists of Moscow, 1809. **2**: p. 327-344.
55. Lyklema, J., *Fundamentals of Interface and Colloid Science.* Vol. 2. 2001, San Diego, CA: Academic Press.
56. Hamann, K., *Characterization of Powder Surfaces.* 1976, London, UK: Academic Press.
57. Probstein, R.F., *Physicochemical Hydrodynamics: An Introduction.* 1994: Wiley-Interscience, N.Y.
58. Giddings, J.C., Science, 1993. **260**: p. 1456-1465.
59. Pennathur, S. and J.G. Santiago, *Electrokinetic Transport in Nanochannels. 1. Theory.* Analytical Chemistry, 2005. **77**: p. 6772-6781.
60. Griffiths, S.K. and R.H. Nilson, *Charged Sepcies Transport, Separation, and Dispersion in Nanoscale Channels: Autogenous Electric Field-Flow Fractionation.* Anal. Chem., 2006. **78**: p. 8134-8141.
61. Herr, A.E., et al., *Electroosmotic Capillary Flow with Nonuniform Zeta Potential.* Anal. Chem., 2000. **72**: p. 1053-1057.
62. Rice, C.L.a.R.W., *Electrokinetic Flow in a Narrow Cylindrical Capillary.* Journal of Physical Chemistry, 1965. **69**: p. 4017-4024.
63. Yaroslavtsev, A.B., V.V. Nikonenko, and V.I. Zabolotsky, *Ion transfer in ion-exchange and membrane materials.* Russian Chemical Reviews, 2003. **72**: p. 3930421.
64. Probstein, R.F., *Physicochemical Hydrodynamics: An Introduction.* 1994: Wiley-Interscience.
65. Rubinstein, I. and B. Zaltzman, *Electro-osmotically induced convection at a permselective membrane.* Physical Review E, 2000. **62**: p. 2238-2251.
66. Rubinstein, I. and B. Zaltzman, *Electro-osmotic slip of the second kind and instability in concentraiton polarization at electrodialysis membranes.* Mathematical Models and Methods in Applied Sciences, 2001. **11**: p. 263-300.
67. Dukhin, S.S., *Electrokinetic phenomena of the second kind and their applications.* Adv Colloid Interface Sci, 1991. **35**: p. 173.
68. Mishchuk, N.A. and P.V. Takhistov, *Electroosmosis of the second kind.* Colloids and Surfaces A: Physicochemical and Engineering Aspects, 1995. **95**: p. 119-131.
69. Ben, Y. and H.-C. Chang, *Nonlinear Smoluchowski slip velocity and micro-vortex generation.* Journal of Fluid Mechanics, 2002. **461**: p. 229-238.
70. Bazant, M.Z. and T.M. Squires, *Induced-Charge Electrokinetic Phenomena: Theory and Microfluidic Applications.* Physical Review Letters, 2004. **92**: p. to be correst.

71. Levitan, J.A., et al., *Experimental observation of induced-charge electro-osmosis around a metal wire in a microchannel.* Colloids and Surfaces a-Physicochemical and Engineering Aspects, 2005. **267**(1-3): p. 122-132.
72. Squires, T.M. and M.Z. Bazant, *Induced-charge electro-osmosis.* Journal of Fluid Mechanics, 2004. **509**: p. 217-252.
73. Urbanski, J.P., et al., *Fast AC electro-osmotic micropumps with nonplanar electrodes.* Applied Physics Letters, 2006. **89**(14): p. 3.
74. Levich, V., *The theory of concentration polarization.* Acta Physicochimica U.R.S.S., 1942. **17**: p. 257-307.
75. Chu, K.T., *Asymptotic Analysis of Extreme Electrochemical Transport*, in *Department of Mathematics*. 2005, Massachusetts Institute of Technology: Cambridge. p. 244.
76. Kim, S.J., et al., *Nonlinear Electrokinetic Flow Pattern Near Nanofluidic Channel.* Micro Total Analysis Systems, 2006. **1**: p. 522-524.
77. Mishchuk, N.A. and S.S. Dukhin, *interfacial electrokinetics and electrophoresis*, ed. A.V. Delgado. 2002, New York, NY: Marcel Dekker.
78. Mishchuk, N.A. and S.S. Dukhin, *Electrophoresis of solid particles at large peclet numbers.* Electrophoresis, 2002. **23**: p. 2012-2022.
79. Maletzki, F., H.W. Rossler, and E. Staude, *Ion Transfer across electro-diffusional membranes in the overlimitng current range: stationary voltage current characteristics and current noise power spectra under different conditions of free convection.* J. Membrane Sci., 1992. **71**: p. 105-115.
80. Petersen, N.J., et al., *Study of interface conductivity and its possible applications.* Proc. Micro Total Analysis Systems, 2004: p. 348-350.
81. Shannon, M.A., et al., Micro Total Analysis Systems, 2003: p. 5-8.
82. Leinweber, F.C. and U. Tallarek, *Nonequilibrium Electrokinetic Effects in Beds of Ion-Permselective Particles.* Langmuir, 2004. **20**: p. 11637-11648.
83. Petersen, N.J., et al. *Study of Interface conductivity and its possible applications.* in *Micro Total Analysis Systems 2004*. 2004.
84. Madndersloot, W. and R.E. Hicks, Ind. Eng. Chem. Process Des. Dev., 1965. **4**: p. 304.
85. Mao, P. and J. Han, *Fabrication and characterization of 20 nm planar nanofluidic channels by glass-glass and glass-silicon bonding.* Lab Chip, 2005. **5**: p. 837-844.
86. Rubinstein, I., et al., *Experimental Verification of the Electroosmotic Mechanism.* Russian Journal of Elelctrochemistry, 2002. **38**(853-863).
87. Hjerten, S., *High-Performance Electrophoresis Elimination of Electroosmosis and Solute Adsorption.* Journal of chromatography, 1985. **347**: p. 191-198.
88. Paul, P.H., D.W. Arnold, and D.J. Rakestraw. *Electrokinetic Generation of High Pressures Using Porous Microstructures.* in *Micro Total Analysis Systems 1998*. 1998.
89. Ramos, A., et al., *AC electrokinetics: a review of forces in microelectrode structures.* Journal of Physics D: Applied Physics, 1998. **31**: p. 2338-2353.
90. Ajdari, A., *Pumping liquids using asymmetric electrode arrays.* Physical Review E, 2000. **61**: p. R45-R48.
91. Pejcic, B., R.D. Marco, and G. Parkinson, *The role of biosensors in the detection of emerging infectious diseases.* Analyst, 2006. **131**: p. 1079-1090.

92. Nakamura, R.M., *Immunochemical Assays and Biosensor Technology for the 1990s.* 1992, Washington, D.C.: American Society for Microbiology.
93. Edwards, R., *Immunoassays essential data.* 1996, Huddersfield, UK: H. Charlesworth & Co. Ltd.
94. Wild, D., *The Immunoassay Handbook.* 3rd ed. 2005, Oxford, UK: ELSEVIER Ltd.
95. Corey, E., et al., *Characterization of 10 new monoclonal antibodies against prostate-specific antigen by analysis of affinity, specificity and function in sandwich assays.* Int. J. Cancer, 1997. **71**: p. 1019-1028.
96. Yalow, R.S. and S.A. Berson, *Assay of plasma insulin in human subjects by immunological methods.* Nature, 1959. **184**: p. 1648-1649.
97. Self, C.H., *Enzyme amplification: a general method applied to provide an immunoassisted assay for placental alkaline phosphatese.* J. Immunol. Methods, 1985. **75**: p. 389-393.
98. Sano, T., C.L. Smith, and C.R. Cantor, *Immuno-PCR: very sensitive antigen detection by means of specific antibody-DNA conjugates.* Science, 1992. **258**: p. 120-122.
99. Patolsky, F., G. Zheng, and C.M. Lieber, *Nanowire sensors for medicine and the life sciences.* Nanomedicine, 2006. **1**: p. 51-65.
100. Kusnezow, W., et al., *Kinetics of antigen binding to antibody microspots: Strong limitation by mass transport to the surface.* Proteomics, 2006. **6**: p. 794-803.
101. Mol, N.J.d., et al., *Kinetic Analysis of the Mass Transport Limited Interaction between the Tyrosine Kinase Ick SH2 Domain and a Phosphorylated Peptide Studied by a New Cuvette-Based Surface Plasmon Resonance Instrument.* Analytical Biochemistry, 2000. **279**: p. 61-70.
102. Cesaro-Tadic, S., et al., *High-sensitivity miniaturized immunoassays for tumor necrosis factor alpha using microfluidic systems.* Lab on a Chip, 2004. **4**: p. 563-569.
103. Huber, D.L., et al., *Programmed Adsorption and Release of Proteins in a Microfluidic Device.* Science, 2003. **301**: p. 352-254.
104. Morais, S., A. Maquieira, and R. Ruchades, *Immunofiltration: A Methodology for Preconcentration and Determination of Organic Pollutants.* Analytical Chemistry, 1999. **71**: p. 1905-1909.
105. Pal, A. and T.K. Dhar, *An Analytical Device for On-Site Immunoassay. Demonstration of Its Applicability in Semiquantitative Detection of Aflatoxin B1 in a Batch of Samples with Ultrahigh Sensitivity.* Analytical Chemistry, 2004. **76**: p. 98-104.
106. Herr, A.E., et al., *On-Chip Native Gel Electrophoresis-Based Immunoassays for Tetanus Antibody and Toxin.* Analytical Chemistry, 2005. **77**: p. 585-590.
107. Lim, T.-K., H. Hota, and T. Matsunaga, *Microfabricated On-Chip-Type Electrochemical Flow Immunoassay System for the Detection of Histamine Released in Whole Blood Samples.* Analytical Chemistry, 2003. **75**: p. 3316-3321.
108. Mekala, D.J., R.S. Alli, and T.L. Geiger, Proc Natl Acad Sci U S A, 2005. **102**: p. 11817-2.
109. Wang, Y.-C., M.H. Choi, and J. Han, *Two-Dimensional Protein Separation with Advanced Sample and Buffer Isolation Using Microfluidic Valves.* Analytical Chemistry, 2004. **76**(15): p. 4426-4431.

110. El-Ali, J., P.K. Sorger, and K. Jensen, *Cells on chips.* Nature, 2006. **442**: p. 403-411.
111. Grodzinski, P., M. Silver, and L.K. Molnar, *Nanotechnology for cancer diagnostics: promises and challenges.* Expert review of molecular diagnostics, 2006. **6**: p. 307-318.
112. Song, S. and A.K. Singh, *On-chip sample preconcentraiton for integrated microfluidic analysis.* Analytical and bioanalytical chemistry, 2006. **384**: p. 41-43.
113. Whitby, M. and N. Quirke, *Fluid flow in carbon nanotubes and nanopipes.* Nature Nanotechnology, 2007. **2**: p. 87-94.
114. Wang, Y.-C. and J. Han, *Nonlinear Electroosmosis and Biomolecule Electrokinetic Trapping Induced by Ion Selective Nanofluidic Channels.* APS March Meeting, 2006.